2021

Characterization of Micronutrient Dependent Growth by Several Temperate Freshwater Phytoplankton

Purnank Shah
shah4680@mylaurier.ca

Characterization of Micronutrient Dependent Growth by Several Temperate Freshwater Phytoplankton

by

Purnank Shah
BSc Biochemistry, University of Waterloo, 2017

THESIS
Submitted the Department of Geography and Environmental Studies
at Wilfrid Laurier University
in fulfillment of the
requirements for the degree of
Master of Science
in
Geography

Waterloo, Ontario, Canada, 2021

Abstract

Harmful algal blooms (HABs) are a growing problem in many freshwater water bodies in Canada and around the world. HABs have wide-ranging impacts to ecosystems and economies. Since the 1970s, the primary focus of policies with respect to curbing HABs has been to lowering the inputs of P into waters. However, reports of HABs continue to increase even with all these P-removing policies in place. Some jurisdictions have chosen to focus on N-removal instead or in conjunction with P-removal to help with HABs. However, because some cyanobacteria have the ability to fix atmospheric N_2, N-removal might only lead to the dominance of N-fixing HABs. Recent research has suggested that micronutrients, such as Fe and Co, are key in algal bloom development and biochemistry.

The goals of this thesis are to assess their dependence on micronutrients and investigate how micronutrients impact algal bloom growth, to assess possible mitigation strategies and to explore new techniques to help in answering these questions. Chapters 2 and 6 explore how Fe and Co may play a role in phytoplankton bloom development and growth of N-fixing cyanobacteria. Chapters 4 and 5 explore how Fe(II) removal might impact cyanobacterial growth and affect HABs. Chapters 3 and 7 use modified and new techniques to study algal growth by using stable isotopes to characterize growth of phytoplankton in culture and using a smartphone app to quantify algal biomass.

We found the nutrient threshold concentrations (below which growth ceases) and relative affinities for Fe at low concentrations for seven different phytoplankton. We determined that N-fixing cyanobacteria in N-replete conditions have the lowest iron threshold at 76 ± 2pM, green algae have a mean iron threshold of 245 ± 5pM, the non-fixer *Microcystis aeruginosa* has a threshold of 663 ± 17pM, and N-fixing cyanobacteria that are grown without nitrate have a mean iron threshold of 736 ± 17pM. At low Fe concentrations, *Microcystis aeruginosa* had the highest affinity, followed by N-fixing cyanobacteria grown in N-replete conditions, then N-fixing cyanobacteria who had to fix N_2 and green algae had the lowest affinity at low Fe concentrations. These findings reinforce the importance of Fe in HABs growth and development and provide insight into how certain species and species types could dominate at low concentrations of Fe.

By using a simple mixing-model, we were able tease apart the isotopic composition of newly accumulated biomass from the measured bulk samples, we found that estimated isotopic composition of new biomass differed up to 15‰ from the measured bulk sample. We characterized the growth of cultures of ten different phytoplankton species using the new estimates of isotopic composition and found that fractionation factors between dissolved nutrient and biomass vary largely with time and in diazotrophic species, the fractionation factor is much higher than previously reported. We used these newly estimated isotopic compositions and fractionation factors and correlated them to instantaneous growth rates and found moderate correlations among growth rates and carbon isotopic fractionation factors.

Fe is an important nutrient from algal bloom development and recent research has pointed specifically to Fe(II). We assessed the impacts of Fe(II) removal on cyanobacterial growth using a colourometric Fe(II) chelator, ferrozine (FZ). We found that adding FZ

in a variety of FZ:Fe molar ratios does not impact the growth of phytoplankton in the conditions we used. Therefore, we must continue to explore the efficacy and impacts of Fe(II) removal on HABs in the environment.

This work let to further exploration of the properties of FZ while other chelators, like citrate and EDTA are present. We also studied the impacts of other metal chelators on the formation of the Fe-FZ complex. While citrate did not inhibit the formation of the Fe-FZ complex, EDTA might play an Fe oxidizing role in cell medium.

Like Fe, increases in Co can increase growth and N-fixation in cyanobacteria. However, unlike Fe, the mechanism of how this occurs is largely unknown. We investigated the impacts of increasing Co concentrations on the growth and heterocyst abundance of filamentous N-fixing cyanobacteria. Our results show that increasing Co significantly increases the percentage of heterocysts found in cultures of N-fixing filamentous cyanobacteria. We also combined our culture studies with field and literature data and found similar results. This may point to a possible role of Co in heterocyst synthesis and thus N-fixation and how that might impact algal bloom growth and development, especially in environments with low N.

All of this work relied on the optical measurement of algal biomass using a spectrophotometer. However, this method is not feasible when it comes to field measurements or engaging citizens to participate in monitoring efforts. We devised an unique and simple strategy to accurately measure algal biomass using a smartphone app, using the RGB colour model. A good linear relationship between algal absorbance at 750nm using a spectrophotometer and $(R + B + G)/G$ was found. We also correlated this relationship to cell numbers in culture at a species level. This method offers a promising detection method for algal biomass determination with simple operation, fast response and low cost.

This work highlights the importance of Fe and Co to the growth and proliferation of HABs and attempts to use this micronutrient dependence to control the problem. We also show the use of new and innovative models and methods to make the characterization of this complex problem more efficient and accurate.

Acknowledgements

Firstly, I want to thank Dr. Jason Venkiteswaran. Jason, thank you for always having a slightly-ajar office door and for always listening to my latest rants about what culture died on that given week. Thank you for all your support and patience over the years and for making the lab a place that puts the people first. I was sold on the idea of joining your lab from that one-fateful afternoon when you gave me a tour of Cold Regions back in 2017 and I have not regretted it.

I also want to thank Dr. Lewis Molot and Dr. Sherry Schiff for being a part of my advisory committee. Lewis, thank you for going through *every single one* of my many drafts with a fine-toothed comb, for offering advice whenever I came calling and for all the support you have given me over the years. Sherry, thank you always for your thoughtful questions, your out-of-the-box ideas and for your amazing energy, they made me a better researcher. I also want to thank Dr. Sue Watson, she took a chance on me back in 2013 and hired me as a co-op student in her HABs lab and first inspired and fostered the love for algae I have today.

No work gets done in the EGL group without Richard Elgood. Rich, thank you not just for processing all the samples I left to you, but for years of advice, for the laughter, for your support and for teaching me a lot of the lab techniques and procedures we use. I am sorry for having a terrible success rate in finding samples whenever I went cooler-diving. To Sarah Sine, thank you for always running my ridiculously high N samples with no idea of where the concentrations will be. I didn't make it easy, but you always managed to get it done.

While they've both moved on to bigger and better things, I want to thank Dr. Kateri Salk and Dr. Megan Larsen. Thank you both for taking the time and teaching us the basics of R and statistics. You turned us all into R-masters and I will forever be grateful. Both of you were the first post-doctoral fellows I worked with, and I want to thank you both for your guidance, your ear and your example.

To Jenn Mead, Pieter Aukes, Jeremy Leathers, Mackenzie Shultz, Matthew Roberts, Catherine Goltz and to the other graduate students I had the privilege of working with, thank you always for listening to my inane ramblings about algae. Whether they made sense or not, know that I always appreciated you listening and I am always in awe of your ideas and your work. I think I hit the proverbial-jackpot when I started grad school the same time as Rachel Henderson, Emily Barber and Jordyn Atkins. I am better researcher, a better TA and a better person because I have your friendship. You made the struggle bearable and I can't wait to see where we go from here.

To my friends outside of grad school, thank you for always having my back, for always cheering me on, and for spending hours just listening to me lecture you all about algal blooms. You did not sign up to be friends with a mega-nerd when you met me, but you have all stuck through for the better part of a decade. Your support, your company and your love helped me push through some of the dark days of experimentation-failures and I cannot thank you enough.

Finally, I want to thank my family. Having a scientist in a family of business people is not easy to understand. I certainly did not make it easy with my constant moving, and the far flung co-ops and the field trips to ELA or Lake Erie, but you have supported me through it all. Thank you for celebrating every step forward, every pretty graph and every little success. Thank you for welcoming a set of my algae cultures into our home when the pandemic first began, and being more concerned about them than I was. Thank you for always having my back, for always reminding me to get back up and get to work and for supporting my love for science.

Table of Contents

List of Tables

List of Figures

Abbreviations

A_{750} Absorbance at 750nm 27, 41, 43, 44, 54, 60, 78, 79, 93–96, 99, 122, 123, 131–134

abs absorbance 22, 96

BBM Bold's Basal Medium (modified) 26, 41, 59, 92, 122

BG-11 Blue-Green Medium Num. 11 26, 41, 59, 77, 92, 122

BG-11_0 Blue-Green Medium Num. 11 (no $NaNO_3$) 26, 41, 77, 78, 92, 122

CCMs carbon concentrating mechanisms 6

cHABs cyanobacterial harmful algal blooms 1–4, 8, 22, 25, 39, 57, 58, 75, 91

ChlA chlorophyll *A* 8, 91, 92

CPCC Canadian Phycological Culture Centre 16, 26, 41, 59, 77, 92, 122

cyanotoxins toxins produced by cyanobacteria 2

DIC dissolved inorganic carbon 5, 38, 41–44, 49, 54

DIN dissolved inorganic nitrogen 30, 38, 42–44, 49, 55

DOC dissolved organic carbon 5, 7, 8, 38, 41, 42, 44, 54

DOM dissolved organic matter 7, 15, 103

DOP dissolved organic phosphate 8

ECCC Environment and Climate Change Canada 16, 77

EDTA ethylenediaminetetraacetic acid 22, 59, 63, 67–70, 73, 103

ELA IISD Experimental Lake Area 16, 20, 41, 59, 74, 77, 79, 85, 103

FZ ferrozine 22, 57, 59–61, 63–65, 67, 69, 70, 72, 73, 103

GF-AAS graphite furnace atomic absorption spectrometry 27

HABs harmful algal blooms 1–4, 9, 24, 36, 37, 39, 40, 58, 65, 75, 90, 91

IVF *In vivo* fluorometry 91

NIES Microbial Culture Collection at the National Institute for Environmental Studies 16, 41, 77, 92, 122

PBS phycobilisomes 91

PCC Pasteur Culture Collection of Cyanobacteria 16, 26, 41, 59, 64, 77, 86, 92, 122

POC particulate organic carbon 5, 38, 43, 49

POM particulate organic matter 38, 39, 42, 43, 55, 56

PON particulate organic nitrogen 38, 43, 49

PSII photosystem II 11

RGB red, green, blue colour model 90, 94

SAG Sammlung von Algenkulturen at the University of Göttingen 16, 41, 92, 122

TDN total dissolved nitrogen 42, 44, 54, 55

Chapter 1

Introduction

Canada is home to over a million lakes and many more ponds (Pick, 2016). The Laurentian Great Lakes, the largest freshwater system on Earth, contains approximately 21% of the world's freshwater and is the source of drinking water for millions of people (Frey and Mutz, 2006). Since the 1960s, phosphorus (P) loading into lakes has led to a rise in harmful algal blooms (HABs) as well as a large increase in the possible toxin-producing cyanobacterial harmful algal blooms (cHABs) (Winter et al., 2011). Harmful algal blooms can pose a significant threat to human health and the economy due to the production of potent toxic compounds (Downing et al., 2001). While eutrophication, the presence of excessive nutrients in a water body, seems to be the primary driver of HABs and cHABs, other factors play an important role in the proliferation of HABs and in determining the species that dominate. Since the 1970s, there have been laws and policies such as the Canada-USA Great Lakes Water Quality Agreement signed in 1972 and revised in 1978, 1987 and 2012, to mitigate and stop the rise of HABs (Pick, 2016). However, our lack of understanding of what drives the growth of HABs and what factors determine which species will dominate leaves us unable to effectively control this ever-proliferating problem.

1.1 HABs and cHABs

There has been an increase in the report of algal blooms all over the world (Pick, 2016). However, "algal bloom" is not a well-defined term. A bloom is commonly

defined as a large growth of phytoplankton in a water body (Smayda, 1997). Some groups distinguish between nuisance algal blooms and harmful algae blooms. HABs are algal blooms associated with adverse health effects while nuisance algal blooms have been defined to have more general harms (Ho and Michalak, 2015). Many different researchers and organizations define a bloom more specifically, usually by looking at biomass. For example, a bloom is defined as algal counts above 200,000 cells/L by the Intergovernmental Oceanographic Commission (Anderson et al., 2017). Several Canadian jurisdictions define cHABs based on cell counts of greater than 20,000 cyanobacterial cells/mL, while some define it as greater than 100,000 cyanobacterial cells/mL (Watson et al., 2008; Health Canada, 2012).

1.1.1 Impacts of HABs and cHABs

These blooms have a number of wide-ranging impacts associated with them. They leave foul-smelling and unsightly clusters of dead and dormant cells on shores and water surfaces which interfere with recreational uses. High algal biomass can deplete environments of oxygen as the bloom decay, resulting in harm to aquatic life (Anderson et al., 2002). Some cHABs produce toxins which can kill aquatic wildlife, poison livestock and even humans. These toxins produced by cyanobacteria (cyanotoxins) have been linked to many different diseases including carcinomas (Downing et al., 2001). Metabolic by-products of phytoplankton include taste and odour compounds that are difficult to remove from the drinking water treatment process (Downing et al., 2001).

Lakes in Canada are a large source of income through fisheries, tourism and other industries (Hudnell, 2010). However, algal blooms lower such incomes because of the resulting costs due to losses in recreational and industrial activities, clean up and treatment efforts add up. It was estimated that from 2011 to 2014, HABs in Lake Erie cost between $2.25 million to $5.58 million USD in just decreased sales of fishing licenses due to harm caused by HABs to fisheries (Wolf et al., 2017). A conservative estimate of annual costs due to HABs is $2.2 billion to $4.6 billion USD to the United States economy (Hudnell, 2010). These costs are found to be increasing as the severity and the

occurrence of HABs increases throughout the world.

1.1.2 Diversity of HABs and Nitrogen Fixation

Phytoplankton are a diverse group of photosynthetic organisms, they include classes of organisms such as diatoms, dinoflagellates, chlorophytes and cyanobacteria (Simon et al., 2009). They are found in a host of environments such as frozen rocks, caves, hotsprings, soil, inland waters and many others (Padisák et al., 2016). There are tens of thousands of branches of phytoplankton on the evolutionary tree of life. Despite this wide variety and diversity of organisms in the world, thousands of species are often binned together in groups that perform similar ecological function to simplify analyses and to help in making conceptual and quantitative models (Mutshinda et al., 2016). Phytoplankton are split into groups such as silicifying diatoms, mixotrophic dinoflagellates, calcifiers, toxin-producing cyanobacteria, or nitrogen fixing cyanobacteria (Mutshinda et al., 2016; Hood et al., 2006; Irwin et al., 2012).

A key characteristic differentiating cyanobacteria is whether the species can fix atmospheric nitrogen (N_2) into a more bioavailable form of nitrogen. This is called diazotrophy. This process involves breaking the triple bond in N_2 and converting it to ammonia. In many N-depleted environments, this cyanobacterial N-fixation plays an important role in adding to the pool of bioavailable N (Bauersachs et al., 2009). Nearly half the nitrogen fixation activity in the world is done by oceanic cyanobacteria (Galloway et al., 2004).

1.1.3 Theories of Causation of cHABs

The exact cause of cHABs has been a puzzle for ecologists. Historically, cHABs occurred annually in nutrient-rich, eutrophic environments. However, cHABs are increasingly reported in low-nutrient lakes, bays and reservoirs (Dodds et al., 2009; Verschoor et al., 2017). Many factors have been proposed to explain the occurrence of cHABs such as phosphorus and nitrogen loading and low mixing and flushing rates (Kane et al., 2014; Michalak et al., 2013; Paerl et al., 2011; Smith and Schindler, 2009).

With increasing lake temperatures, a focus has also been on studying the impacts of increasing water temperatures on the occurrence of HABs and the dominance of cHABs. Cyanobacteria grow at wider and warmer temperature range than other phytoplankton in lab conditions (Paerl et al., 2011).

Over the years of studying cHABs, the dominant hypothesis has been that increased loading of nitrogen and phosphorus is the driving force behind bloom proliferation (Kane et al., 2014; Elser et al., 1990; Schindler, 1974; Steel, 1971). However, as noted above, because some cyanobacteria taxa can fix atmospheric N, P is the limiting nutrient that controls the biomass in a bloom (Higgins et al., 2017; Schindler et al., 2008; Schindler, 1974, 1975). Current management practices and models are focused on P and/or N but overlook other factors that may help the cyanobacteria dominate (Schindler, 2006). Evidence has suggested that trace elements such as Co, and more importantly Fe, might play a crucial role in cHABs formation (Molot et al., 2014; Saito et al., 2004). The conceptual model of Molot et al. (2014) hypothesizes that phytoplankton biomass is controlled by N and P but cyanobacteria dominance is controlled by the availability of Fe(II) (Molot et al., 2014). When sediments are oxidized, cHABs do not occur (Molot et al., 2021).

1.2 Nutrients

1.2.1 Macronutrients

Macronutrients for phytoplankton are elements that are needed in relatively high abundance in order to live. These include elements such as: carbon (C), phosphorus (P), nitrogen (N), hydrogen (H), oxygen (O), potassium (K), sulfur (S), calcium (Ca), magnesium (Mg), silicon (Si), chloride (Cl) and sodium (Na) (Graham et al., 2016). These macronutrients play a myriad of roles and functions within a phytoplankton cell (see Table 1.1). If the nutrients are not enough, it results in deformity, lower growth rates, discolouration, stressed cells and possibly cell death (Barker et al., 2015).

Table 1.1: Macronutrients commonly needed by phytoplankton and some uses (Graham et al., 2016; Berg et al., 2002)

Element	Examples of Function or Location in Cell
C	building block
P	ATP, DNA, phospholipids
N	amino acids, nucleotides, chlorophyll, phycobilins
H	proton gradient, acid-base reactions
O	respiration
K	agar and carrageenan, osmotic regulation (ionic form), cofactor for many enzymes
S	some amino acids, nitrogenase, thylakoid lipids, CoA, carrageenan, agar, DMSP, biotin
Ca	alginates, calcium carbonate, calmodulin
Mg	chlorophyll
Si	diatom frustules, silicoflagellate skeletons, synurophyte scales and stomatocyst walls, walls of the ulvophyte Cladophora
Cl	oxygen production in photosynthesis, trichloroethylene, perchloroethylene
Na	nitrate reductase

1.2.1.1 Carbon

Carbon (C) is an essential building block of life as it is the subunit in all biomolecules. C can form long and strong bonds with itself (C-C bonds) and with a variety of other elements such as N, O, P, S, metals and many more (Burrows et al., 2017; Demming, 2010). Carbon containing molecules can be variable and stable which allows for life to exist. In freshwater systems, C exists as either dissolved inorganic carbon (DIC), dissolved organic carbon (DOC) or particulate organic carbon (POC). Most of the carbon in a lake is found in the particulate form (Einola et al., 2011).

DIC refers to C existing as a species of the carbonate buffer system: carbon dioxide, bicarbonate, carbonate or carbonic acid. The presence of DIC and light can determine instantaneous rates of photosynthesis and can impact phytoplankton growth and proliferation considerably. At an ecologically relevant pH, the concentration of HCO_3^- is greater than CO_2 (Graham et al., 2016).

$$CO_2 + H_2O \longrightarrow H_2CO_3 \rightleftharpoons HCO_3^- + H^+ \rightleftharpoons CO_3^{2-} + 2\,H^+ \tag{1.1}$$

Oxygenic photosynthesis is a key characteristic of almost all phytoplankton. Phytoplankton use light dependent oxidation of water (Eq. 1.2) to produce energy to carry out the light independent carbon fixation (Eq. 1.3) (Graham et al., 2016).

$$H_2O + NADP^+ + ADP + P_i \longrightarrow O_2 + ATP + NADPH \tag{1.2}$$

$$CO_2 + NADPH + ATP + H^+ \longrightarrow CH_2O + NADP^+ + H_2O + ADP + P_i \tag{1.3}$$

The light-dependent reaction (Eq. 1.2) harnesses solar energy through the photosystems (containing light-harnessing pigment molecules such as chlorophyll and phycocyanin) and oxidizes a H_2O molecule to generate the reducing power needed to reduce CO_2 by Rubisco enzyme. The light-independent reaction (Eq. 1.3) uses the reducing power generated from the light-dependent reaction (NADPH and ATP) to generate carbohydrates (CH_2O). This is done by the enzyme Rubisco, which has Mg cofactors (shown in green within Fig. 1.1) (Taylor et al., 2001).

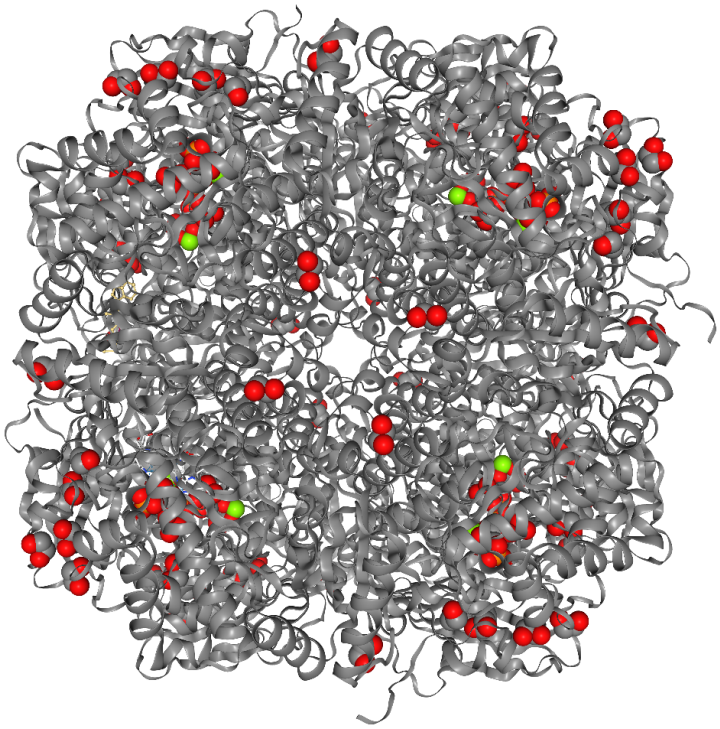

Figure 1.1: Structure of Rubisco from *Chlamydomonas reinhardtii*. Mg cofactors are green (Taylor et al., 2001)

Phytoplankton have carbon concentrating mechanisms (CCMs) to keep rates of

photosynthesis high as when environmental concentrations of CO_2 are low at commonly found pH of freshwater systems. To increase intracellular concentrations of CO_2, phytoplankton store HCO_3^- by converting it to CO_2 using the enzyme carbonic anhydrase to catalyze the conversion (Graham et al., 2016; Falkowski and Raven, 2007). Carbonic anhydrase is known to have metallic cofactors, most commonly Zn but Cd and Co can also be found (Graham et al., 2016; Suzuki et al., 2011) (shown in light purple within Fig. 1.2).

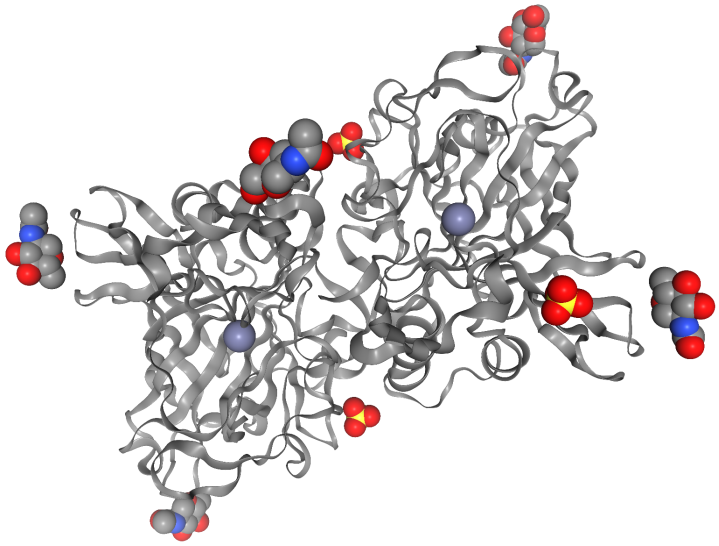

Figure 1.2: Structure of carbonic anhydrase from *Chlamydomonas reinhardtii* (Suzuki et al., 2011)

Another form in which C is found within a freshwater system is DOC or dissolved organic matter (DOM). DOC and DOM are terms used to describe C-based molecules. This can include small molecules such as free-floating amino acids or those as large as humic acids, which have multiple large subunits as parts of their structures (Leenheer and Croué, 2003). DOC that can be derived from terrestrial sources (allochthonous) or be from in-lake processes (autochthonous)(Williamson et al., 1999). DOC can be a source of nutrition for life living in the lake, but it can also be lost to sedimentation, photodegradation or exported out of the lake through outflows downstream (Hanson et al., 2011). DOM has the ability to bind to metals and introduce bioavailable micronutrients to a lake (Creed et al., 2018).

1.2.1.2 Phosphorus

Phosphorus (P) is also an essential building block element for all organisms. It forms important biomolecules such as nucleic acids, phospholipids and adenosine triphosphate (ATP) which acts as an important energy currency in cellular reactions (see Eqs. 1.2 and 1.3 for examples) (Van Mooy et al., 2009; Knowles, 1980). As with all organisms, P plays a key role in phytoplankton physiology and growth. In temperate lakes, chlorophyll *A* (ChlA) is related to total P as a positive log-linear function (Filstrup and Downing, 2017). The relationship of increased P-availability increase risk of occurrence of cHABs is known (Downing et al., 2001). This directly ties P concentrations to algal biomass, showing the importance of P as a nutrient in algal growth.

P is available to phytoplankton through internal and external sources. P is absorbed by plants on the land through various mechanisms that involve uptake of free P from the soil, which is rare. Dead biomass decomposed by bacteria can make more P available to plants and also enhanced release of P from soil apatites by oxalic acid-producing mycorrhizal fungi can make P more bioavailable for plants (Smil, 2000). P from the terrestrial environment enters the aquatic system much like DOC, as dissolved organic phosphate (DOP). Terrestrial inputs such as decaying biomass, or animal waste contain significant amounts of P (Khan and Ansari, 2005).

Once in the lake, P can go through many forms and many phases. It can precipitate out of the water column as an insoluble mineral or be absorbed by aquatic life and incorporated in to the biomass (Orihel et al., 2017). Once the mineral settles, or the biomass dies and settles, the P is part of the sediment. Anoxia at the sediment-water-interface can cause particulate P to solubilize and diffuse into the water column and become available for the biota once more. This is called "internal loading" of P (Orihel et al., 2017; Khan and Ansari, 2005; Molot et al., 2014). Internal P loading can be done through various other ways such as hydrolysis of organic matter, desorption of P from molecules or minerals, dissociation of P from humic complexes or through resuspension of solid P (Orihel et al., 2017).

During the 1970s, laws and policies such as the Canada-USA Great Lakes Water

Quality Agreement were put into effect to curb the impacts of eutrophication due to high P loading of the 1960s/early 1970s (Pick, 2016; Dolan and McGunagle, 2005). While P loading has been at or below target levels, release of legacy P from the sediments still poses a challenge for managers and policy makers to mitigate the occurrences of HABs (Schindler, 2012).

1.2.1.3 Nitrogen

Nitrogen is used to make proteins, nucleic acids, photosynthetic pigments and other molecules. In most cases, NO_3^- and NH_4^+ are imported into the cell from the environment, but some algal species have been known to import small amides (like acetamide), amino acids and urea as well (Graham et al., 2016). Phytoplankton prefer to use NH_4^+ because it can be directly used as a substrate in the synthesis of biomolecules.

Phytoplankton can use the enzyme nitrate reductase, to convert NO_3^- back to NO_2^- within the cell which then gets further reduced to NH_4^+ using the enzyme nitrite reductase. This process of nitrate assimilation is a Fe and Mo cofactor dependent process (Graham et al., 2016; Ullrich, 1983). This ammonium is then used for biosynthesis for necessary molecules.

Nitrogen Fixation Nitrogen makes up 78% of the atmosphere, but the N_2 gas form is unusable for many organisms (Wallace and Hobbs, 2006). There are three ways in which this nitrogen gas can become bioavailable.

The first is by the energy of a lightning strike that would split N_2 into two radical and those individual N-radicals would then react with the O present in the air and form NO_x. This would further react to form water soluble HNO_3^- which is usable by organisms (Hill et al., 1980; Tuck, 1976).

Some cyanobacteria can fix atmospheric N_2 through an energy-intensive metabolic process called diazotrophy. This gives these cyanobacteria a competitive edge over other organisms in N-limited waters (Graham et al., 2016). The reaction of biological N-

fixation is:

$$N_2 + 16\,ATP + 8\,e^- + 8\,H^+ \longrightarrow 2\,NH_3 + H_2 + 16\,ADP + 16\,P_i \tag{1.4}$$

The reaction is carried out by the nitrogenase enzyme (see Fig. 1.3). Nitrogenase has two sets of dimeric proteins that join and form the tetramer and it contains metallic cofactors of Fe and Mo, (shown in orange and teal in Fig. 1.3) (Schindelin et al., 1997). The widespread use of synthetic nitrogenous fertilizers, produced via the Haber-Bosch process resulted in record crop yields, but this reactive N is now one of the largest sources of NO_3^- to aquatic systems (Sutton and Bleeker, 2013; Farrar et al., 2014; Braun, 2007).

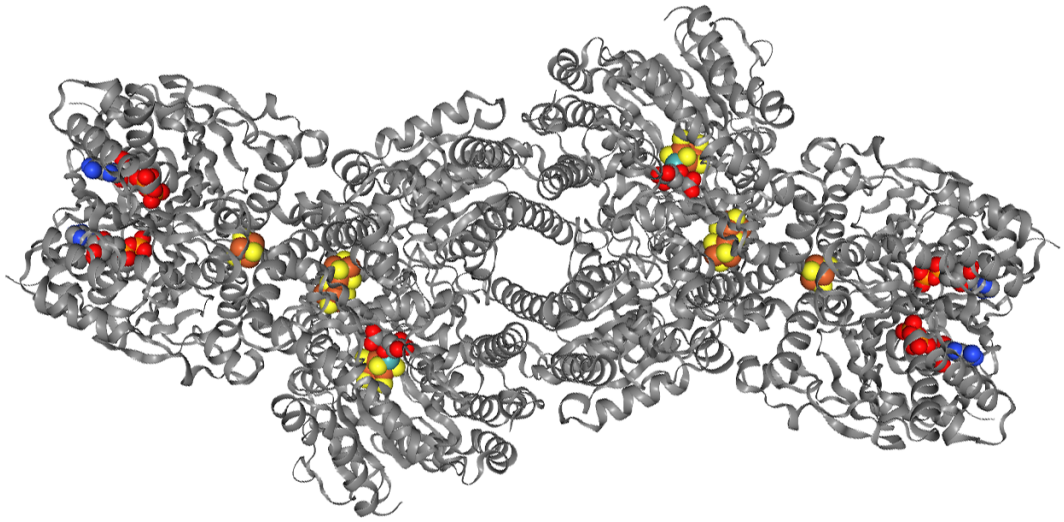

Figure 1.3: Structure of nitrogenase from *Azotobacter vinelandii* (Schindelin et al., 1997)

Heterocyst Differentiation Nitrogenase is an oxygen-sensitive enzyme that is deactivated by the presence of oxygen (Kangatharalingam et al., 1992). To control this, filamentous cyanobacteria such as *Anabaena* and *Aphanizomenon* create specialized cells called heterocysts to house the nitrogen fixation machinery separate from vegetative cells which photosynthesize (Chaurasia and Apte, 2011). Heterocyst differentiation is a complex process which can classified into four phases: induction, patterning, commitment and morphogenesis (see Fig. 1.4) (Videau et al., 2016).

Heterocyst differentiation is triggered by nitrogen starvation and the resulting

synthesis of the global nitrogen regulator, NtcA protein (Harish and Seth, 2020). In addition to heterocyst differentiation, NtcA is needed to express genes used in ammonium and nitrate assimilation. NtcA mutant strains are unable to grow without nitrate being made available, and heterocyst differentiation is never initiated (Kumar et al., 2010). NtcA activation in low nitrogen environment initiates the synthesis of HetR, a specific master regulator for the production of hetercoysts (Harish and Seth, 2020).

Once HetR is activated, proteolysis within the protoheterocysts increase and so does the expression of HetP and PatS (Wolk, 1996; Harish and Seth, 2020). HetR upregulates the expression of its own inhibitor, PatS. PatS will move laterally along the filament to inhibit HetR in cells that are to remain vegetative. Other pattern determining proteins in the Pat-family are also involved in this process (Xu et al., 2020; Thiel, 2005).

HetR also upregulates the expression of HetP which upregulates the expression of key genes in pathways that cause physiological changes that form the heterocysts. HetP is thought to be the involved in the commitment of the cell to irreversibly turn it into a heterocyst (Harish and Seth, 2020).

Heterocysts are very different from vegetative cells in physiology. During morphogenisis, protoheterocysts undergo a variety of changes to make the make the cell environment microoxic, in order to maximize nitrogenase efficiency. These changes include the development of a characteristic multilayer envelope made of specialized glycolipids (Hgl) and polysaccharaides (Hep) for hetercoysts, the creation of narrow junctions to adjacent vegetative cells for nutrient transfer and the rearrangement of the intracellular membrane system (Pernil and Schleiff, 2019; Kumar et al., 2010).

Respiration is enhanced to maintain low O_2 levels. Reductants needed for nitrogenase and respiration are produced via photosynthesis in vegetative cells and transferred to heterocysts (Wolk, 1996). The activity of oxygen-generating photosystem II (PSII) is deactivated during morphogenisis as is the ability for the cell to divide (Zhao and Wolk, 2008). Nitrogenase, glutamine synthase and hydrogenase synthesis is promoted by NtcA and occurs late in the differentiation process (18 - 24 hours) (Kumar et al., 2010).

Heterocysts have many metalloproteins within them, chief amongst them being

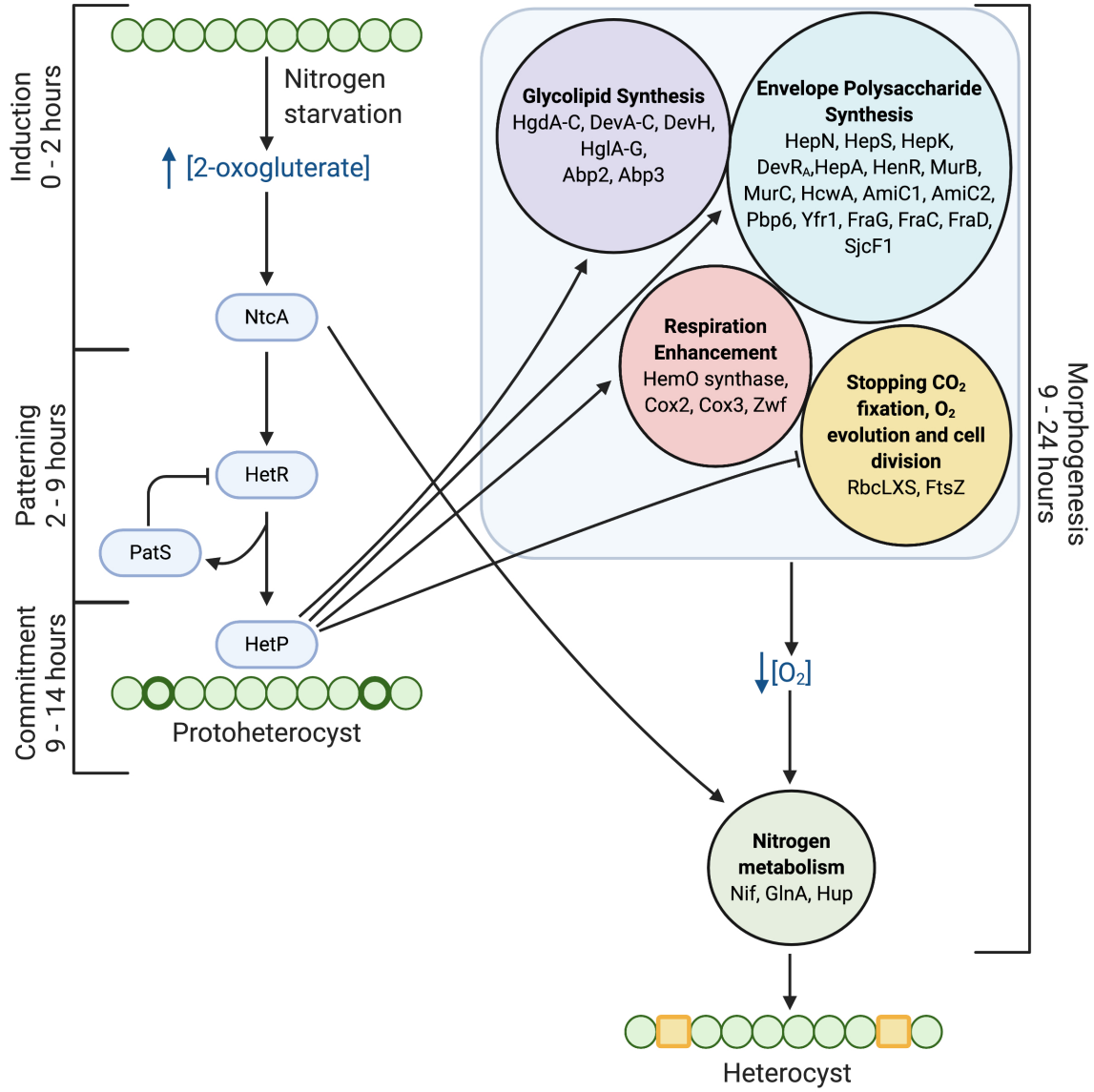

Figure 1.4: Stages of heterocyst differentiation. This model shows a simplified view of the some of the genetic and proteomic machinery involved in heterocyst formation. The temporal divisions are shown on the side. Arrows indicate activation and T-bars represent deactivation or inhibition. Not all regulatory relationships are shown for simplicity. Image adapted from Zhao and Wolk (2008); Thiel (2005); Qiu (2018); Harish and Seth (2020)

nitrogenase which needs iron and molybdenum. Other metalloenzymes in the heterocysts are known and need elements such as Fe, Cu, Mo, Ni, Mn, V, and Zn (Pernil and Schleiff, 2019).

1.2.2 Micronutrients

Micronutrients for phytoplankton are elements that are needed only in small amounts. These include elements such as: iron (Fe), cobalt (Co), molybdenum (Mo), zinc

Table 1.2: Micronutrients commonly needed by phytoplankton and some uses (Graham et al., 2016)

Element	Examples of Function or Location in Cell
Fe	ferredoxin, cytochromes, nitrogenase, nitrate and nitrite reductase, catalase, glutamate synthetase, superoxide dismutase cofactor
Co	vitamin B_{12}
Mo	nitrate reductase, nitrogenase
Mn	oxygen-evolving complex of photosystem II, superoxide dismutase
Zn	carbonic anhydrase, alcohol dehydrogenase, glutamic dehydrogenase
Cu	plastocyanin, cytochrome oxidase
V	bromoperoxidase, some nitrogenases
Br or I	halogenated compounds with antimicrobial, anti-herbivore, or allelopathic functions

(Zn), copper (Cu), manganese (Mn), boron (B), vanadium (V), bromine (Br) or iodine (I) (Graham et al., 2016). As noted with examples above, many of these micronutrients serve as important cofactors within enzymes of phytoplankton (see Table 1.2). Without these cofactors important reactions will not occur at the rate needed to sustain life.

Approximately 40% of over 1300 enzymes with known structures require a metal cofactor. This ranges from 36% to 59% in the different classes of enzymes as shown in Fig. 1.5 (Andreini et al., 2008). Enrichment of eutrophic lakes in New Zealand with B, Co, Cu or Mo increased primary productivity in lakes by 40% (Downs et al., 2008) suggesting the potential for micronutrient limitation in watersheds with low micronutrient geology.

1.2.2.1 Iron

Fe is considered so important for cellular growth that some consider it to be a macronutrient (Goldman, 1966). Fe, specifically Fe(II), is thought to be very important to biological activity is because dissolved Fe(II) was more prevalent in the primordial anoxic waters than it is today when cyanobacteria evolved (Wilhelm, 1995). This led to the dependence on Fe for many biological activities like intracellular redox chemistry (Graham et al., 2016). An abiotic chemical reaction network has been described that is promoted by Fe(II) in which pyruvate and glyoxylate build 9 of the 11 intermediates

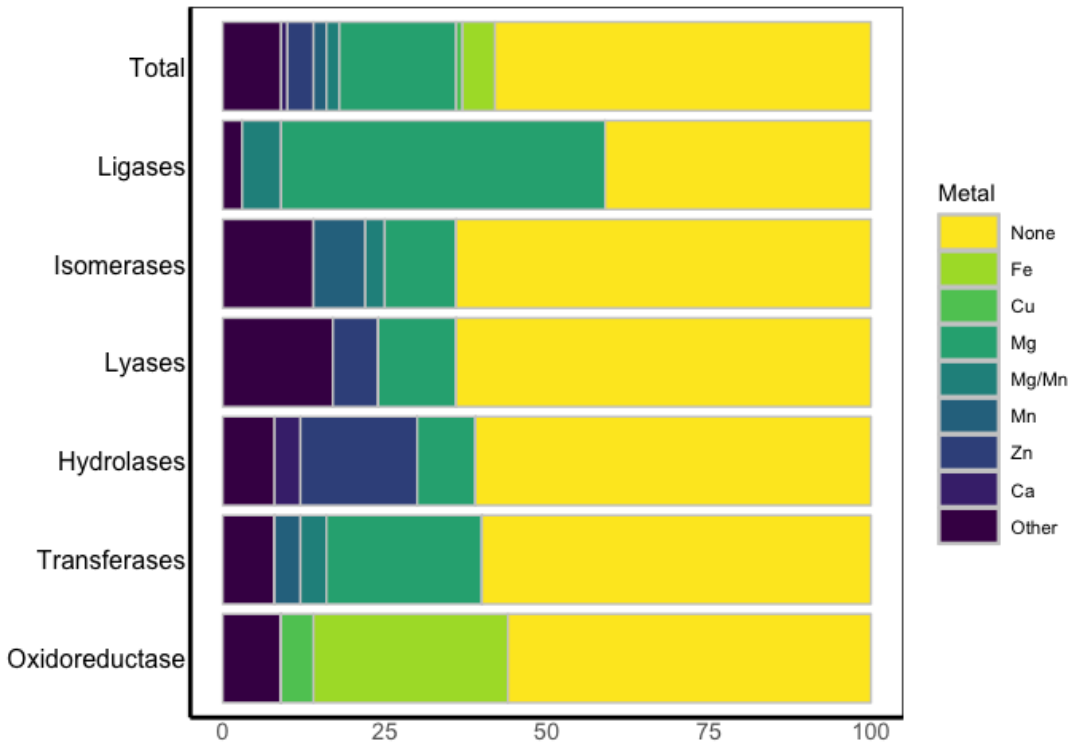

Figure 1.5: Relative occurrences of metallic cofactors in six enzymatic classes. Number of enzyme structures examined: Total = 1371, Ligases = 63, Isomerases = 71, Hydrolases = 432, Transferases = 365 and Oxidoreductases = 310. Figure adapted from Andreini et al. (2008)

of the Krebs cycle. This Fe(II) promoted reaction network resembles and overlaps with Krebs and glyoxylate cycles and may represent an ancient, prebiotic precursor to the reactions of the essential metabolic pathways (Muchowska et al., 2019). Fe is found as the centre of metalloproteins that carry out the many redox reactions in a cell. These proteins function in important electron transfer pathways such as cellular respiration and photosynthesis which release and generate energy in cells. Other biological processes that Fe is a part of are reduction of a substrate by adding H_2, hydrogenation and nitrogen fixation (see Fig. 1.6) (Kendall et al., 2012; Shi et al., 2007).

The model proposed by Molot et al. (2014, 2021) points to the evidence that cyanobacteria have a higher requirement for Fe than their eukaryotic counterparts and are also unable to transport Fe(III) through their cell member (Molot et al., 2010, 2014; Kranzler et al., 2014). This suggests that while factors like macronutrient concentrations might play a role in controlling the biomass in the bloom, the cyanobacterial dominance

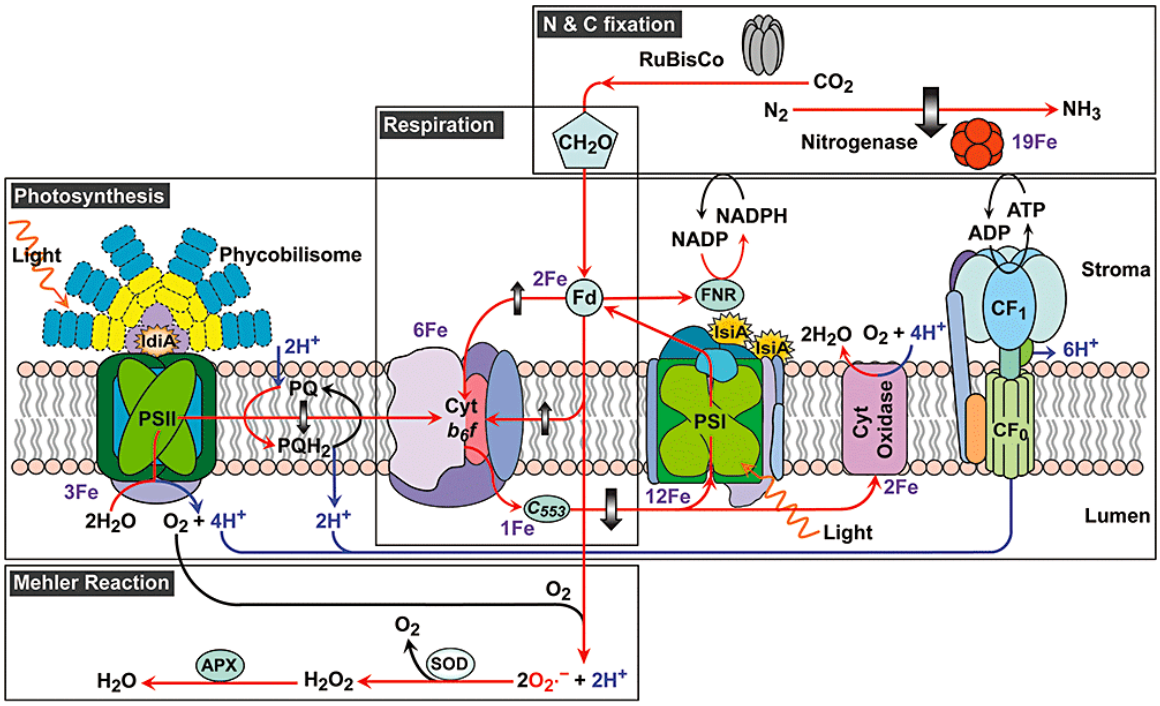

Figure 1.6: Schematic model of Fe-included metabolic pathways; photosynthesis, nitrogen fixation, respiration and Mehler reaction pathways in *Trichodesmium erythraeum*. Red arrows, electron transport; blue arrows, proton transport (Shi et al., 2007).

is determined by the availability of Fe(II), which in turn is controlled by the extent of sediment anoxia, specifically sediment redox which controls internal Fe(II) loading (Molot et al., 2014, 2021). Determining the sources of Fe(II) and how Fe is used by phytoplankton is a challenge because in oxygenated water Fe(II) is quickly converted to Fe(III), resulting in quick removal of Fe(II) unless the Fe(II) is chelated to DOM (Verschoor and Molot, 2013).

1.2.2.2 Cobalt

Co is an important micronutrient for cyanobacteria. Its role as a cofactor in key molecules such as vitamin B_{12} make it significant to cyanobacterial growth and function (Goldman, 1966). More than 150 species of phytoplankton have an obligate need for exogenous vitamin B_{12} which suggests that supply of cobalt-containing vitamin B_{12} could play a role in determining which species out competes others when conditions are ripe for a bloom to occur (Croft et al., 2006).

Co behaves much like Fe in the water column, both exist in very low concentrations

in oxic waters and have similar redox states (Co (II) or Co (III)) with the Co (III) state being insoluble. Co has been known to be able to be replaced or replace other metallic cofactors such as, Zn and Cd, when nutrients are limited. This complicating factor makes studying Co biogeochemistry very difficult (Saito et al., 2004). It has been found that increasing Co concentrations led to an increase in photosynthetic activity and increased rates of N-fixation in cyanobacteria (Goldman, 1966; Granéli and Haraldsson, 1993; Holm-Hansen et al., 1954; Iswaran and Rao, 1964; Hallsworth et al., 1960; Kelly et al., 2021). These studies show ample evidence that Co is important for cyanobacterial growth, but there is no clear picture of the mechanism yet.

1.3 Cell Culture

Cell culture is a common technique for understanding how organisms behave while still being able to keep controls on the conditions of the experiment. Culture studies are advantageous in terms of costs, ease of control and manipulation and volumes of media required (Andersen, 2005). The significant disadvantage to using cell cultures is that organisms may not behave the same way they would in the environment. In addition, changes in cell morphology or changes in function have been observed (de Figueiredo et al., 2011). However, cell cultures are an important step in understanding the complex phenomena observed in the environment because of the control they offer.

The objectives of this thesis were met by studying cultures of phytoplankton obtained from a variety of different sources. Some cultures were purchased from the Canadian Phycological Culture Centre (CPCC) (Waterloo, ON), Pasteur Culture Collection of Cyanobacteria (PCC) (France), Sammlung von Algenkulturen at the University of Göttingen (SAG) (Germany) and the Microbial Culture Collection at the National Institute for Environmental Studies (NIES) (Japan). Some cultures were lake water isolates from IISD Experimental Lake Area (ELA) lakes and some isolates from other lakes were provided by Dr. Arthur Zastepa at Environment and Climate Change Canada (ECCC) (Burlington, ON) (see Table 1.3).

Table 1.3: Species and characteristics of phytoplankton studied

Organism	Type	N-Fixer?	Source
Anabaena flos-aqaue	Cyanobacteria	N-Fixing	CPCC 67
Aphanizomenon flos-aqaue	Cyanobacteria	N-Fixing	NIES 81
Coelastrum proboscideum	Eukaryotic Algae		SAG 217-2
Chlorella vulgaris	Eukaryotic Algae		CPCC 90
Chlamydomonas reinhardtii	Eukaryotic Algae		CPCC 243
Microcystis aeruginosa	Cyanobacteria		PCC 7005
Dolichospermum lemmermanii	Cyanobacteria	N-Fixing	Lake Erie (ECCC)
Aphanizomenon skuja	Cyanobacteria	N-Fixing	Lake 227 (ECCC)
Dictyosphaerium pulchellum	Eukaryotic Algae		Lake 227 (ELA)

1.4 Growth Kinetics

Every population has different characteristics, for example how mobile it can be or how it occupies the space in which it is located. The growth of a population, in numbers and in density, is a way to characterize different populations. Phytoplankton, along with many organisms as a logistic growth curve. Growth rates are essential to studying different population dynamics. Growth rate is defined as the net rate of change in biomass (see Eq. 1.5) (Graham et al., 2016).

$$rN = \frac{dN}{dt} \tag{1.5}$$

dN/dt represent the change in biomass over a unit of time. This represents the population growth rate, or gross growth rate. This change is equal to r (net growth rate) multiplied by the biomass, N. We can further isolate r by dividing both sides of Eq. 1.5 by N.

$$r = \frac{\frac{dN}{dt}}{N} \tag{1.6}$$

$$r = \mu - \lambda \tag{1.7}$$

where μ represents the gross growth rate and λ represents the death rate. If the differential equation in Eq. 1.5 is solved, it results in a exponential equation.

$$N = N_o e^{rt} \tag{1.8}$$

According to Eq. 1.8, a population will grow indefinitely, which is not realistic. Therefore an upper limit called the "carrying capacity," K which is equal to max N, was introduced, thus making the growth model have an end.

$$\frac{dN}{dt} = rN\frac{(K-N)}{K} \tag{1.9}$$

In this equation K has the same units as N (biomass/volume).

1.4.1 Growth and Nutrient Uptake

The Monod growth model considers that population growth is a function of nutrient concentration and follows similarly to the Michaelis-Menten equation (Graham et al., 2016).

$$\mu = \mu_{max}\frac{S}{K_S + S} \tag{1.10}$$

In this equation, S is the concentration of the substrate of interest, μ is the growth rate, μ_{max} is maximum rate of reproduction and K_S is the half-saturation constant for growth as a function of S (Monod, 1950; Owens and Legan, 1987). The initial slope of the Monod curve is given by μ_{max}/K_S which is a relative indicator of competitive ability at low substrate concentration (Molot and Brown, 1986).

The minimal concentration of substrate needed to commence all growth is defined as the "nutrient threshold concentration," below this concentration, no growth will occur and in a Monod growth model, it may look like negative growth or no growth (see Fig. 1.7) (Jiang et al., 2019). The Monod equation (Eq. 1.10), can be modified to include the threshold concentration ($S_{Threshold}$) (see Eq. 1.11) (Kilham, 1975; Jiang et al., 2019).

$$\mu = \mu_{max}\frac{S - S_{Threshold}}{K_S + S - S_{Threshold}} \tag{1.11}$$

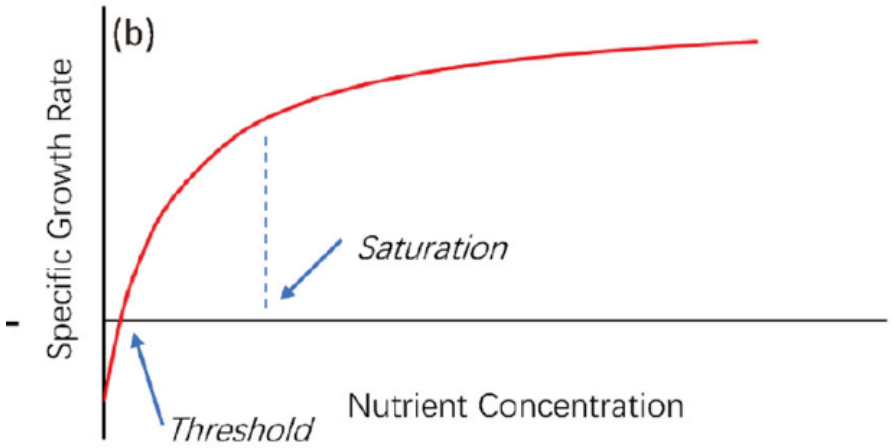

Figure 1.7: Indication of threshold concentration on Monod growth curve (Jiang et al., 2019)

1.5 Stable Isotopes

Stable isotopes are a form of an element which have a different atomic mass. They exist in nature in more numbers than radioactive isotopes. For example, carbon has two stable isotopes ^{12}C and ^{13}C and nitrogen has ^{14}N and ^{15}N. Likewise, iron has four stable isotopes: ^{54}Fe (5.85% abundant), ^{56}Fe (91.75% abundant), ^{57}Fe (2.12% abundant) and ^{58}Fe (0.28% abundant) (Sheftel et al., 2018). The δ^{56}Fe is the deviation of the ^{56}Fe/^{54}Fe ratio present in a sample from a standard (IRMM-014) and is reported as δ in units per mil (‰) (Coplen, 2011). Isotopic fractionation factors (δ) are defined as the ratio of isotopic composition of the same element between substances (Coplen, 2011). They are useful in understanding how different processes change the isotopic composition of a sample. Fractionation factors for common processes are known and by observing δ in different pools, a better idea of what processes are occurring can be gleaned. Processes such as nitrogen fixation by cyanobacterial cultures have a been shown to have a fractionation factor of $2 - 3‰$ of δ^{15}N while nitrate utilization has been shown to have a fractionation factor of $4 - 19‰$ of δ^{15}N (Bauersachs et al., 2009). Fractionation processes of other processes are known, however, the fractionation of Fe during phytoplankton uptake of Fe is unknown.

δ^{56}Fe can be used as a tool to track sources and cycling of Fe in freshwater systems.

Processes, both biotic and abiotic, can fractionate Fe isotopes and isotopic fractionation have been associated with redox changes (Johnson et al., 2008; Johnson and Beard, 2006; Wu et al., 2011). Fe isotopes have been used to study biogeochemical processes in oceans, rivers and groundwater (Fehr et al., 2008; Bergquist and Boyle, 2006; Teutsch et al., 2005). Not many studies have been done on freshwater systems, and most of them have been in environments containing high Fe concentrations, which are rare (Schiff et al., 2017). Thus, using stable isotopes of Fe to study lake Fe-cycling and its impacts on cyanobacterial dominance is novel.

1.6 Lake 227

This research is part of a larger project to understand iron cycling in Lake 227, located at ELA. ELA is a natural laboratory of 58 lakes and their watersheds located in northwestern Ontario near Kenora, ON. Lake 227 is a purposely eutrophied lake and the data set of different chemical and biological parameters of Lake 227 spans 50 years. Since 1969, N (as nitrate) and P (as phosphate) have been added to Lake 227 at different ratios during the ice-free season. From 1969 to 1974 the N:P ratio was 27:1 (a P-limited system), from 1975 to 1989 the ratio was lowered to 9:1 (a somewhat N-limited system) and from 1990 to present, only P has been added (a N-limited system) (Findlay et al., 1994).

Throughout the years, phytoplankton species have been enumerated and tracked. With varying nutrient input regimes, the composition of the phytoplankton too has changed (see Fig 1.8). At present, the seasonal pattern of phytoplankton is an early season N-fixing bloom of *Aphanizomenon skuja* followed by a later season bloom of eukaryotic chlorophytes after the crash of the *Aphanizomenon* bloom (Schindler et al., 2008).

Based on previous work, δ^{56}Fe in Lake 227 has been found to span the known range of δ^{56}Fe, with significant differences in different parts and phases of the lake (see Fig 1.9) (Schiff et al., 2017). Given this data set and history of experimentation and understanding of the system, Lake 227 is an ideal model system for this work.

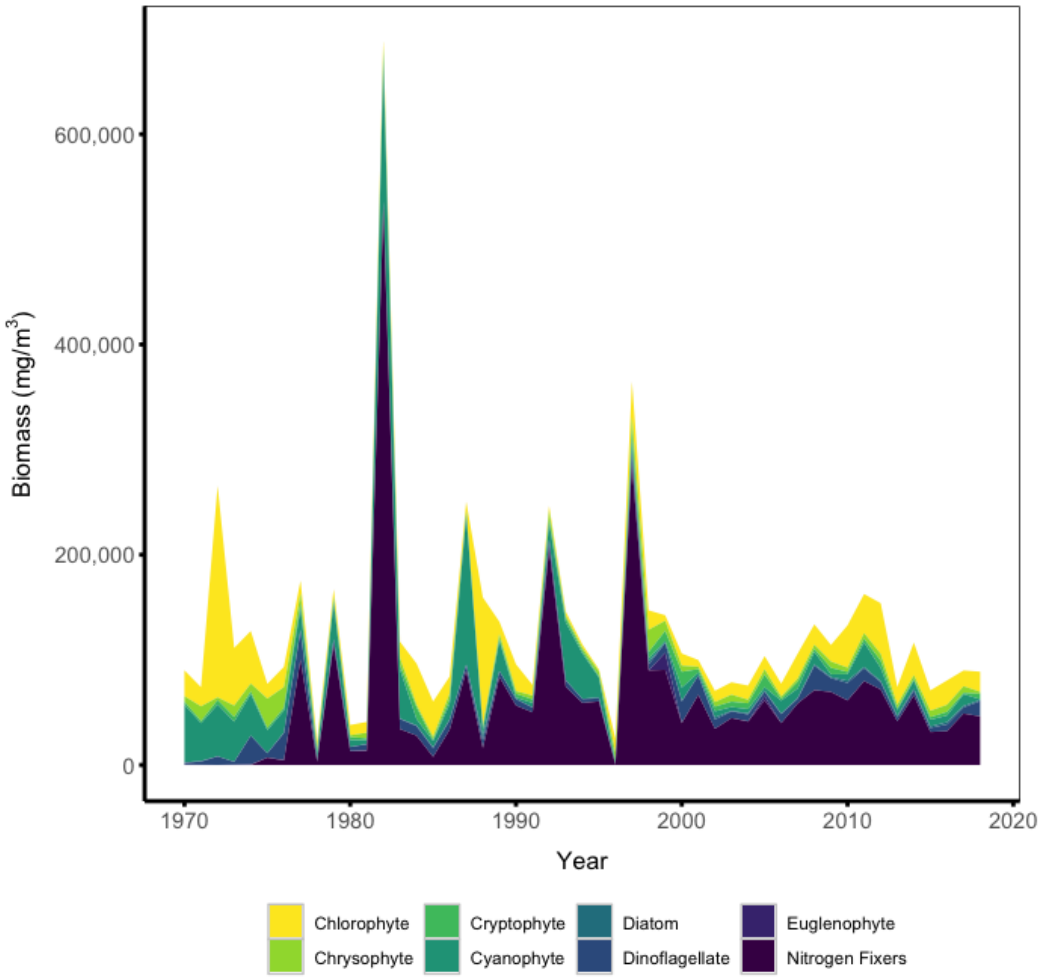

Figure 1.8: Epilimnetic phytoplankton community composition of Lake 227 from 1970 to 2018 adapted from Schindler et al. (2008) and extended with data provided from IISD-ELA. Cyanophyte refers to non N-fixing cyanobacterial species.

1.7 Objectives

The objectives of this thesis are:

1. To determine the Fe threshold concentrations of different taxa of phytoplankton. This will characterize the growth kinetics of different phytoplankton taxa at low Fe concentrations. Differences in growth kinetics and threshold concentrations can inform on which species might become dominant, even in low Fe environments and if Fe requirements change in N-fixing conditions.
2. To determine a new model of determining the isotopic composition and fractionation factors of newly accumulated biomass between two sampling

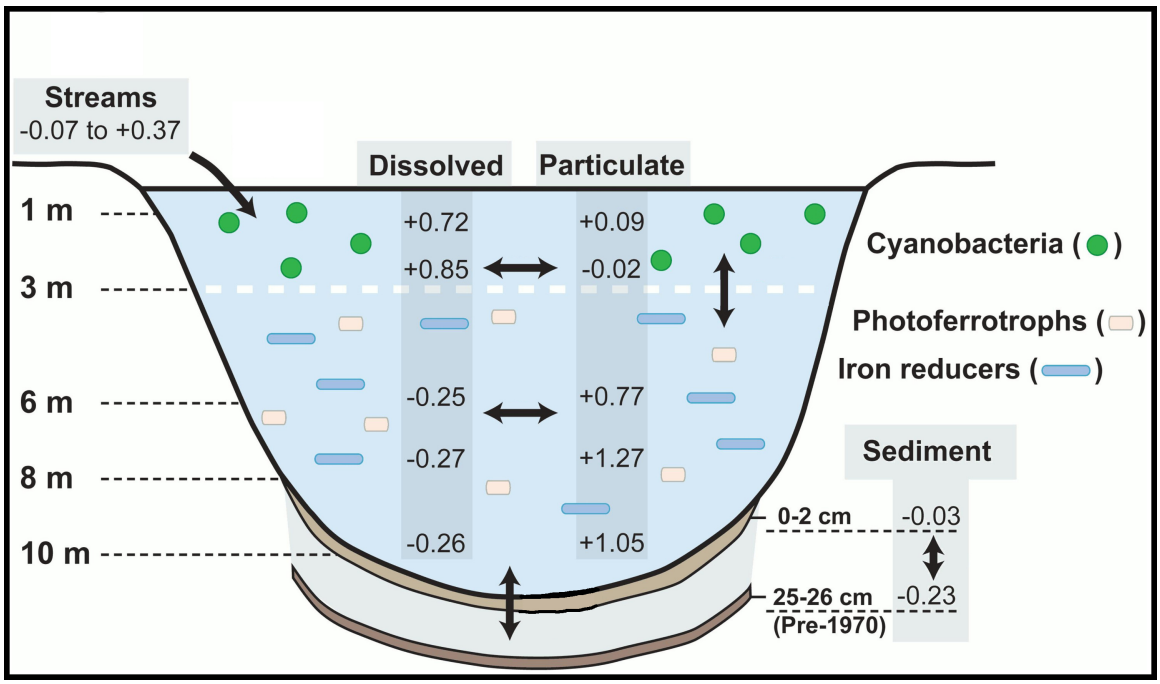

Figure 1.9: Natural abundance of Fe isotopes in Lake 227

events from the bulk sample. This will aim to help understand how isotopic composition and fractionation differ during growth of phytoplankton and make relationships and correlations to better understand the growth dynamics of phytoplankton in the environment.

3. To determine if cyanobacterial growth can be prevented in culture by adding a Fe(II) specific chelator. This will help inform on possible Fe(II) removal strategies for freshwater systems to mitigate cHABs.

4. To determine the relative strength of ferrozine (FZ) as a potential Fe chelator to ethylenediaminetetraacetic acid (EDTA) or citrate. This will help determine if the formation of the Fe:FZ complex can be impacted by EDTA or citrate under certain conditions.

5. to determine if Co plays a role in heterocyst formation of N-fixing cyanobacteria. This will fill a gap in the understanding of the role of Co as a cofactor in cyanobacterial cells.

6. To propose an alternative proxy to measuring algal cell culture growth to absorbance (abs) using a smartphone app and items found easily.

Chapter 2

Threshold Concentrations and Transport Affinity of Iron By Various Freshwater Phytoplankton

Abstract

Harmful algal blooms are an ever-increasing problem in many waterways and waterbodies in Canada and around the world. Many policies have focused on lowering phosphorus inputs to waters to curb the growth of algal blooms which cause damages to industries such as fishing and tourism. However, even with decreasing phosphorus inputs into rivers and lakes, the reported occurrences of harmful algal blooms are increasing. Are there other nutrients in play along with phosphorus in the growth and proliferation of algal blooms? Here, we quantify the ability of seven different phytoplankton taxa to grow at low initial total dissolved Fe concentrations and determined that N-fixing cyanobacteria in N-replete conditions have the lowest iron threshold (below which growth ceases) at 76 ± 2pM, green algae have a mean iron threshold of 245 ± 5pM, the non-fixer *Microcystis aeruginosa* has a threshold of 663 ± 17pM, and N-fixing cyanobacteria that are grown without nitrate have a mean iron threshold of 736 ± 17pM. Furthermore, growth rates at low Fe varied almost 7-fold. These results show that low

iron concentrations can potentially play a role in determining which species is dominant as we did not find that the Fe_T patterns hold the same at low Fe concentrations. At low Fe, the non-fixer *Microcystis aeruginosa* had the highest initial slope in a plot of uptake vs Fe concentration, followed by N-fixing cyanobacteria in N-replete conditions, then N-fixing cyanobacteria that are grown without nitrate and finally eukaryotic algae. These initial slopes indicate relative competitiveness of these species at low Fe concentrations, if their threshold concentrations are exceeded.

2.1 Introduction

Harmful algal blooms are an increasing problem in freshwaters over the world (Huisman et al., 2018). Phytoplankton are diverse organisms. They include a variety of different genera and phyla and are found in almost any environment (Simon et al., 2009; Padisák et al., 2016). HABs can make aquatic toxins, foul taste and odour compounds and millions of dollars in economic damages (Downing et al., 2001; Wolf et al., 2017). Developing a management plan and targets of nutrient loading is essential for restoring systems. We can make realistic and attainable management plans if we understand the relationship between increasing nutrient concentrations and a species' growth. Previous work has focused on the limitation of available N and P to stop the formation of algal blooms (Schindler, 1974, 1975), however the problem of HABs still persists and is growing. We have increasingly found HABs in oligotrophic lakes, bays and reservoirs (Verschoor et al., 2017; Winter et al., 2011).

Iron is an important micronutrient for the growth and proliferation of phytoplankton. Fe is used in major biochemical pathways within the cell such as cellular respiration, photosynthesis and N-fixation (Shi et al., 2007). Abiotic reaction networks that represent an ancient prebiotic precursor to life is promoted by Fe(II), indicating the importance of Fe in chemistry which is necessary for life (Muchowska et al., 2019). Fe is found as a co-factor in approximately 30% of known enzymes used in redox reactions in the cell (Andreini et al., 2008). We also know that cyanobacteria have a higher requirement for

Fe and that they are very depended on transport of Fe(II) (Molot et al., 2014, 2021). However, we do not yet know the threshold concentrations of Fe needed for the growth of phytoplankton. Previous work with N and P have demonstrated that using the Monod model to find threshold concentrations could lead to realistic management goals (Xu et al., 2015; Jiang et al., 2019).

Previous studies have shown that cyanobacteria need more iron than their eukaryotic counterparts yet we have not quantified the iron thresholds needed to begin growing in cell cultures (Sunda and Huntsman, 2015; Molot et al., 2014). Kilham (1975) and Jiang et al. (2019) have used similar equations as Eq. 2.1 to find the nutrient thresholds for Si, N and P for algal growth and Braddock et al. (1984) have found Fe growth thresholds for *Thiobacillus ferrooxidans*.

The relationship between nutrient concentration and specific growth rate of a species (μ) is non-linear. Establishing nutrient thresholds, the concentration of nutrient below which growth does not occur, can be an effective way for mitigating and preventing cHABs formation (Xu et al., 2015). The conventional method of establishing the threshold concentrations is using the Monod model (Monod, 1950; Williams et al., 2016; Xu et al., 2015). The Monod model is used to characterize the relationship between the growth rate of a population and the concentration of a nutrient being studied (Monod, 1950). This model can be modified to find the nutrient thresholds for a species as described in Eq. 2.1 (Kilham, 1975; Jiang et al., 2019).

$$\mu = \mu_{max} \frac{Conc_{Fe} - Fe_T}{K_{Fe} + Conc_{Fe} - Fe_T} \tag{2.1}$$

Where μ is the specific growth rate, μ_{max} is the maximum specific growth rate of the species, $Conc_{Fe}$ is the concentration of Fe, Fe_T is the threshold concentration of Fe and $K_{Fe} + Fe_T$ is the half-velocity constant which is the concentration of Fe when the μ is half of μ_{max}. Eq. 2.1 is the same is Eq. 1.11 but the variables are changed to better describe the experiment. The initial slope, $\mu_{max}/(K_{Fe}\text{-}Fe_T)$ (modified from Molot and Brown (1986)), gives the relative growth ability at low substrate rates. This slope is an important predictor of competition outcomes of various taxa at low concentrations of a certain

nutrient where a higher initial slope indicates a higher growth rate at low concentrations (Molot and Brown, 1986).

The objective of this paper is to quantify the threshold concentrations of Fe for seven common temperate freshwater phyto- plankton taxa to gain insight into why certain taxa become dominant, even in low Fe conditions and to use these values to make better management decisions for impaired waters.

2.2 Materials and Methods

2.2.1 Experimental Organisms and Growth Conditions

We obtained algal cultures of *Anabaena flos-aqaue* (CPCC 67), *Aphanizomenon skuja* (Lake 227), *Microcystis aeruginosa* (PCC 7005), *Chlamydomonas reinhardtii* (CPCC 243) and *Chlorella vulgaris* (CPCC 90) from various sources as listed in Table 1.3. These phytoplankton were grown at 20°C on a 12:12h light/dark cycle at 100 $\mu mol/m^2$/s in either Blue-Green Medium Num. 11 (BG-11) for the cyanobacteria, or Bold's Basal Medium (modified) (BBM), for the chlorophytes, containing no Fe and an equivalent amount of Co as $CoSO_4$ instead of $Co(NO_3)_2$ (Rippka et al., 1979; Stein et al., 1973). *Anabaena flos-aqaue* and *Aphanizomenon skuja* were also grown in Blue-Green Medium Num. 11 (no $NaNO_3$) (BG-11_0) and are referred to below as "N-fixing" to distinguish those cultures from those with $NaNO_3$. A 12:12h light cycle was selected to mimic the circadian cycle of cyanobacteria and to ensure that N-fixation rates remained constant throughout the experiment (Chen et al., 1998).

All species were grown in 1nM Fe as $FeCl_3$ for three transfers before 1mL of exponentially growing cells from 1nM Fe starter culture was used to inoculate metal-free tubes of BG-11, BG-11_0 or BBM containing varying concentrations of Fe. To ensure that there was no trace metal contamination, all reagents used were trace metal grade, all flasks and bottles were soaked in 10% HCl over 48 hours and then in Milli-Q water for another 24 hours. Only acid-washed clear pipette tips were used throughout this experiment. All media, glassware and supplies such as pipette tips were UV sterilized

under a Laminar flow hood for 15 minutes as autoclave steam can introduce trace metal contamination (Keller et al., 1988).

2.2.2 Determining Iron Concentrations

After all growths were completed, the samples were digested using a combination of trace-metal grade HNO_3 and HCl as described by the Environmental Protection Agency (1983). Due to the use of very low concentrations of Fe, Fe concentrations were determined after the growth. All samples contained varying concentrations of Fe and thus there were no replicates at the same Fe concentration. To avoid external Fe contamination, all digestions were done inside a fume hood and samples were heated on a heating block using only metal-free plastic tubes. Total Fe concentration in each digested sample was measured using graphite furnace atomic absorption spectrometry (GF-AAS), detection limit of 0.06μg/L (Perkin-Elmer Pinaacle 900T AAS).

2.2.3 Calculations and Equations

Absorbance at 750nm (Absorbance at 750nm (A_{750})) was used to measure growth of samples. At 750nm, interference from photosynthetic pigments is minimal and can be used as a consistent proxy for cellular growth (Chioccioli et al., 2014). Cell numbers were estimated by counting cells with a hemocytometer and generating standard curves for each organism to correlate cell number to A_{750} (see Appendix A).

A_{750} was plotted against time and the R package *growthcurver*(version 0.3.0) was used to find the growth rate of each sample (Sprouffske and Wagner, 2016). The package *growthcurver* finds the best fit of a given dataset to the logistic growth equation (Eq 2.2).

$$N_t = \frac{K}{1 + (\frac{K - N_0}{N_0}) e^{-rt}} \tag{2.2}$$

where N_t is the A_{750} at a given time, K is the carrying capacity, N_0 is the starting A_{750}, r is the growth rate (μ) and t is time. Eq. 2.2 is the solution of Eq 1.9.

After the μ are found, the data were fitted to the modified Monod equation (Eq.

2.1) using the *nls* function in R with bootstrapping (number of iterations = 10,000) (McClanahan and Humphries, 2012). *nls* is used to solve non-linear regressions using the sum of least squares. This function was used to solve for μ_{max}, Fe_T and K_{Fe}. Initials slopes were then calculated using $\mu_{max}/(K_{Fe}\text{-}Fe_T)$.

2.3 Results

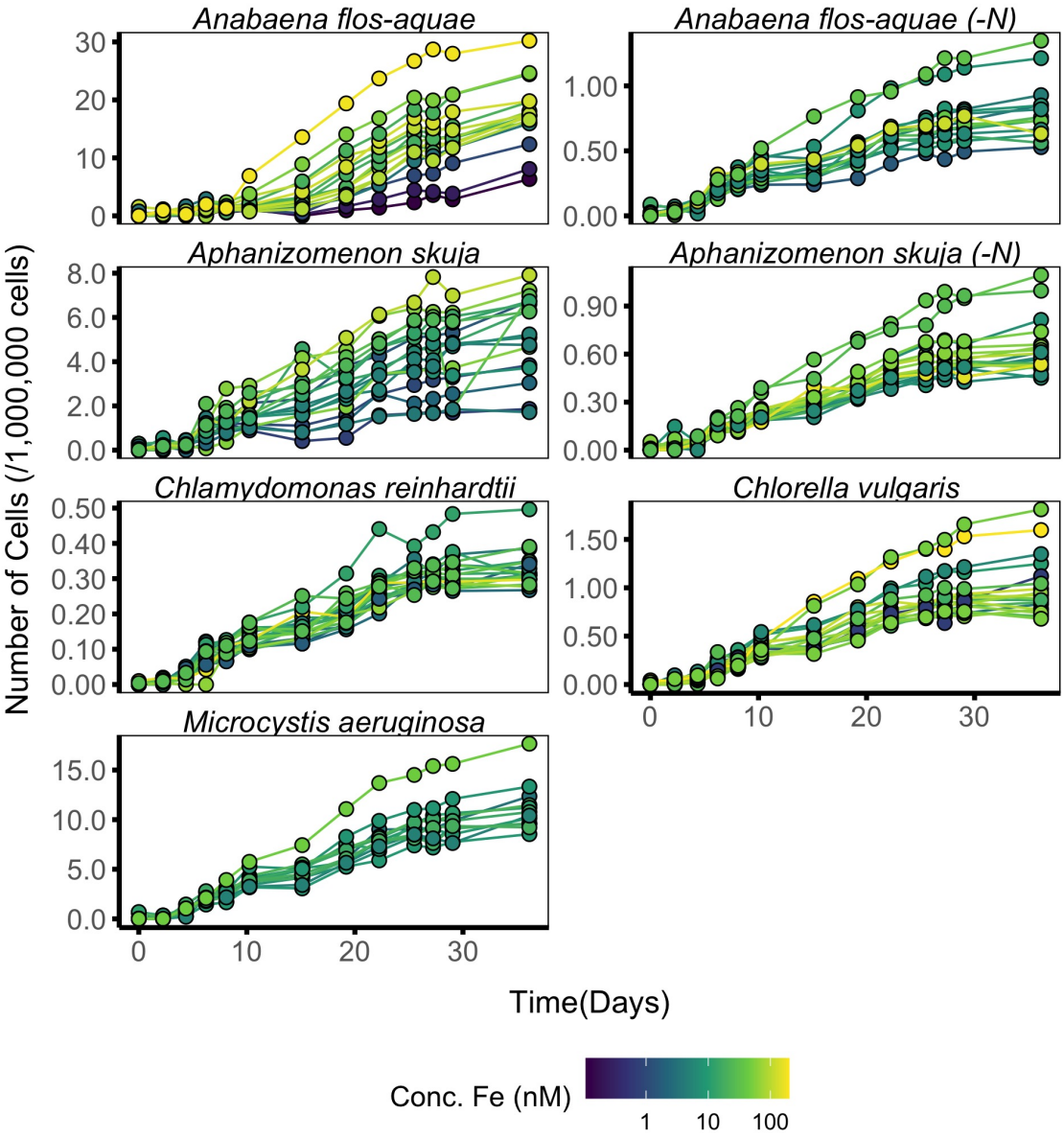

Figure 2.1: Growth curves of the phytoplankton species at different concentrations of Fe. Species labelled with (-N) are grown without inorganic N in the media and are N-fixing.

Growth curves of phytoplankton follow a S-shaped curve (Fig. 2.1). We calculated the mean and 95% confidence interval and used the mean bootstrap predictions to calculate the model curve for the Monod plots shown in Fig. 2.2. Low root mean squared errors (RMSE) shown in Fig. 2.2 indicate that the parameters estimated are a good fit for the data.

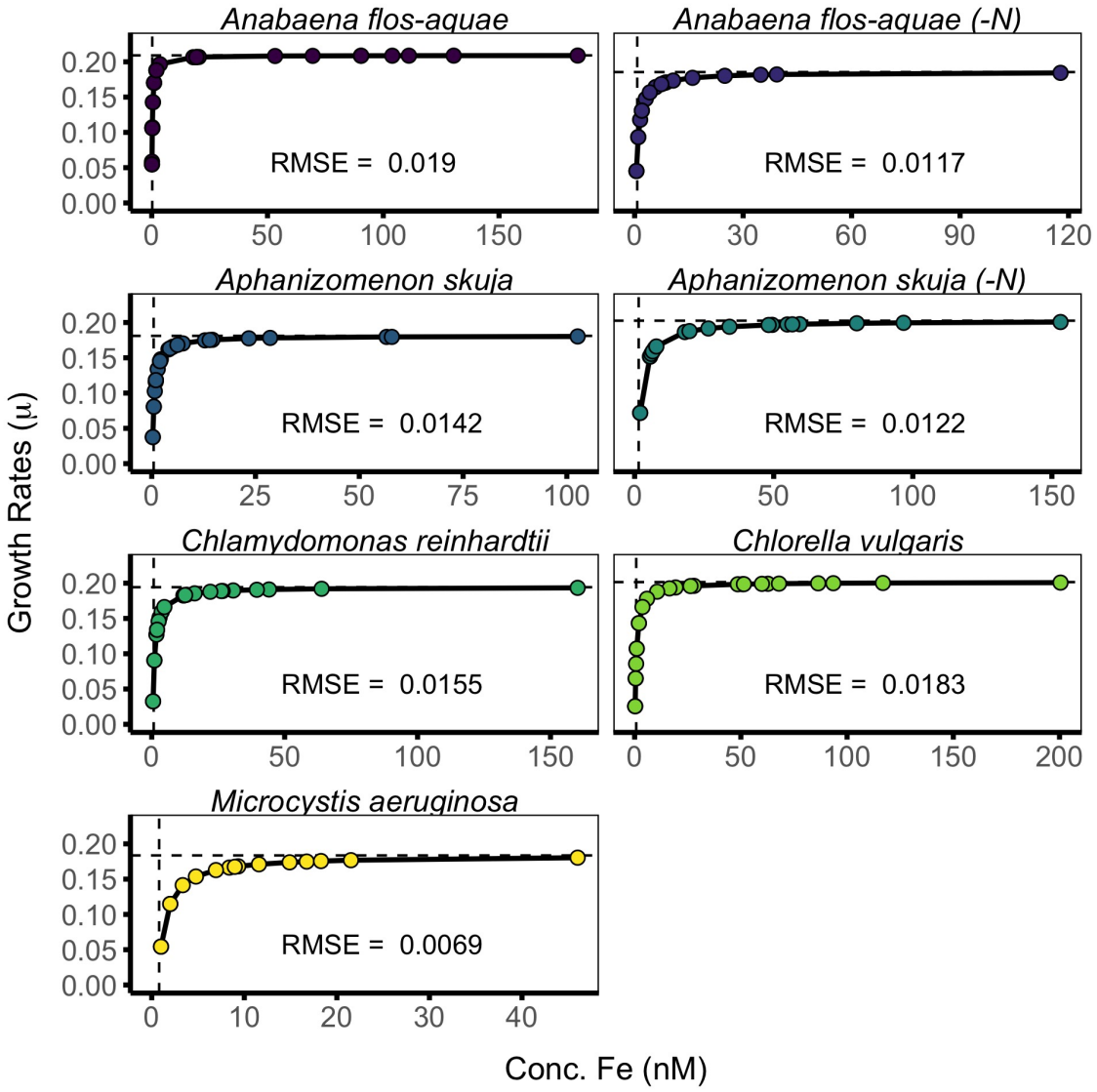

Figure 2.2: Monod plots of the different species with the model line drawn. Horizontal dashed lines indicate μ_{max} and vertical dashed lines indicate K_{Fe}. RMSE between experimental and modelled μ are shown. Species labelled with (-N) are grown without inorganic N in the media and are N-fixing.

We compared the parameters estimated using two-way pairwise ANOVAs comparing the iron thresholds, half-velocity constants and maximal growth rates (see Tables

Table 2.1: Output of two-way ANOVA of Terms by Species

term	df	sumsq	meansq	statistic	p.value
Term	2	10549	5275	26700	$< 2 \times 10^{-16}$
Species	6	12092	2015	10201	$< 2 \times 10^{-16}$
Term:Species	12	6799	567	2868	$< 2 \times 10^{-16}$
Residuals	209979	41482	0		

2.1 and 2.3). The results of the Tukey's HSD for the ANOVA used to test for different species and different N conditions for N-fixing species are statistically different are shown in Fig. 2.3. We averaged the estimates for Fe_T, K_{Fe} and μ_{max} for each species type and did another two-way pair-wise ANOVA to see if different types of alga taxa have different iron thresholds. The results of this are shown in Tables 2.3 and 2.4 and Fig. 2.4.

The results in Table 2.4 and Fig. 2.4 show that all three variables have means that are statistically different from one another. The μ_{max} for the three different classes are similar (approximate μ of 0.194) meaning that the phytoplankton will have a similar maximal growth rate, given enough nutrients.

The K_{Fe} found in this study for the species and species type are statistically different, where N-fixing, N-replete cyanobacteria have the lowest K_{Fe} at 0.341nM, 95% CI[0.339, 0.343], followed by eukaryotic algae at 0.745nM, 95% CI[0.741, 0.749], non-N-fixing, N-replete cyanobacteria (*Microcystis aeruginosa*) have a mean K_{Fe} of 0.802nM, 95% CI[0.795, 0.808] and finally the N-fixing cyanobacteria without dissolved inorganic nitrogen (DIN) at 1.093nM, 95% CI[1.085, 1.101].

We found the relative growth ability at low concentrations of Fe by the initial slope of the Monod curve, $\mu_{max}/(K_{Fe}\text{-}Fe_T)$ shown for each species and species type in Tables 2.5 (Molot and Brown, 1986). A higher slope indicates a competitive advantage for the species or species type at lower concentrations of Fe. At an initial concentration of 1nM Fe, *Chlorella vulgaris*, the eukaryotic algae, has the lowest initial slope at 0.332, while the N-replete cyanobacteria, *Anabaena flos-aqaue* and *Microcystis aeruginosa* have initial slopes greater than 1 indicating that these cyanobacteria species are highly competitive under culture conditions.

Table 2.2: Groups of the Post-Hoc of ANOVA analysis using Tukey's-HSD for the two-way Species ANOVA (Table 2.1). The N-fixers, *Anabaena flos-aquae* and *Aphanizomenon skuja*, were grown with DIN (N-replete) and without DIN. Groups indicate results of Tukey's-HSD only within each parameter at $p < 0.05$.

Species	Species Type	Term	ANOVA Grouping	Mean Value	95% CI	5% CI
Anabaena flos-aquae	Cyanobacteria	Fe_T	f	0.021	0.022	0.021
Anabaena flos-aquae (N-Fixing)	Cyanobacteria	Fe_T	d	0.268	0.274	0.261
Aphanizomenon skuja	Cyanobacteria	Fe_T	e	0.131	0.134	0.128
Aphanizomenon skuja (N-Fixing)	Cyanobacteria	Fe_T	a	1.204	1.235	1.174
Chlamydomonas reinhardtii	Chlorophyte	Fe_T	c	0.347	0.356	0.339
Chlorella vulgaris	Chlorophyte	Fe_T	e	0.142	0.146	0.139
Microcystis aeruginosa	Cyanobacteria	Fe_T	b	0.663	0.68	0.647
Anabaena flos-aquae	Cyanobacteria	K_{Fe}	f	0.222	0.224	0.221
Anabaena flos-aquae (N-Fixing)	Cyanobacteria	K_{Fe}	d	0.726	0.731	0.721
Aphanizomenon skuja	Cyanobacteria	K_{Fe}	e	0.46	0.463	0.457
Aphanizomenon skuja (N-Fixing)	Cyanobacteria	K_{Fe}	a	1.461	1.472	1.449
Chlamydomonas reinhardtii	Chlorophyte	K_{Fe}	c	0.741	0.747	0.736
Chlorella vulgaris	Chlorophyte	K_{Fe}	c	0.748	0.755	0.742
Microcystis aeruginosa	Cyanobacteria	K_{Fe}	b	0.802	0.808	0.795
Anabaena flos-aquae	Cyanobacteria	μ_{max}	a	0.209	0.209	0.209
Anabaena flos-aquae (N-Fixing)	Cyanobacteria	μ_{max}	e	0.185	0.186	0.185
Aphanizomenon skuja	Cyanobacteria	μ_{max}	g	0.181	0.181	0.181
Aphanizomenon skuja (N-Fixing)	Cyanobacteria	μ_{max}	b	0.203	0.203	0.202
Chlamydomonas reinhardtii	Chlorophyte	μ_{max}	d	0.194	0.194	0.194
Chlorella vulgaris	Chlorophyte	μ_{max}	c	0.201	0.202	0.201
Microcystis aeruginosa	Cyanobacteria	μ_{max}	f	0.184	0.184	0.183

2.4 Discussion

The Monod model is a steady-state model derived from the Michaelis-Menten model of enzyme kinetics (Healey, 1980). In enzymology, affinity by an enzyme for a substrate has been indicated by the coefficient K_m (analogous to K_{Fe} in the equation), where the lower the K_m, the higher the affinity. However, this is incorrect when applying this model to organisms. Competitive ability between species is best indicated by the initial slope of the Monod curves for concentrations above threshold values. The K_{Fe} values in the Monod model are empirical and will differ between species and reflect the ambient conditions (Walker, 1998; Healey, 1980). The affinity for uptake of a nutrient by an organism is dependent on many factors such as genetics, cell size, and uptake

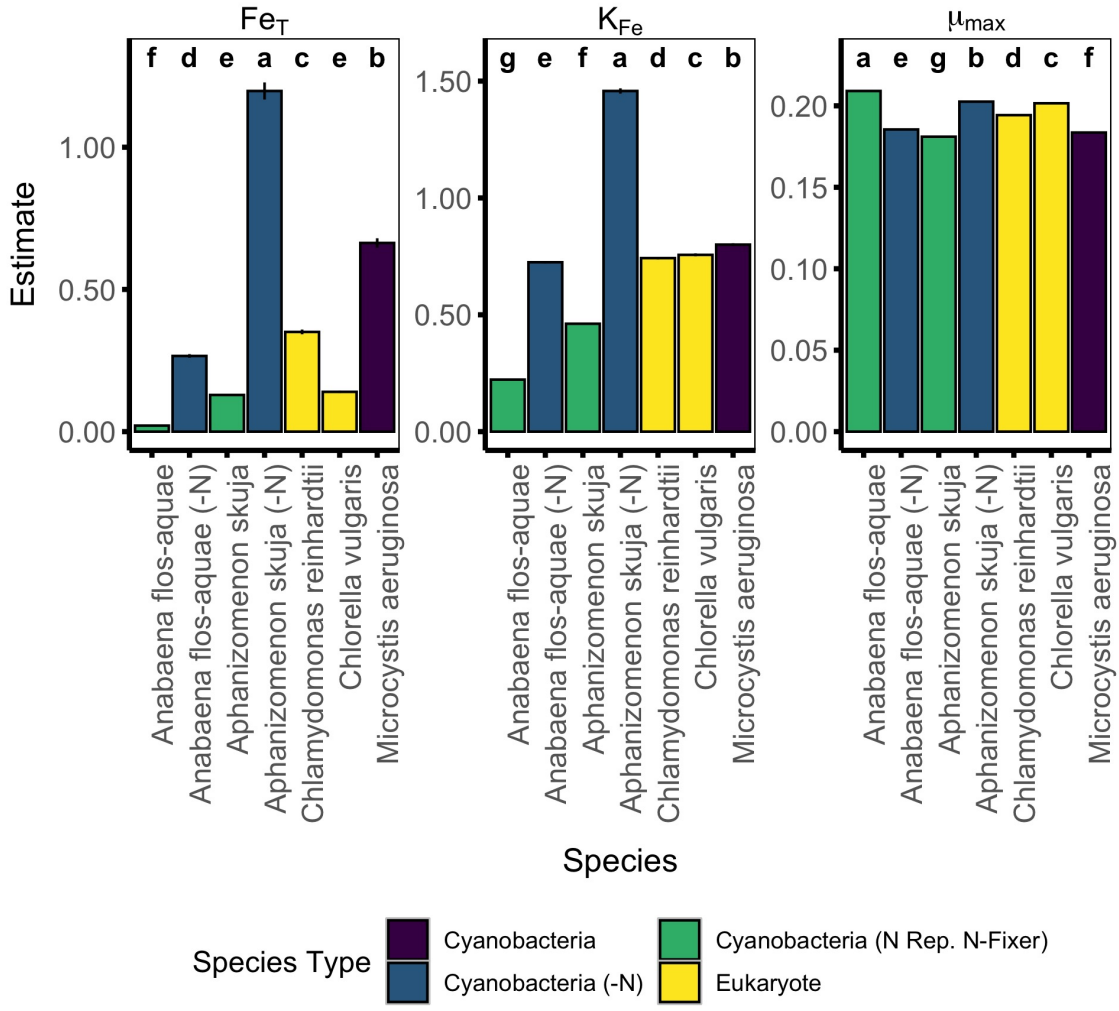

Figure 2.3: Fe_T, K_{Fe} and μ_{max} for each species, colour indicates species type. Lettered groupings indicate statistically different means as shown by the pair-wise two-way ANOVA (results shown in Tables 2.1 and 2.2) and are ordered from highest to lowest mean-value. Error bars indicate 95% confidence intervals. Species labelled with (-N) are grown without inorganic N in the media and are N-fixing.

mechanisms (Sunda and Huntsman, 2015; Healey, 1980) and whether uptake rate (the numerator) is expressed per unit volume or cell surface area. In this study, the K_{Fe} also appears to be affect N availability, specifically when comparing N-replete and N-fixing cyanobacteria. If we treat the half-saturation constant as an analogy for affinity for iron, then we should observe similar $K_{Fe} + Fe_T$ values within a species but this did not occur.

We can better indicate affinity by the initial slope of the Monod curve. When concentration of Fe is very low, a relatively higher slope of the Monod curve can indicate competitiveness because it reflects a higher growth rate at a given substrate concentration.

Table 2.3: Output of two-way ANOVA of Terms by Species type

term	df	sumsq	meansq	statistic	p.value
Term	2	10549	5275	22545	$< 2 \times 10^{-16}$
Species Type	3	7109	2370	10128	$< 2 \times 10^{-16}$
Term:Species Type	6	4136	689	2947	$< 2 \times 10^{-16}$
Residuals	209988	49129	0.23		

Table 2.4: Groups of the Post-Hoc of ANOVA analysis using Tukey's-HSD for the two-way Species Type ANOVA (Table 2.3). *Anabaena flos-aquae* and *Aphanizomenon skuja* have been pooled dependent on the availability of DIN in culture and *Chlorella vulgaris* and *Chlamydomonas reinhardtii* were pooled. Letters indicate statistically different means within each parameter at $p < 0.05$.

Species Type Type	Term	ANOVA Grouping	Mean Value	95% CI	5% CI
Cyanobacteria	Fe_T	b	0.663	0.680	0.647
Cyanobacteria (N Rep. N-Fixer)	Fe_T	d	0.076	0.078	0.074
Cyanobacteria (N-Fixing)	Fe_T	a	0.736	0.753	0.719
Chlorophyte	Fe_T	c	0.245	0.250	0.240
Cyanobacteria	K_{Fe}	b	0.802	0.808	0.795
Cyanobacteria (N Rep. N-Fixer)	K_{Fe}	d	0.341	0.343	0.339
Cyanobacteria (N-Fixing)	K_{Fe}	a	1.093	1.101	1.085
Chlorophyte	K_{Fe}	b	0.745	0.749	0.741
Cyanobacteria	μ_{max}	d	0.184	0.184	0.183
Cyanobacteria (N Rep. N-Fixer)	μ_{max}	b	0.195	0.195	0.195
Cyanobacteria (N-Fixing)	μ_{max}	c	0.194	0.194	0.194
Chlorophyte	μ_{max}	a	0.198	0.198	0.198

A comparatively higher initial slope, the better the taxa will do at lower concentrations of the nutrient (Molot and Brown, 1986; Healey, 1980).

This study offers an opportunity to compare iron threshold of growth among a variety of different types of phytoplankton taxa. The iron thresholds for the four species types are different where N-fixing cyanobacteria in N-replete conditions (*Anabaena flos-aquae* and *Aphanizomenon skuja*) have the lowest iron threshold with a mean threshold of 0.076nM, 95% CI[0.074, 0.076], followed by eukaryotic algae (*Chlamydomonas reinhardtii* and *Chlorella vulgaris*) with a mean iron threshold of 0.245nM, 95% CI[0.240, 0.250], followed by non-N-fixing cyanobacteria (*Microcystis aeruginosa*) with a threshold of 0.663nM, 95% CI[0.647, 0.680] and the N-fixing cyanobacteria (*Anabaena flos-aquae* and *Aphanizomenon skuja*) with have an iron threshold at 0.736nM, 95%

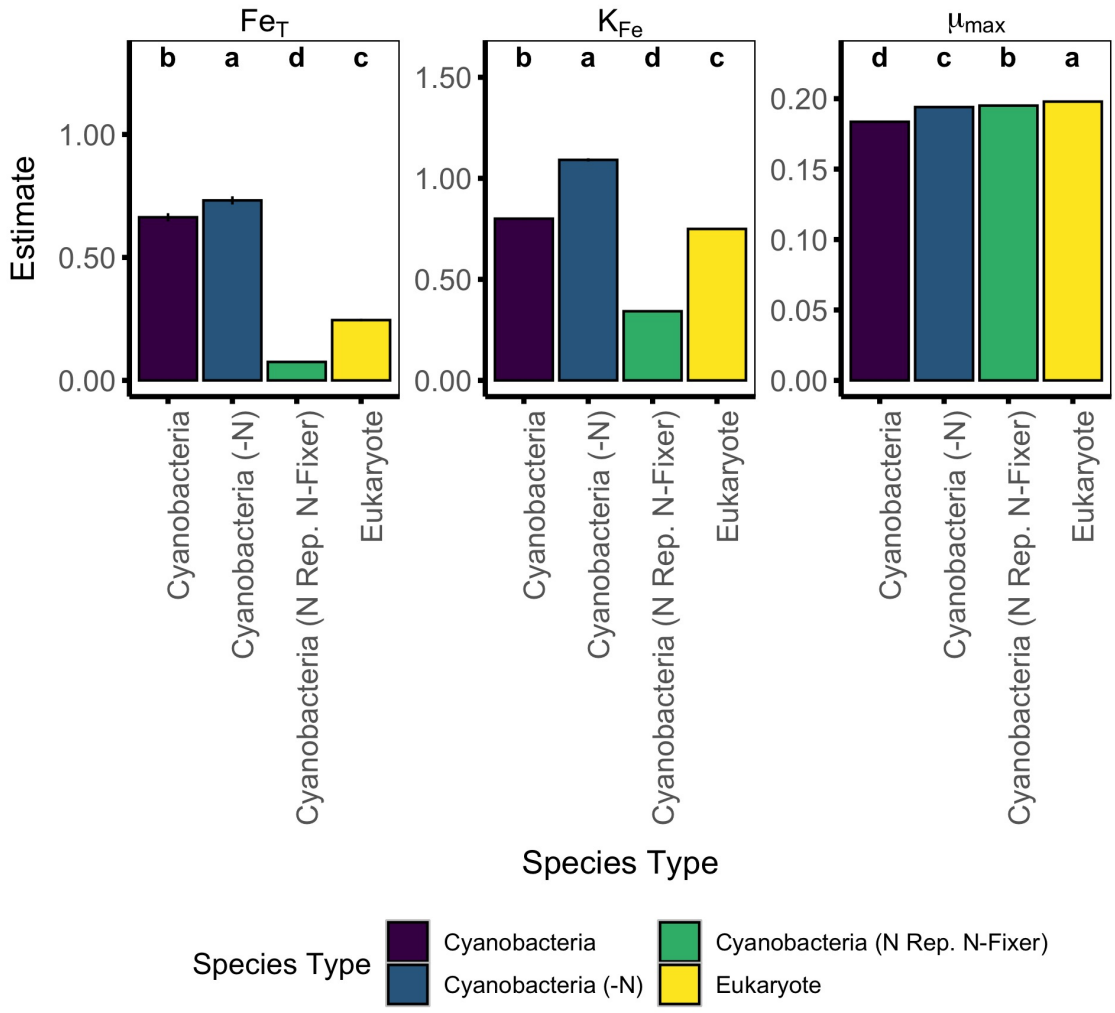

Figure 2.4: Average estimates of the variables; Fe_T, K_{Fe} and μ_{max} for each species type, colour indicates species type. Lettered groupings indicate statistically different means as shown by the pair-wise two-way ANOVA (results shown in Tables 2.3 and 2.4) and are ordered from highest to lowest mean-value. Error bars indicate 95% confidence intervals. Species labelled with (-N) are grown without inorganic N in the media and are N-fixing.

CI[0.719, 0.753].

N-fixing cyanobacteria have a higher Fe threshold than their N-replete counterparts (Fig. 2.4). When diazotrophic species switch to N-fixation, their the Fe_T increases almost an order of magnitude. This is in line with other studies that show that iron quotients of N-fixing cyanobacteria are higher than those of their N-replete counterparts (Molot et al., 2014). Nitrogenase increases demand for Fe but cells do not lower their Fe_T to meet this extra demand. Rather, they increase it. This could possibly be because lowering the Fe_T may be too energy intensive at a time when energy is needed to fix atmospheric nitrogen.

Table 2.5: Relative growth abilities of phytoplankton taxa and species types at low concentrations of Fe found by the initial slope of the Monod curve. ± indicate propagated 95% confidence intervals.

Species	$\mu_{max}/(K_{Fe}\text{-}Fe_T)$
Anabaena flos-aquae	1.040 ± 0.008
Anabaena flos-aquae (N-Fixing)	0.404 ± 0.007
Aphanizomenon skuja	0.550 ± 0.007
Aphanizomenon skuja (N-Fixing)	0.790 ± 0.085
Chlamydomonas reinhardtii	0.492 ± 0.012
Chlorella vulgaris	0.332 ± 0.004
Microcystis aeruginosa	1.324 ± 0.172
Species Type	$\mu_{max}/(K_{Fe}\text{-}Fe_T)$
Cyanobacteria	1.324 ± 0.172
Cyanobacteria (N Rep. N-Fixer)	0.736 ± 0.008
Cyanobacteria (N-Fixing)	0.543 ± 0.026
Chlorophyte	0.396 ± 0.005

Each nitrogenase complex has 32 to 36 Fe atoms as metallic co-factors and this apparent increase in iron threshold could be evidence of increased use of nitrogenase by the cyanobacteria (see fig 1.3) (Schindelin et al., 1997; Graham et al., 2016). However, the nutrient thresholds determined in this study are also dependent on the other conditions. Factors like temperature and light are known to impact nutrient thresholds (Yuan et al., 2007; Hill et al., 2009) but these factors were considered and kept constant during this experiment.

Affinity for iron at low concentrations may play an important role in the ability of phytoplankton species to be competitive. *Microcystis aeruginosa* has the highest initial slope but will out-compete *Anabaena flos-aqaue* only when the concentration of Fe is higher than 0.6nM which is the iron threshold for *Microcystis aeruginosa*. The chlorophyte *Chlorella vulgaris*, has a low iron threshold at 0.142nM, however, because the initial slope is lower it will not be competitive at low concentrations of iron. Outcome of competition between species at low Fe concentrations will depend on their species-specific threshold and affinity values.

Threshold concentrations for N and P have been used to set targets for nutrient loading in Lake Taihu, China (Yin et al., 1992; Xu et al., 2015; Jiang et al., 2019). Threshold concentrations can help inform on determining nutrient loading standards for

management of HABs (Hill et al., 2009). Additionally, in the case of Fe, these nutrient thresholds combined with the initial slopes can help us understand what is involved in determining dominance by one species over another at different concentrations of Fe.

2.5 Conclusion

In this study we quantified the Fe thresholds for several common freshwater phytoplankton using a modified Monod equation and used the initial slopes as measures of relative competitiveness in low Fe environments to better understand how Fe impact growth dynamics of different potentially bloom forming species.

The data presented in this study show that N fixing cyanobacteria in N-replete conditions have the lowest iron threshold, followed by chlorophytes, then *Microcystis aeruginosa* and finally, N-fixing cyanobacteria. We also show that *Microcystis aeruginosa* has the highest initial slope, followed by N-fixing cyanobacteria in N-replete conditions, then N-fixing cyanobacteria and finally chlorophytes, showing the relative competitiveness of these species types at low Fe concentrations.

We confirmed previous work which showed that N-fixation increases iron demand and we show that the increased demand does not decrease the Fe_T, but increases it. We also quantify and show that while cyanobacteria have a high Fe_T than eukaryotic algae, the initial slopes indicate that in low Fe environments, the cyanobacteria will outcompete the eukaryotic algae.

These findings reinforce the importance of Fe in harmful algal bloom growth and development and mitigation strategies should be designed to limit both Fe and P below the threshold concentrations for phytoplankton. Further research into these technologies is required.

Chapter 3

Using a Mixing-Model to Estimate Phytoplankton Growth Rates Using Carbon and Nitrogen Stable Isotope Fractionation

Abstract

Lakes, bays and reservoirs are important sources of drinking water, recreation and economic activity. Eutrophication has led to the increased and persistent presence of harmful algal blooms (HABs) that can potentially cause great damage to water quality. Understanding the biogeochemical processes that occur in freshwater is key to understanding the drivers to forming HABs. The use of stable isotopes is a common strategy to understand the movement of elements and growth rates of species through an aquatic system. However, measurements of stable isotopic composition of particulate matter report only one value for the bulk sample and distinguishing between old and newly accumulated biomass values in a bulk sample has been challenging. In this study, we propose the use of a mixing-model to estimate the δ^{13}C and the δ^{15}N of the newly accumulated phytoplankton biomass between two sampling events in culture. We show

that the difference in the isotopic compositions of the new particulate organic matter (POM) and the measured bulk POM can be as large as 15‰. Using this model, we show that the fractionation factors, the discrimination between the isotopes (α and ϵ) change during the growth of phytoplankton cultures and we used this model to correlate the growth rate of the phytoplankton with the changing fractionation factors and found good correlations ($R^2 > 0.7$) between species grown in N-replete conditions and the $\epsilon^{13}C$. This technique and model can be used with environmental samples to better understand the biogeochemical processes that contribute to the growth of new algal biomass and to better understand the growth of the species in the environment.

3.1 Introduction

Macronutrients such as nitrogen and carbon are essential for growth of any organism. C and N are a part of almost all the major molecules involved in biology from carbohydrates, to proteins, to DNA and RNA (Graham et al., 2016). Carbon and nitrogen exist in freshwater in the dissolved phase, as dissolved inorganic carbon (DIC), dissolved organic carbon (DOC) or dissolved organic nitrogen (??), or in the particulate phase as particulate organic carbon (POC) or particulate organic nitrogen (particulate organic nitrogen (PON)). Most of the biomass is found in the particulate phase dependent on the filter size (Kurihara et al., 2018; Einola et al., 2011). DIC and DIN are used by phytoplankton for cellular function and growth (Graham et al., 2016).

C and N, along with P are considered to be the three most important macronutrients for phytoplankton (Graham et al., 2016). In oligotrophic areas of the oceans, cyanobacteria account for more than 50% of primary productivity and can introduce N in bioavailable forms through N-fixation (Bauersachs et al., 2009). The abilities of phytoplankton to fix atmospheric carbon and sometimes nitrogen has led to the understanding that phosphorus is the key macronutrient driving harmful algal bloom biomass in freshwaters (Schindler et al., 2008). However, studying C and N is important to understanding how these vital macronutrients are cycled through the ecosystem.

HABs and cHABs are large growths of phytoplankton that can cause harm to the environment that they grow in (Graham et al., 2016). cHABs are especially problematic because they are capable of producing toxic and/or foul smelling compounds and causing fish and aquatic wildlife death by creating anoxic conditions formed due to the accumulation of scum. All of these problems are expensive to solve (Downing et al., 2001; Winter et al., 2011; Michalak et al., 2013).

The use of stable isotopes as a technique to understand biogeochemical processes began in the 1960s (Park and Epstein, 1961). Since then, stable isotopes have been useful in differentiating between biotic, abiotic, and a variety of other processes involving C, N and other elements (Dauphas et al., 2017; Johnson and Beard, 2006; Gu et al., 1994; Mackensen and Schmiedl, 2019; Guiry, 2019; Bauersachs et al., 2009).

There are a several factors that have an impact on the isotopic composition of phytoplankton. In freshwater systems dominated by phytoplankton, the stable isotopic composition of the POM (δ^{13}C and δ^{15}N) is dependent on the concentration and the stable isotopic composition of the dissolved nutrient and the isotopic fractionation (α and ϵ) of the dissolved nutrients during uptake and usage (Gu et al., 2006; Lehmann et al., 2004). The isotopic fractionation is the ratio of heavy to light isotope ratio for two pools of interchanging species and is represented by α. These α can be converted into permil fractionation factor, ϵ, by presenting the α as a deviation from 1. The fractionation between the dissolved nutrient and the particulate for many processes are known and studied. The carbon isotopic fractionation is approximately -29‰ for eukaryotic algae and between -22 and -25‰ in cyanobacteria (Falkowski and Raven, 2007). The nitrogen isotopic fractionation during nitrate assimilation is 5-6‰ (Waser et al., 1998; Karsh et al., 2014). Amount of biomass present, the instantaneous growth rate (μ_i) and nutrient concentration all can impact the fractionation factors between the dissolved nutrients and the particulate matter (Holben and Ostrom, 2000; Burkhardt et al., 1999; Kukert and Riebesell, 1998). Laws et al. (1997) determined the relationship between ϵ^{13}C and μ of *Phaeodactylum tricornutum* cultures. However, due to the technological constraints, the practical applications of this methods are limited (Zhen and Zhu, 2018). Popp et al.

(1998) found that introducing the size and surface area of a cell will help make the relationship between ϵ^{13}C and μ stronger, however, this formulation involves variables such as carbon fixation rates, flow and CO_2 diffusion across cell membranes, making the process of using stable isotopes to calculate growth rate more complicated. Tanaka et al. (2008) found a positive linear relationship between $\Delta\delta^{13}C_{leaf-DIC}$ and μ. However, the linear fit had a correlation coefficient of 0.39, indicating a weak relationship. Zhen and Zhu (2018) used laboratory cultures of *Microcystis* to build an exponential relationship between the carbon isotopic fractionation and the growth rate. They then used this relationship to find the growth rate of *Microcystis* in Lake Taihu, China.

However, many of these studies only used the isotopic composition of the bulk particulate matter. Bulk samples, especially lake water samples, contain much more than just algal biomass, and can confound results further (Bade et al., 2006). In cell cultures, bulk samples include all accumulated materials which formed when culture conditions were different than the conditions for the instantaneous biomass. Changes in biochemical processes and how nutrients are used and recycled are known for phytoplankton cells (Fogg and Thake, 1987). Understanding how stable isotopic composition of phytoplankton changes during growth in culture can help understand the roles of C and N in the growth of HABs.

The objective of this study is to use a mixing-model to separate the isotopic composition (δ^{13}C and δ^{15}N) of newly accumulated phytoplankton biomass from the bulk sample to better understand how growth changes the isotopic composition and the fractionation factors of several species of temperate freshwater phytoplankton in culture and to use the fractionation factors to build relationships with the growth rates of these species.

3.2 Materials and Methods

3.2.1 Experimental Organisms and Growth Conditions

Cultures were grown in BG-11 media with and without nitrate (BG-11_0) and Bold Basal Media (BBM). Cultures of cyanobateria: *Anabaena flos-aqaue* (CPCC 67) (in BG-11 and BG-11_0), *Aphanizomenon flos-aqaue* (NIES 81) (in BG-11 and BG-11_0), *Aphanizomenon skuja* (isolate from Lake 227, ELA) (in BG-11 and BG-11_0), and *Microcystis aeruginosa* (PCC 7005) (in BG-11) along with cultures of eukaryotic algae: *Coelastrum proboscideum* (SAG 217-2), *Chlorella vulgaris* (CPCC 90), and *Chlamydomonas reinhardtii* (CPCC 243), all grown in BBM, were grown in 4L batch cultures at 20°C on a 12:12h light/dark cycle at 100 μmol/m^2/s with constant aeration. A 12:12h light cycle was selected to mimic the circadian cycle of cyanobacteria and to ensure that N-fixation rates remained constant throughout the experiment (Chen et al., 1998). All media contained equivalent concentrations of $FeCl_3$ instead of ferric ammonium citrate and equivalent amount of $CoSO_4$ instead of $Co(NO_3)_2$ (Rippka et al., 1979; Stein et al., 1973). Growth of the culture was monitored by measuring absorbance of the cell culture at 750 nm (A_{750}). At four time points along the growth, samples for nutrient concentrations, stable isotope analyses of Fe, C and N and DOC spectral characterization were collected. Cultures of nitrogen-fixing cyanobacteria were aerated at less power than cultures grown in nitrate to help maintain integrity of filaments.

3.2.2 Nutrient Analyses

Samples for DIC were collected directly into 12mL exetainers with no headspace and preserved with diluted $HgCl_2$. Analysis was done by withdrawing 6mL of sample while displacing with 6mL of He and transferring to another evacuated 12mL exetainer filled with 12mL He. Both exetainers were acidified using H_2SO_4 and placed on a shaker for 2 hours to allow gas/liquid equilibrium. The concentration of the headspace CO_2 was measured using a Varian CP-3800 Gas Chromatograph and dissolved CO_2 concentrations were determined using Henry's Law for each exetainer.

Samples for dissolved P and Fe concentrations were collected by filtering samples through 0.22μm filters. Dissolved P was analyzed using the molybdenum blue reaction as described by Ota and Kawano (2017). Fe samples were digested using a combination of HNO_3 and HCl digestion as described by Environmental Protection Agency (1983) in acid-washed plastic tubes and analyzed using ICP-OES (emission λ = 238.204).

Samples for total dissolved nitrogen (TDN) and DOC concentration were collected by filtering sample water though 0.45μm filters and analyzed with a Shimadzu Total Organic Carbon (TOC-L) Combustion Analyzer with TNM-1 Module with the precision of ±0.3mg C/L and ±0.3mg N/L.

3.2.3 Isotope Analyses

Samples for δ^{13}C-DIC were collected and prepared as samples for DIC concentration and analyzed by GC-CF-IRMS using an Agilent 6890 gas chromatograph coupled to an Isochrom isotope ratio mass spectrometer (IRMS: Micromass UK) with precision of ±0.3‰ as described in Schiff et al. (2017).

Samples for δ^{13}C-POM and δ^{15}N-POM were collected by filtering sample water through an ashed Whatman QMA filter, nominal pore size of 1μm and analyzed by CF-EA-IRMS (CHNS-O EA1108) coupled with a Delta Plus (Thermo) isotope ratio mass spectrometer with a precision of ± 0.2‰ in δ^{13}C and ± 0.3‰ in δ^{15}N as described by Schiff et al. (2017).

δ^{15}N-DIN for all samples were assumed to be constant throughout the growth of the initial value. For species grown with $NaNO_3$, the $NaNO_3$ powder was analyzed using the same method as δ^{15}N-POM and found to be -15.1‰. For diazotrophic species, the δ^{15}N-DIN was assumed to be 0‰ corresponding to the stable isotopic composition of air.

Isotopic composition were expressed in delta (δ) permil (‰) notation for all samples relative to Vienna Pee Dee Belemite (VPDB) for C and atmospheric N_2 for N.

3.2.4 Calculations and Equations

3.2.4.1 Growth Rates

A_{750} was used to monitor growth. Growth rates (μ) were calculated using the equation:

$$\mu = \frac{ln(\frac{Abs_t}{Abs_0})}{t} \tag{3.1}$$

where μ is the growth rate, Abs_t and Abs_0 are the A_{750} at time t and at time 0 right after the inoculation.

3.2.4.2 Model Development

A simple model was used to determine the isotopic fractionation factors in the new biomass accumulated between two sampling points, similar to the model used to differentiate different sources of the isotopic signature (Dijkstra et al., 2008). New biomass isotopic fractionation factors were determined by first determining the δ^{13}C-POC or δ^{15}N-PON of the new biomass:

$$\delta^A X_{NewPOM} = \frac{(Abs_2 * \delta^A X_2) - (Abs_1 * \delta^A X_1)}{Abs_2 - Abs_1} \tag{3.2}$$

where $\delta^A X_i$ represents either δ^{13}C-POC or δ^{15}N-PON at Time 1 and Time 2, and Abs is the measured A_{750} at those sampling events. The result of eq. 3.2 is the modelled δ^AX-POM of the newly accumulated biomass from the two sampling points used. Error in the isotopic composition of new POM was also calculated (IAEA, 2009).

To determine the permil fractionation factor (ϵ) between the δ^{13}C-POC with δ^{13}C-DIC and δ^{15}N-PON with δ^{15}N-DIN, the fractionation factor (α) was first determined and then that was used to find the ϵ (Farquhar et al., 1989; Farquhar and Richards, 1984; Sharp, 2017):

$$\alpha = \frac{1 + \delta^A X_{Dis.Nutrient\,fromTime1}}{1 + \delta^A X_{NewPOM\,fromTime2}} \tag{3.3}$$

$$\epsilon = (\alpha - 1) * 1000 \tag{3.4}$$

where $\delta^A X_{NewPOM}$ is the isotopic composition of the new biomass accumulated between two sampling events that was calculated from eq. 3.2, and $\delta^A X_{Dis.Nutrient}$ is either extracellular δ^{13}C-DIC or δ^{15}N-DIN from Time 1. The ϵ illustrates the fractionation of the stable isotopes from the dissolved phase into the newly accumulated biomass at each sampling event in permil.

Supplemental Figures and Tables

Please see Appendix B for supplemental figures and tables.

3.3 Results

A_{750} of each culture of phytoplankton are shown in fig. 3.1. The absorbance increases with time as predicted. However, the diazotrophic species grown without nitrogen exhibit lower A_{750} than their N-replete counterparts throughout the whole growth process. The growth rates (μ) for each species by using eq. 3.1. The changing growth rates during the growth are shown in fig. B.1 (located in Appendix B). The instantaneous growth rates are increasing for about 10 in most species and then start lowering.

DIC concentrations for all species are increasing with time except for N-fixing species, which remain relatively low and stable (fig. 3.2). The TDN in all species grown with nitrate ranged from 19.07 - 20.14mM N and in N-fixing cultures 0.01 - 0.04mM N (fig. 3.3). Dissolved P concentrations remain relatively stable in all cultures, ranging from 1.1 - 2.3mM P, with no clear increasing or decreasing trends observed (fig. B.2). Dissolved iron decreased in all cultures getting very close to 0μM of Fe by 29 days (fig. B.3). In cultures grown with NO_3^-, DOC concentrations increased in the medium while DOC concentration in diazotrophic cultures remained low and stable throughout the incubation (fig. B.4).

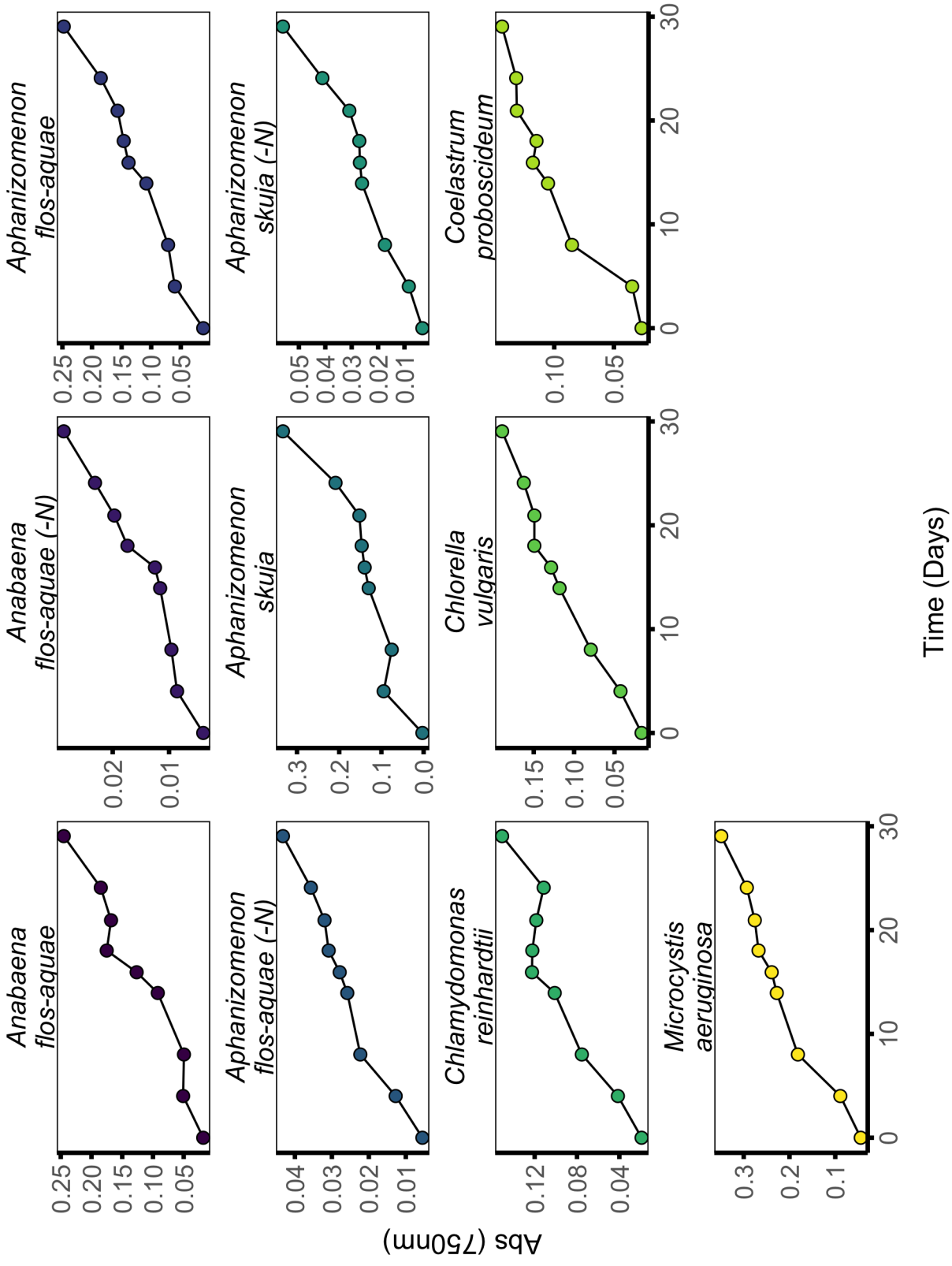

Figure 3.1: Growth curves of the phytoplankton shows the change in A_{750} with time to indicate algal growth in culture. Species labelled with (-N) are grown without inorganic N in the media and are N-fixing.

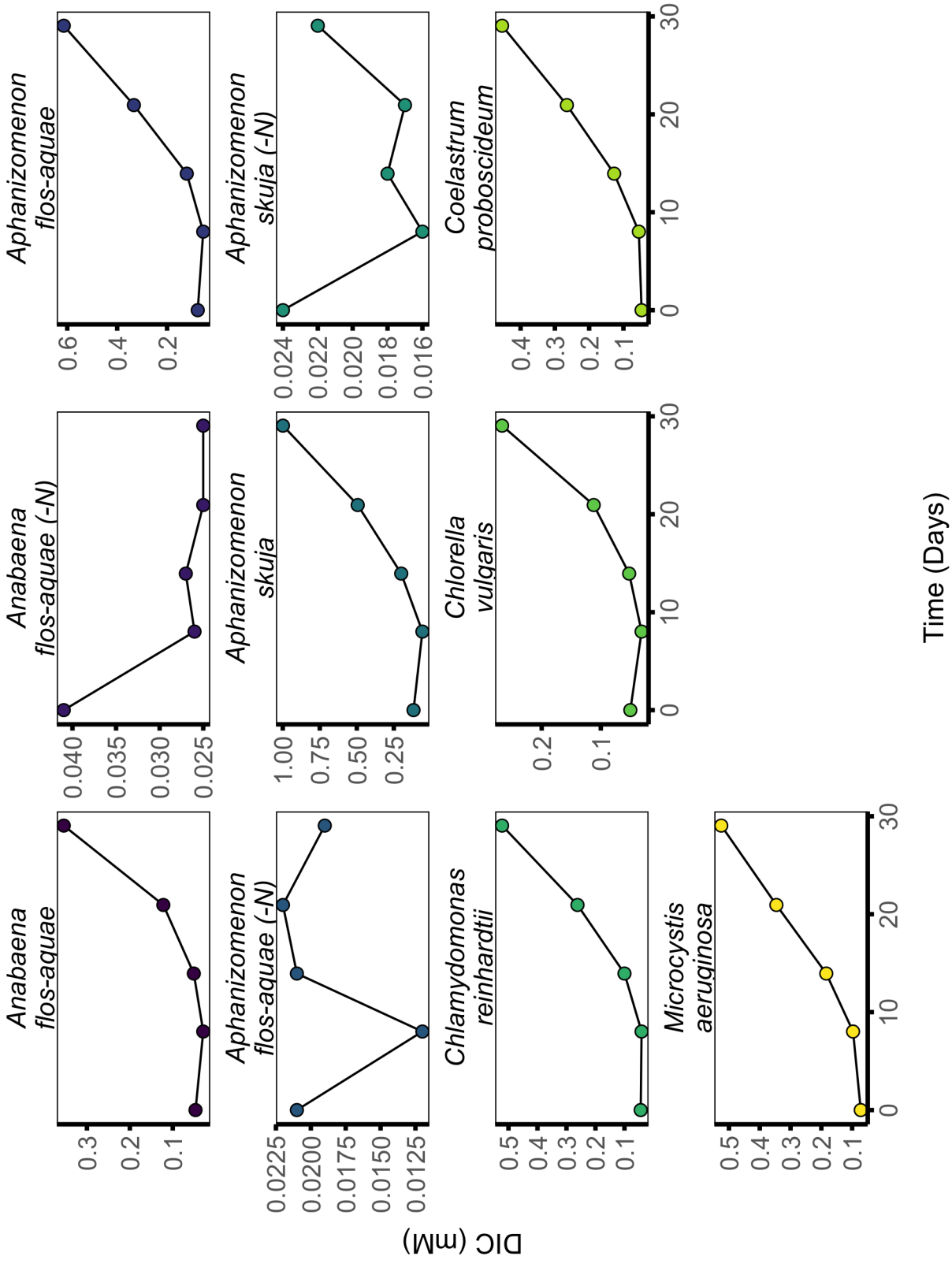

Figure 3.2: Dissolved inorganic carbon (DIC) concentrations during growth of each species. DIC is reported as mM of C. Species labelled with (-N) are grown without inorganic N in the media and are N-fixing.

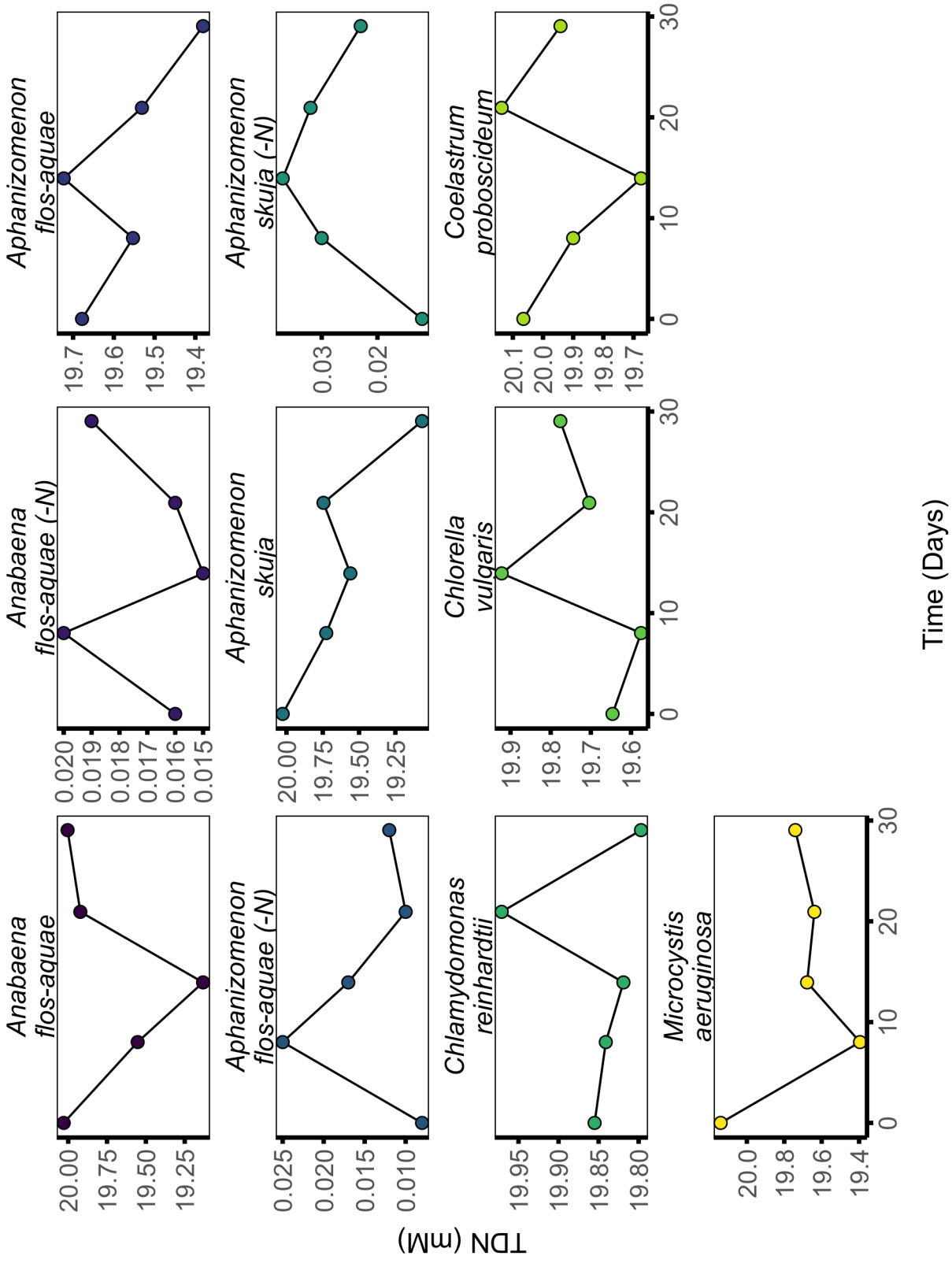

Figure 3.3: Total dissolved nitrogen (TDN) concentrations during growth of each species. TDN is reported as mM of N. Species labelled with (-N) are grown without inorganic N in the media and are N-fixing.Precision is ±0.021mM N.

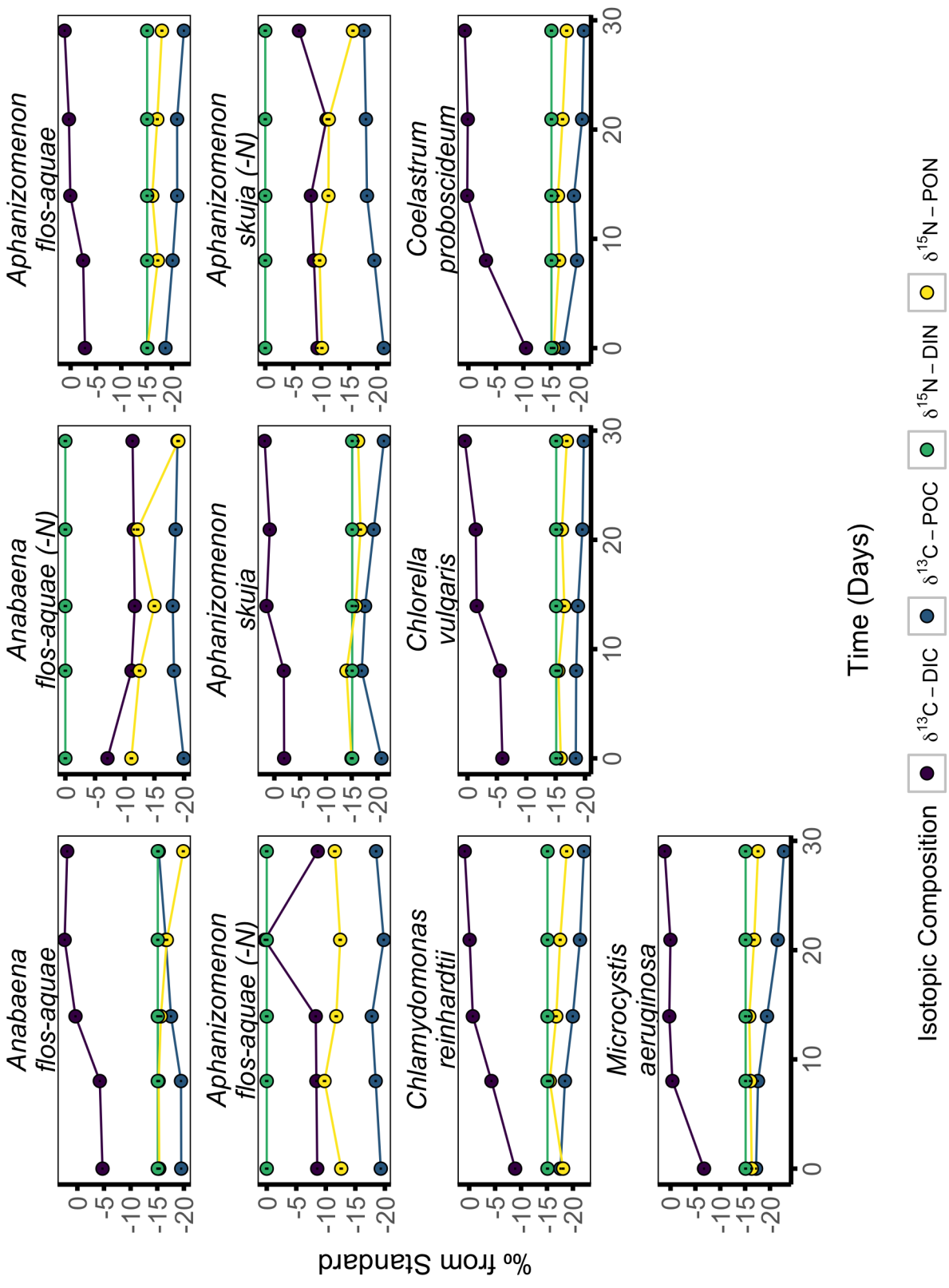

Figure 3.4: Measured δ^{13}C-DIC, δ^{13}C-POC and δ^{15}N-PON along with assumed δ^{15}N-TDN as changing with time during the growth of the various phytoplankton species. δ^{15}N-TDN in cultures grown in nitrate is expected to be a constant -15.1‰, the isotopic composition of the stock $NaNO_3$ and 0‰ for N-fixing cultures which had atmospheric N_2 bubbled in. Precision on δ^{13}C is ±0.2‰ and δ^{15}N is ±0.3‰.

We have shown the isotopic composition of DIC, POC, DIN and PON in fig. 3.4. The δ^{13}C-POC and δ^{15}N-PON shown represent the bulk-particulate matter isotopic composition. δ^{13}C-POC does not follow any discernible trends and ranges mostly between -15 - -22‰. δ^{15}N-PON for N-replete cultures is similar to δ^{13}C-POC also ranging from -15 - -20‰. δ^{15}N-PON for N-fixing cyanobacteria, is decreasing with time. δ^{13}C-DIC increased for all N-replete cultures and plateaued around 0‰. The δ^{13}C-DIC for the N-fixing cyanobacteria is relatively constant around -9‰. δ^{15}N-DIN is assumed to be constant at -15.1‰ for cultures grown with $NaNO_3$ based on the measure δ^{15}N of the $NaNO_3$, and 0‰for N-fixing cultures. The value of -15.1‰ is assumed to be constant because the DIN in those cultures was consistently very high (fig. 3.3), and the value of 0‰is the value of atmospheric N_2, which was the only source for N in diazotrophic cultures.

We calculated the isotopic composition of the newly-accumulated biomass between two sampling points as well as the isotopic fractionation factor (α) and the permil fractionation factor (ϵ) using the model outlined above. The results of each of these calculations are shown in Tables B.1 for δ^{13}C-POC and B.2 for δ^{15}N-PON. Figs. 3.5 and 3.6 show the difference in the δ^{13}C-POC and δ^{15}N-PON of the bulk, analyzed via mass-spectrometry and the δ^{13}C-POC and δ^{15}N-PON of the newly accumulated biomass between two sampling points calculated here for each species. Largest differences between the bulk and the calculated-new biomass POC isotopic compositions occur at approximately 21 days into the growth and the two converge again at day 29 (fig. 3.5). Differences in the isotopic composition of the bulk PON and the calculated-new PON are variable species-to-species and no patterns can be visually distinguished (fig. 3.6).

We then calculated the fractionation factors between the dissolved and particulate fractions of this experiment using Eq. 3.3 and 3.4. Fig. 3.7 shows the permil fractionation factors for both ϵ^{13}C and ϵ^{15}N for all the species and how they change during the growth of the cultures. The ϵ^{13}C appears to be increasing till about 21 days and then decreases again for all species. The ϵ^{15}N for many species appears to increase from 8 to 14 days, then decrease again at 21 days to finally increase again at 29 days. Exceptions to this

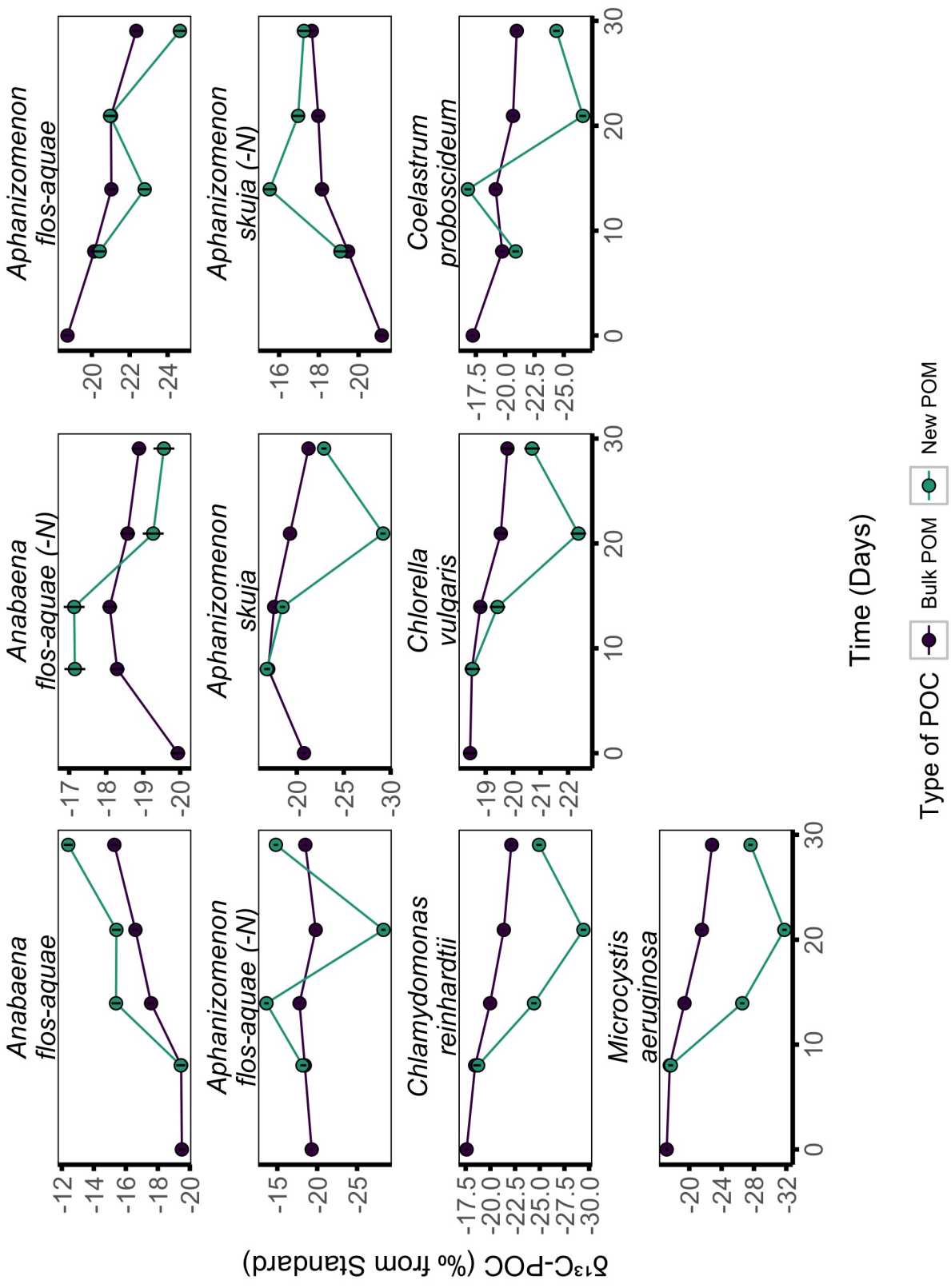

Figure 3.5: δ^{13}C-POC of the measured bulk POC and calculated new POC (from eq. 3.2). Error bars indicate precision for Bulk POM samples, and propagated error for New POM.

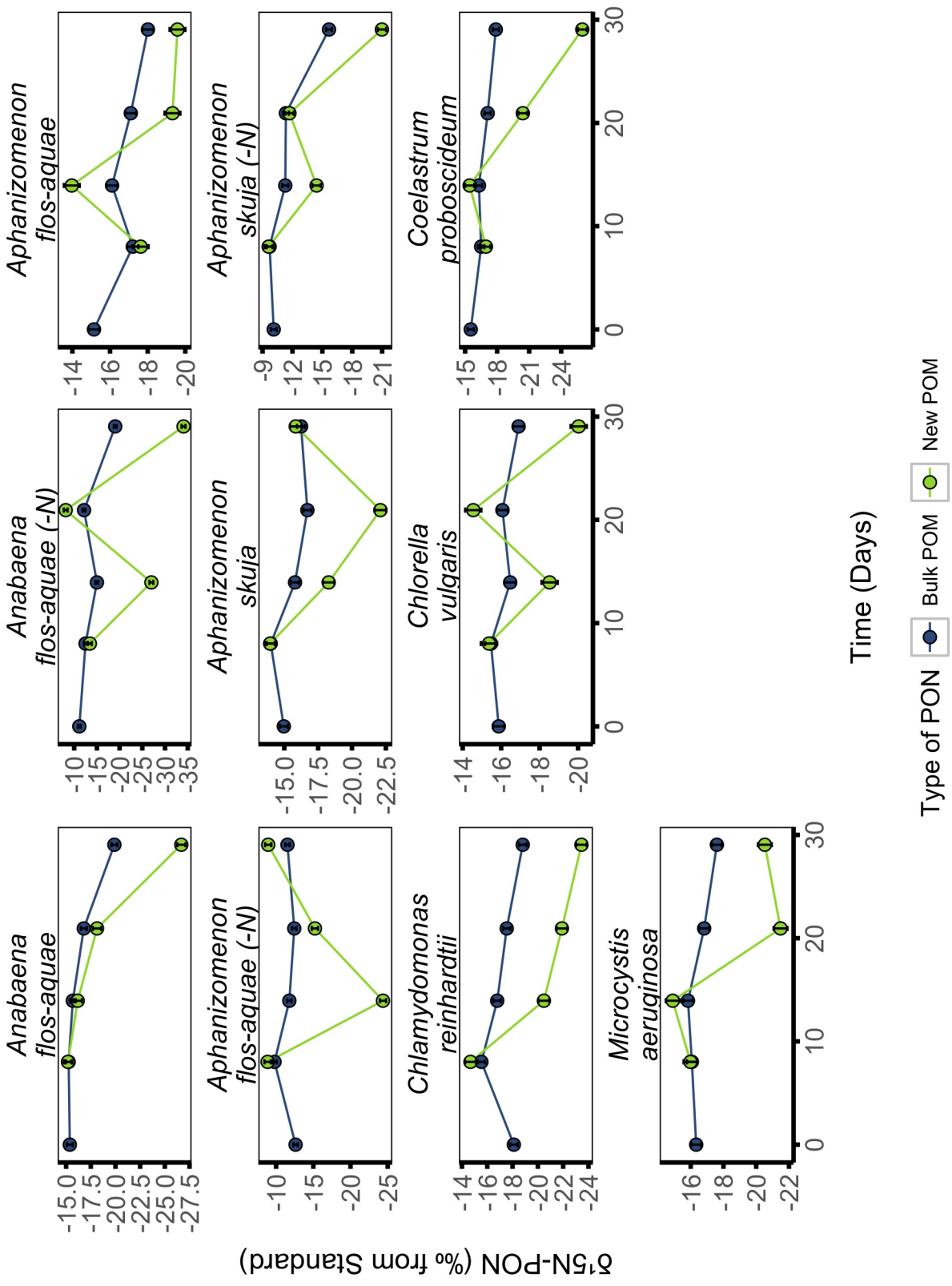

Figure 3.6: δ^{15}N-PON of the measured bulk PON and calculated new PON (from eq. 3.2). Error bars indicate precision for Bulk POM samples, and propagated error for New POM.

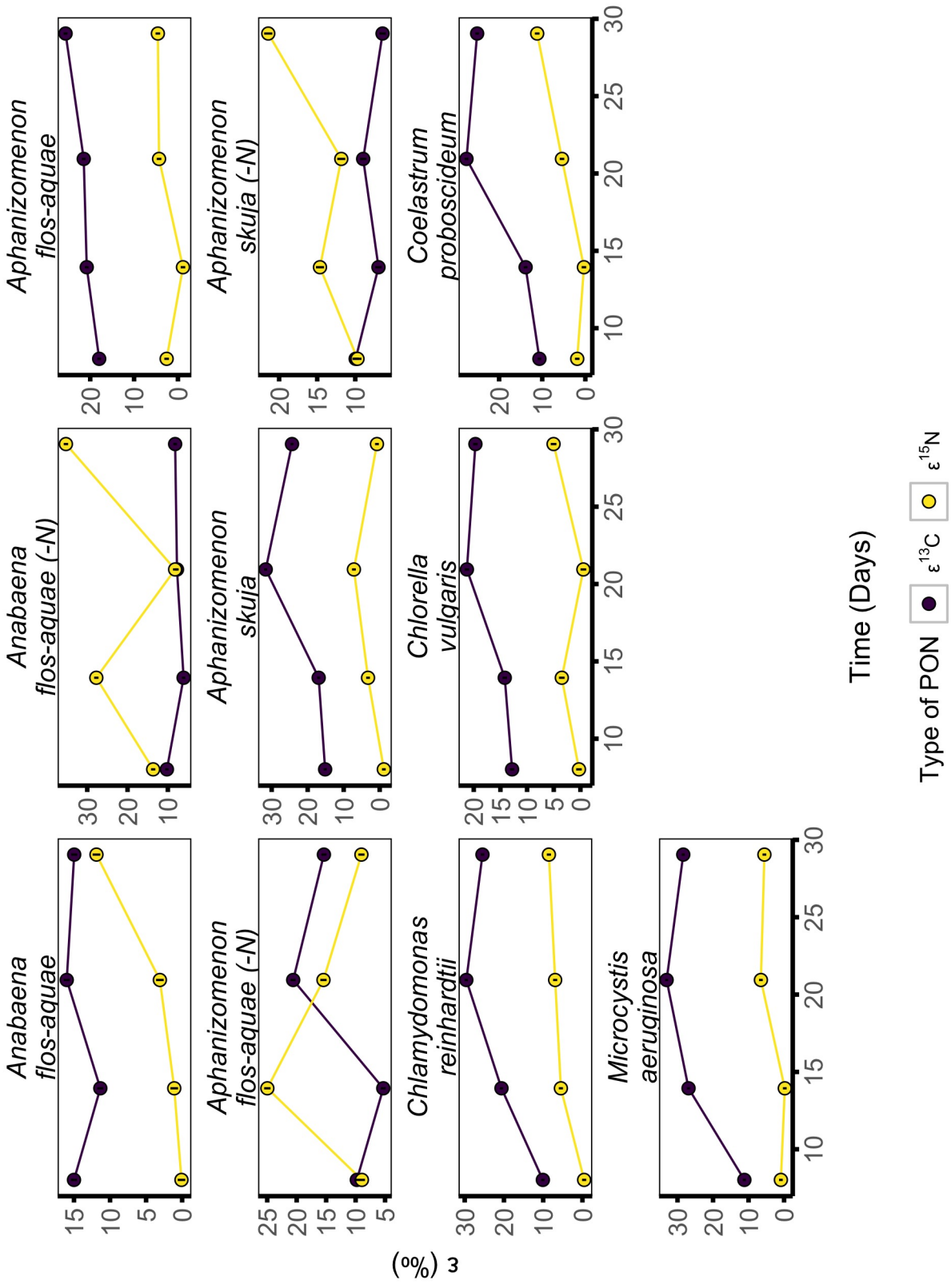

Figure 3.7: The permil fractionation factors (ϵ) between the DIC-POC and DIN-PON in cell culture. Error bars indicate propagated errors from isotopic compositions.

overall pattern in the ϵ^{15}N are *Anabaena flos-aquae* and *Chlamydomonas reinhardtii* which increase as the growth continues.

ϵ	**Species**	**Equation**	$\mathbf{R^2}$
ϵ^{13}C	*Anabaena flos-aquae*	$\mu = 0.2359\epsilon^{-0.293}$	0.0966
	Anabaena flos-aquae (N-Fixing)	$\mu = 0.0215\epsilon^{0.6461}$	0.4311
	Aphanizomenon flos-aquae	$\mu = 103.49\epsilon^{-2.148}$	0.9042
	Aphanizomenon flos-aquae (N-Fixing)	$\mu = 0.2434\epsilon^{-0.352}$	0.2797
	Aphanizomenon skuja	$\mu = 5.6763\epsilon^{-1.034}$	0.7344
	Aphanizomenon skuja (N-Fixing)	$\mu = 0.0176\epsilon^{0.9848}$	0.347
	Chlamydomonas reinhardtii	$\mu = 0.9503\epsilon^{-0.732}$	0.823
	Chlorella vulgaris	$\mu = 5.5462\epsilon^{-1.349}$	0.8203
	Coelastrum proboscideum	$\mu = 0.8167\epsilon^{-0.77}$	0.8321
	Microcystis aeruginosa	$\mu = 0.9544\epsilon^{-0.699}$	0.7583
ϵ^{15}N	*Anabaena flos-aquae*	$\mu = 0.1108\epsilon^{0.065}$	0.8731
	Anabaena flos-aquae (N-Fixing)	$\mu = 0.1215\epsilon^{0.132}$	0.1855
	Aphanizomenon flos-aquae	$\mu = 0.167(\epsilon+2)^{-0.11}$	0.1052
	Aphanizomenon flos-aquae (N-Fixing)	$\mu = 0.1232\epsilon^{0.067}$	0.007
	Aphanizomenon skuja	$\mu = 0.3309(\epsilon+2)^{0.265}$	0.4426
	Aphanizomenon skuja (N-Fixing)	$\mu = 0.9501\epsilon^{0.742}$	0.5271
	Chlamydomonas reinhardtii	$\mu = 0.1532(\epsilon+1)^{0.258}$	0.7941
	Chlorella vulgaris	$\mu = 0.1309(\epsilon+1)^{0.065}$	0.0456
	Coelastrum proboscideum	$\mu = 0.1021\epsilon^{0.156}$	0.3811
	Microcystis aeruginosa	$\mu = 0.1395(\epsilon+1)^{0.251}$	0.4629

Table 3.1: The exponential relationships of ϵ and μ. Any manipulation added to the ϵ is to translate the data towards a positive direction to ensure that no negative ϵ are used when making the regression.

We finally correlated the permil fractionation factors for both C and N to the μ using the power function fit as done by Zhen and Zhu (2018), shown in Table 3.1. The correlation coefficient between ϵ^{13}C and μ are between 0.6 to 1 for all species except the three N-fixing cultures and the nitrate fed *Anabaena flos-aquae*. *Anabaena flos-aquae* and *Chlamydomonas reinhardtii* are the only species with high R^2 values when regressing ϵ^{15}N and μ. Some species required a horizontal translation in ϵ^{15}N to ensure that the data used for the regression are positive in value. *Aphanizomenon flos-aquae* and *Aphanizomenon skuja* (both in N-replete conditions) required all ϵ to increase by 2‰ and *Chlamydomonas reinhardtii*, *Chlorella vulgaris* and *Microcystis aeruginosa* required the increase of 1‰ to all ϵ^{15}N. The regression equations show those manipulations.

3.4 Discussion

This study determined the growth rates, and carbon and nitrogen stable isotopic compositions of the media and laboratory cultures of seven different temperate freshwater phytoplankton taxa using both N-replete and N-fixing conditions for the taxa capable of fixing N_2. We then used a modified mixing-model to determine the stable isotopic composition of the newly created biomass between two sampling events and used that to find the isotopic fractionation factors. We then found the relationship between the growth rates of these species and the carbon and nitrogen fractionation.

Figure 3.1 shows a typical logistic growth curve for the species in this study. Most of the species studied closely follow the logistic growth except for *Aphanizomenon skuja* in nitrogen-fixing and nitrate replete conditions. The N-replete culture follows a dual-limited system, where DIC is low in the beginning of the growth until Fe begins to run low (see fig. 3.2 and B.3). This is seen in the lower $\epsilon^{13}C$ when the DIC concentrations are low in the beginning of the growth. While both DIC and TDN are low in N-fixing cultures, DOC in the media with N-replete cultures increases indicating the growth and death of cells and the release of biologically derived DOM in the process (Loftus and Johnson, 2019).

While growth for the species grown with nitrate appears to follow a predictable pattern, it should be noted that the N-fixing species did not grow much, as evidenced by the low A_{750}. This is most likely due to the use of aquarium bubblers in the cultures to keep the input of CO_2 and N_2 constant during the growth. The increased turbulence from the bubblers resulted in the cyanobacteria not forming stable filaments to grow. This is consistent with the findings from Moisander et al. (2002), which show that *Anabaena* and *Aphanizomenon* carbon and nitrogen fixation activities decrease with increased shearing forces. Bauer et al. (1995) and Herrero et al. (2016) note that in short-filament mutants of *Anabaena*, heterocyst differentiation is often low or completely stopped resulting in very low to no nitrogen fixation by the strains.

Bade et al. (2006) attempted to separate out the algae material from lake water bulk samples and noted that water samples have much more particulate material than

the desired biota from the lake water. The use of eq. 3.2 yielded a δ value for the newly accumulated POM between two sampling events. The difference in the isotopic compositions between the measured bulk-POM and the new POM are noted in figs. 3.5 and 3.6. The differences between these two values indicates that bulk measurements may not be the most accurate representation of the stable isotopic composition.

Determining a relationship between ϵ and μ has been of interest to researchers because that relationship will allow researchers to determine the growth rate of biota in environmental samples without culture work (Burkhardt et al., 1999; Kukert and Riebesell, 1998; Laws et al., 1997; Tanaka et al., 2008; Zhen and Zhu, 2018). This study adds to this knowledge by using the power function model of relationship used by Zhen and Zhu (2018) and applying it to the ten species and variants used in this study for both ϵ^{13}C and ϵ^{15}N. All species grown in nitrate, except *Anabaena flos-aquae*, show a moderate to good correlation of the μ to ϵ^{13}C. We used a similar correlation model as Zhen and Zhu (2018), who found that $\mu = 1.32(1 + \epsilon)^{-0.52}$ for *Microcystis* from Lake Taihu. If the relationship of the Lake Taihu *Microcystis* is to be compared with the relationship of *Microcystis aeruginosa* presented in this study, the two equations follow a similar pattern. However, the Lake Taihu strain consistently indicated that it had a higher growth rate than the strain in this study.

We also explored the relationship of μ with ϵ^{15}N and we did not observe good correlations. This may be because phytoplankton growth and decay play a large role in the process of N-uptake and release, resulting in the δ^{15}N of the medium that is variable during the culture process (Peterson et al., 2001; Zhen and Zhu, 2018). This makes it very difficult to establish a relationship of ϵ^{15}N and μ. In this study, we did not measure the δ^{15}N-DIN and it was assumed to be constant either because the TDN concentrations were very high or because there was no nitrate added.

In this study we found the relationships of ϵ of newly accumulated biomass and the growth rate of freshwater phytoplankton in culture. We show that using ϵ^{13}C can give reasonably good correlations with the μ. However, to use this method in the field to study phytoplankton bloom growth, a few considerations will have to be made; what

is the medium in which the phytoplankton are grown to establish these relationships, what species are studied and do they reflect the biological make-up of the environment in question, and what is the relationship of ϵ^{13}C and μ of N-fixing species which are limited by N throughout the growth.

3.5 Conclusion

The goal of this study was to differentiate the isotopic composition of the newly accumulated POM from the measured bulk sample and to examine if a correlation exists between the growth rates of the phytoplankton species and the isotopic fractionation factors. We did this by using a mixing-model calculation to determine the isotopic composition of the newly accumulated biomass from the bulk sample shown in eq. 3.2. We saw that the newly calculated isotopic composition for the biomass can be as much as 15‰ different than the bulk sample.

We then used the newly determined isotopic fractionation factors to develop relationships between the growth rate of the phytoplankton species and the isotopic fractionation factors. We found that moderate to good correlations ($R^2 > 0.7$) can be found with the growth rates of phytoplankton when grown with nitrogen and the ϵ^{13}C.

We show that by using these models it can be possible to determine growth rates of environmental samples without resorting to laboratory studies by using this model and this method. However, more work needs to be done to better this process, focusing particularly on N-fixing species.

Chapter 4

Inhibitory Effect of Ferrozine on Phytoplankton Growth

Abstract

Cyanobacterial harmful algal blooms (cHABs) are an increasing and costly problem in inland waters. These algal blooms cause economic and health damage through production of foul compounds and toxins. Fe is an important micronutrient needed for many biochemical pathways in phytoplankton. Cyanobacterial dominance of phytoplankton is strongly affected by sediment redox and it is thought that the link between redox and cyanobacteria dominance may be redox control of the availability of Fe(II). This study examined inhibition of the growth of cyanobacterial and chlorophyte cultures by the Fe(II)-chelator, ferrozine (FZ) to further inform on the possible role of Fe(II) in cHAB formation. However, FZ additions to cell culture medium at eight different FZ:Fe molar ratios ranging from 0.1 to 2000 did not inhibit the growth of cyanobacteria significantly possibly due to the availability of Fe(II) due to photoreduction.

4.1 Introduction

Phytoplankton are a large diverse group of organisms that include chlorophytes, cyanobacteria, diatoms and more (Simon et al., 2009). Their roles in nature are as

diverse as their classifications. Some types of phytoplankton are N-fixers, calcifiers, toxin producing or silicieous (Mutshinda et al., 2016). Harmful algal blooms (HABs) and specifically cHABs in inland waters are an increasing problem (Pick, 2016). These blooms pose a serious risk to public health and water quality (Downing et al., 2001).

cHABs have been associated with the availability of nutrients, specifically P (Kane et al., 2014; Schindler, 1974). This has prompted efforts to control the loading P in lakes since the late 1970s (Dolan and McGunagle, 2005). However, there has been a persistence and increasing occurrences of HABs reported even in systems where P concentrations are low necessitating better management practices that go further than P control (Pick, 2016; Verschoor and Molot, 2013; Winter et al., 2011). Existing evidence points to the importance of Fe(II) availability as a potential control for cHABs (Molot et al., 2010; Kranzler et al., 2014). Fe is an important micronutrient in cells because it is used in major biochemical pathways (Shi et al., 2007). It is known that cyanobacteria have a higher demand of Fe than their eukaryotic counterparts and can only transport Fe(II) into the cells (Sunda and Huntsman, 2015; Molot et al., 2014). Thus, cyanobacterial growth can be limited by Fe(II) access unless supply rates are high. Cyanobacteria have several strategies to ensure that even in low Fe environments, the requirements can be met. These include creation and excretion of siderophores, which have high affinities for Fe, these bind to extracellular Fe and then the whole siderophore-Fe complex is transported into the cell (Kranzler et al., 2011). Another strategy is to reduce Fe(III) to Fe(II) at the plasma membrane and the subsequent uptake of the Fe(II) (Lis et al., 2015).

Ferrozine (FZ, 3-(2- pyridyl)-5,6-bis(4-phenylsulfonic acid)-1,2,4-triazine) is a colourless iron-binding complex which turns purplish when bound to Fe(II) (Fig. 4.1) (Stookey, 1970). Ferrozine has been used to quantify amount of Fe(II) colourometrically because it preferentially binds Fe(II) over Fe(III) (Stookey, 1970; Verschoor and Molot, 2013) and has also been used to probe Fe(II) transport in cyanobacteria (Shaked et al., 2004; Kranzler et al., 2011; Lis et al., 2015). Previous work by Molot et al. (2010) showed that cyanobacteria are more sensitive to oxine (8-hydroxyquinoline), a strong Fe oxidizing chelator, than chlorophytes when oxine was added to mesocosms.

The objective of this study was to determine whether FZ could be used as an Fe(II)-removing agent to shift phytoplankton dominance from cyanobacteria to chlorophytes. This experiment was conducted by growing laboratory cultures of five different species of cyanobacteria and chlorophytes at different ratios of FZ to Fe.

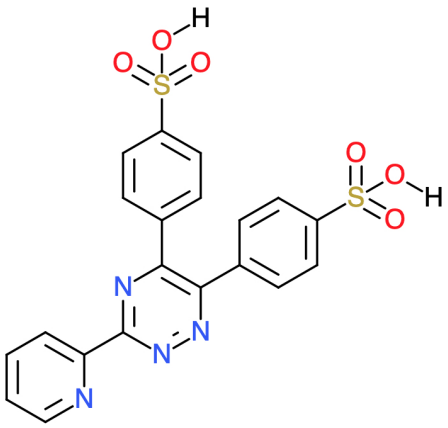

Figure 4.1: Chemical structure of Ferrozine

4.2 Materials and Methods

4.2.1 Experimental Organisms and Growth Conditions

Cultures of *Anabaena flos-aqaue* (CPCC 67), *Aphanizomenon skuja* (isolate from Lake 227, ELA), *Chlamydomonas reinhardtii* (CPCC 243), *Chlorella vulgaris* (CPCC 90), and *Microcystis aeruginosa* (PCC 7005) were grown at 20°C on a 12:12h light/dark cycle at 100 μmol/m^2/s in either BG-11 or BBM media containing varying molar ratios of Fe (as $FeCl_3$) and FZ (Table 4.1) (Rippka et al., 1979; Stein et al., 1973). N was added at a final concentration of 17.6mM in BG-11 and 2.9mM in BBM and P was added at a final concentration of 0.23mM in BG-11 and 1.72mM in BBM and both media contained EDTA at concentration of 2.6μM in BG-11 and 27μM in BBM.

FZ:Fe ratios of 2000:1, 200:1 and 20:1 were used along with the others to mimic ratios used in previous studies (Kranzler et al., 2011), who found inhibition of Fe uptake in the unicellular *Synechocystis* sp. PCC 6803. The Fe(II)FZ_3 complex is pH sensitive and to maintain the pH between 7.8-8.1 (Lis et al., 2015), pH was measured and adjusted

with 0.1M HCl if pH > 8.1 or with 0.1M NaOH if pH < 7.8. All cultures were grown in duplicate.

Table 4.1: FZ to Iron molar ratios

Conc. Fe(μM)	Conc. FZ (μM)	FZ:Fe Molar Ratio
3	0	0:1
3	9	3:1
15	9	3:5
3	30	10:1
45	30	10:15
0.1	200	2000:1
1	200	200:1
10	200	20:1

4.2.2 Monitoring Growth

Growth was assayed by taking absorbance at 750nm (A_{750}) using a Cary 100 spectrophotometer. A_{750} was selected for analysis of phytoplankton growth absorption at 750nm by photosynthetic pigments is minimal and is good indicator of particulate matter (Borowitzka and Moheimani, 2013). A_{750} was used to compare growths at different molar ratios of FZ:Fe in each species. Absorbance was converted into cell numbers for each species by using previously determined linear relationships of absorbance to cell number for each species (see Appendix A).

Growth rates (μ) were found for each incubation were found using the *growthcurver* (version 0.3.0) package in R (Sprouffske and Wagner, 2016). Statistical differences in the mean growth rates within each species were found by using an ANOVA followed by a Tukey's HSD.

4.3 Results

Figures 4.2 - 4.6 show the change in cell number with time of the species studied at different FZ:Fe ratios. While there are no incubations where there is no growth, it appears as if growth is lower at FZ:Fe of 2000:1 and 200:1 in most of the species.

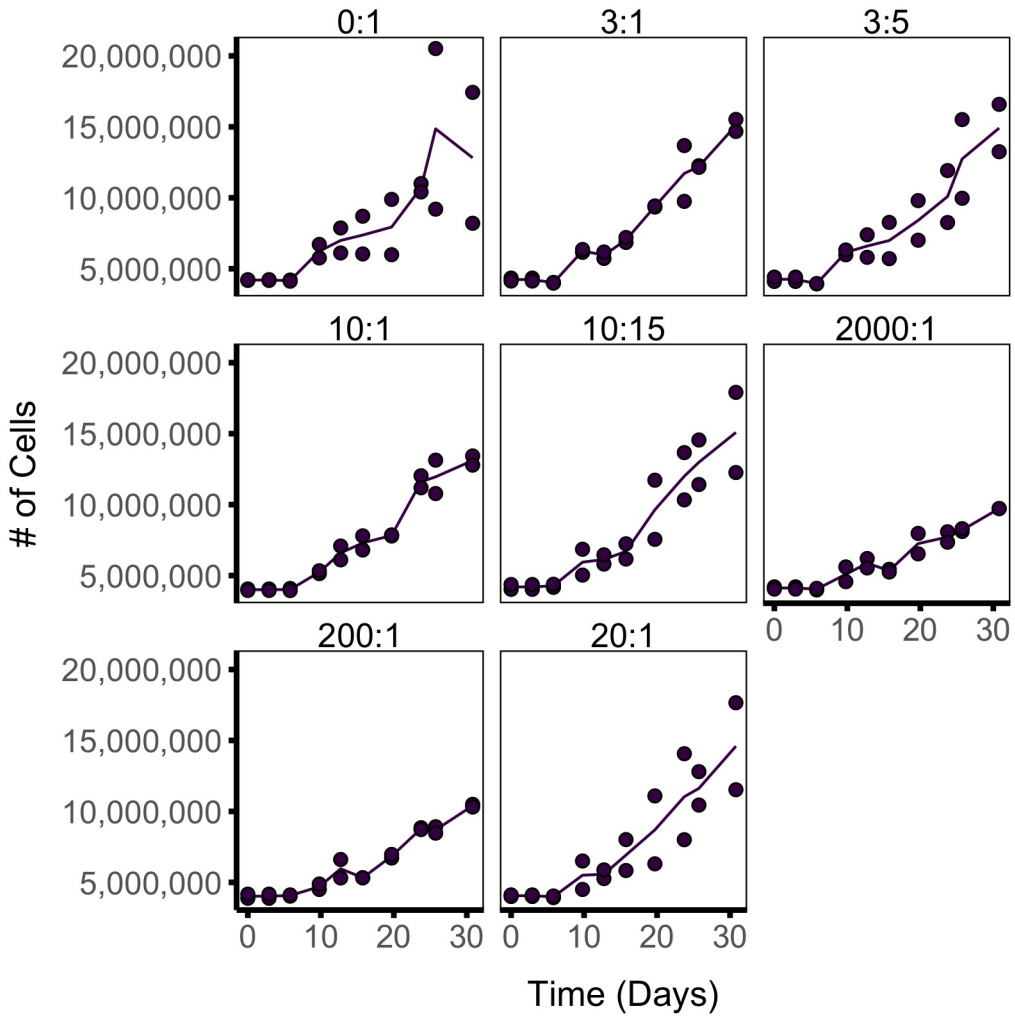

Figure 4.2: Growth of *Anabaena flos-aquae* in different molar ratios of FZ:Fe. Line connects mean cell numbers and points are duplicate measurements of each of two incubations.

Fig. 4.7 shows the growth rates of the studied species at the different FZ:Fe molar ratios. The lettered groupings obtained as a results of a Tukey's HSD compares the growth rates at varying FZ:Fe molar ratios within each species separately. The growth rates for *Anabaena flos-aquae*, *Aphanizomenon skuja*, *Chlamydomonas reinhardtii* and *Microcystis aeruginosa* are not significantly different from one another at any FZ:Fe molar ratio. The growth rates for *Chlorella vulgaris* are variable. Visual inspection of the Fe concentrations does not show an apparent pattern.

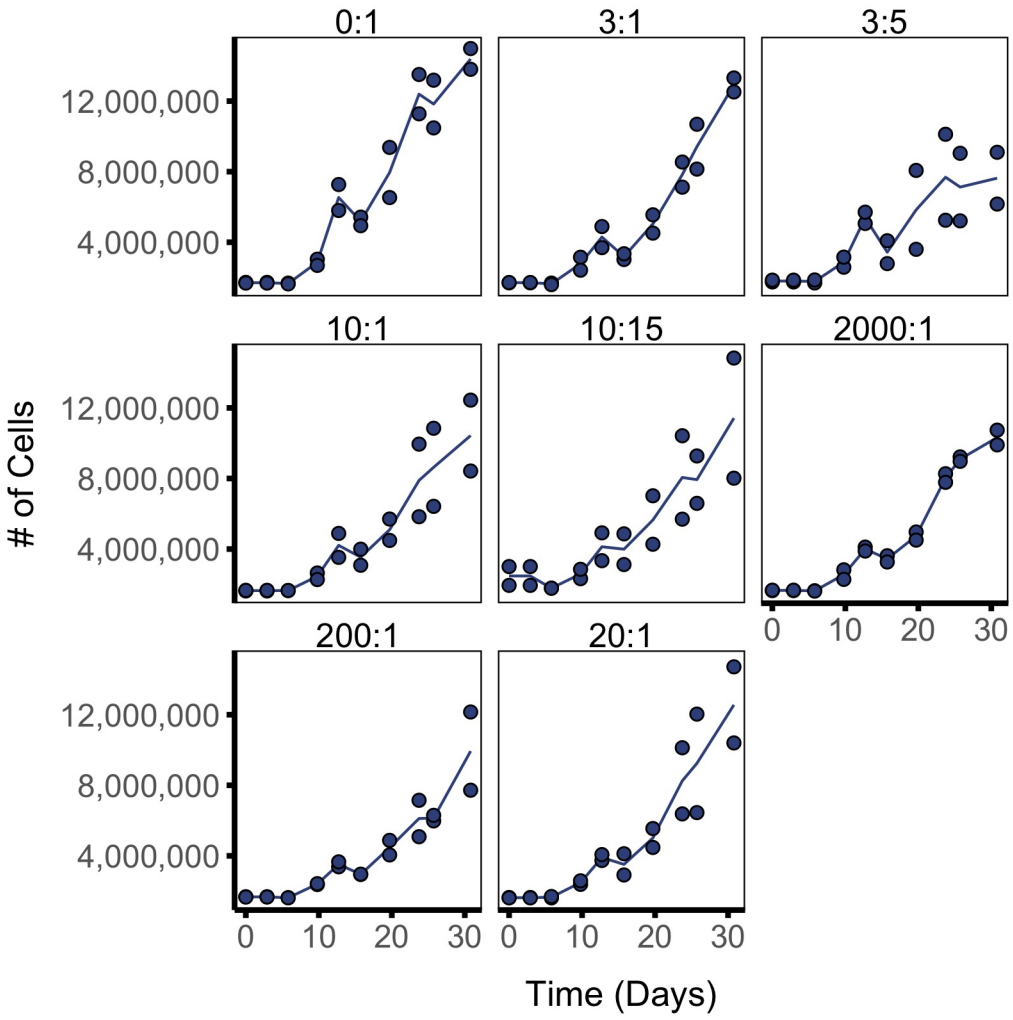

Figure 4.3: Growth of *Aphanizomenon skuja* in different molar ratios of FZ:Fe. Line connects mean cell numbers and points are duplicate measurements of each of two incubations.

4.4 Discussion

Figures of growth for each species (Figs 4.2 - 4.6) and 4.7 do not show any significant difference in the growth patterns of any of the phytoplankton species studied except for the growth rates of *Chlorella vulgaris*. As cyanobacteria are strongly dependent on Fe(II) (Kranzler et al., 2014), the growth rates of cyanobacteria (*Anabaena flos-aquae*, *Aphanizomenon skuja*, and *Microcystis aeruginosa*) but not the eukaryotic algae (*Chlamydomonas rienhardtii* and *Chlorella vulgaris*) were expected to be inhibited at high molar ratios of ferrozine, e.g., higher than 10.

There are a few possible explanations why the growth of cyanobacteria in this study

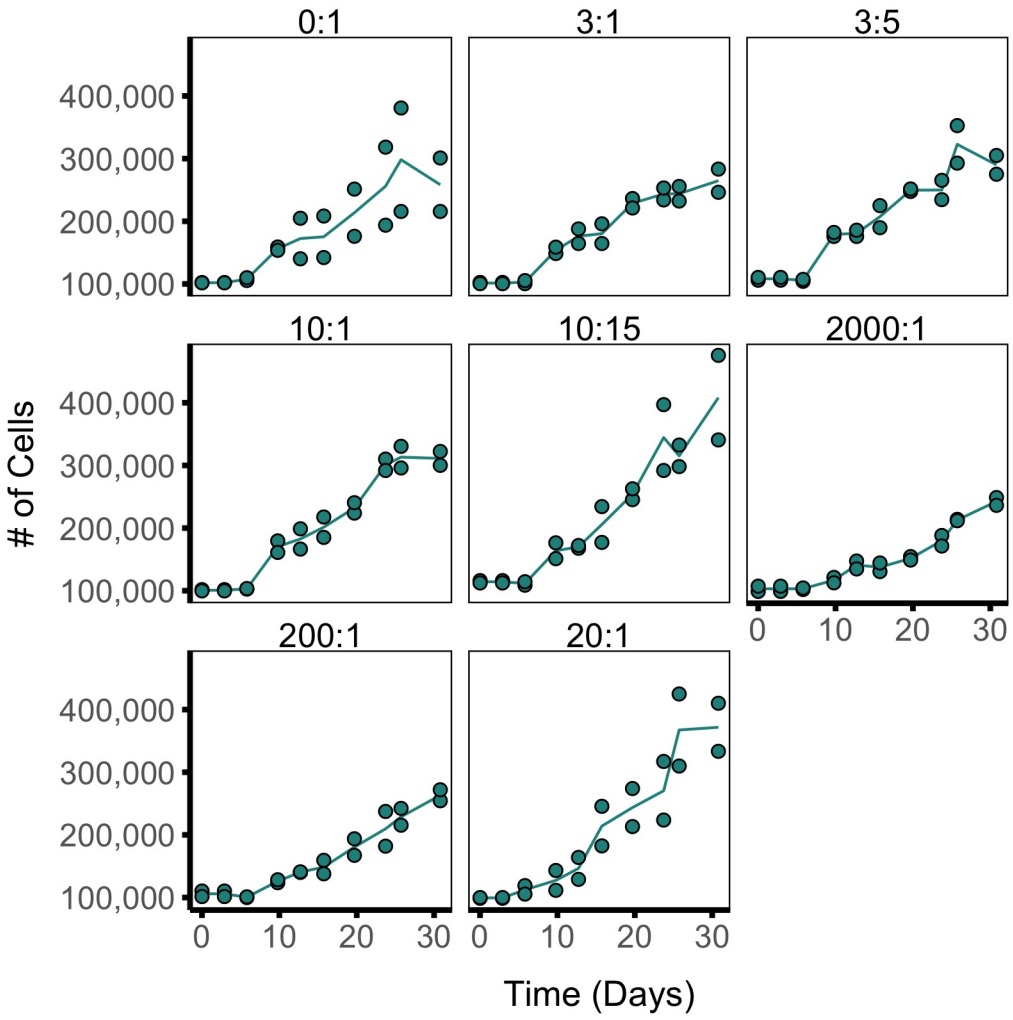

Figure 4.4: Growth of *Chlamydomonas reinhardtii* in different molar ratios of FZ:Fe. Line connects mean cell numbers and points are duplicate measurements of each of two incubations.

was not inhibited by the addition of FZ in contrast to inhibition of *Synechocystis* (Kranzler et al., 2011). Perhaps the filamentous and colonial cyanobacteria strains used in this study were able to scavenge Fe(II) with a ferrous siderophore that competed with ferrozine or perhaps they have an ability to use ferrozine-bound Fe as a potential source of Fe(II), reflecting a siderophore-like uptake (Kranzler et al., 2011). Another possible reason for this result could be that EDTA, the chemical chelator which is used in media keep metallic salts in solution could be out-competing the FZ for the available Fe-pool and the phytoplankton could get iron through EDTA-chelation (see Ch.5) (Rippka et al., 1979; Stein et al., 1973).

Kranzler et al. (2011) found contradictory results to this study using the unicellular

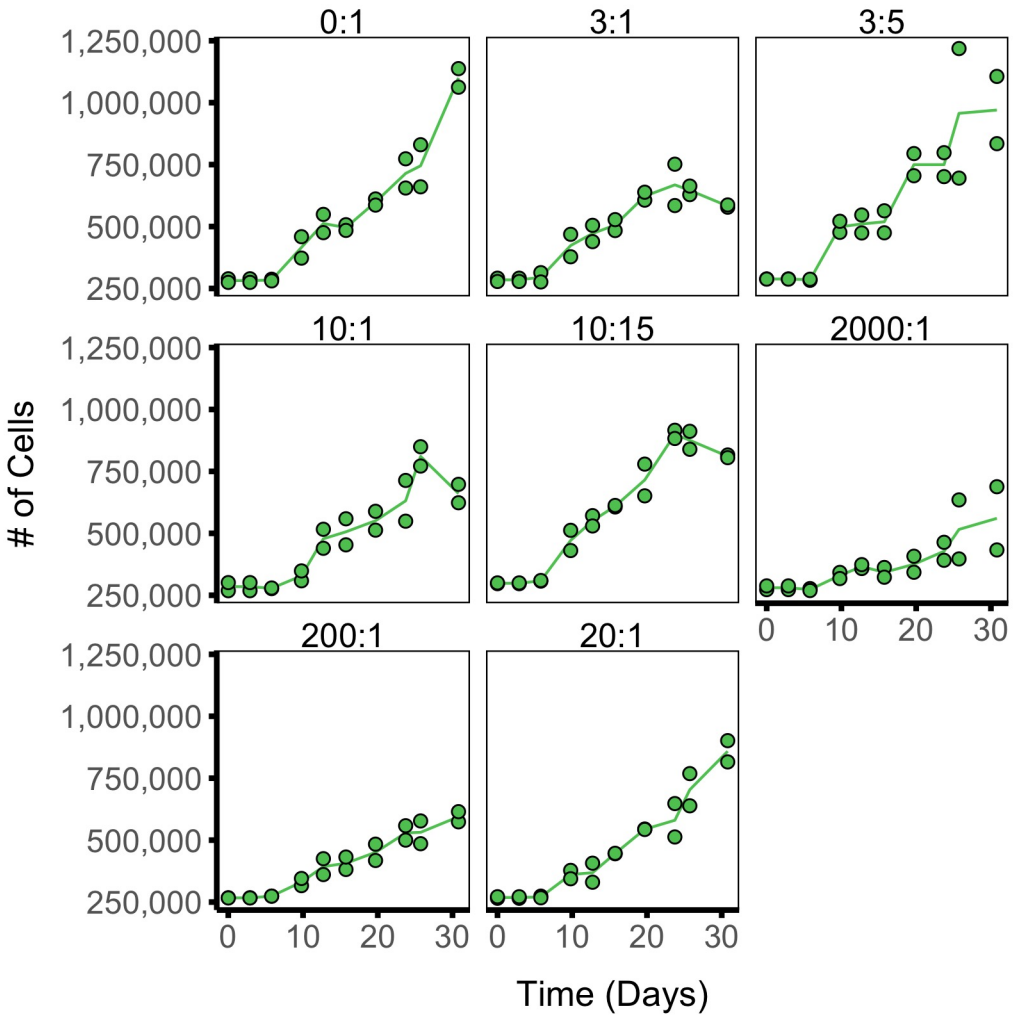

Figure 4.5: Growth of *Chlorella vulgaris* in different molar ratios of FZ:Fe. Line connects mean cell numbers and points are duplicate measurements of each of two incubations.

cyanobacterium, *Synechocystis* sp. strain PCC 6803. This could be due to the differences in growth conditions used. To reduce the photoreduction of Fe, Kranzler et al. (2011) used red light growth conditions, while we used full spectrum lighting to mimic environmental light conditions. The photoreduction of Fe, even at lower concentrations may have been enough Fe(II) for the cyanobacteria used in this study to grow from.

4.5 Conclusion

The goal of this study was determine if FZ could be used to remove Fe(II) in cell media to inhibit the growth of cyanobacteria but not eukaryotic algae. We found that

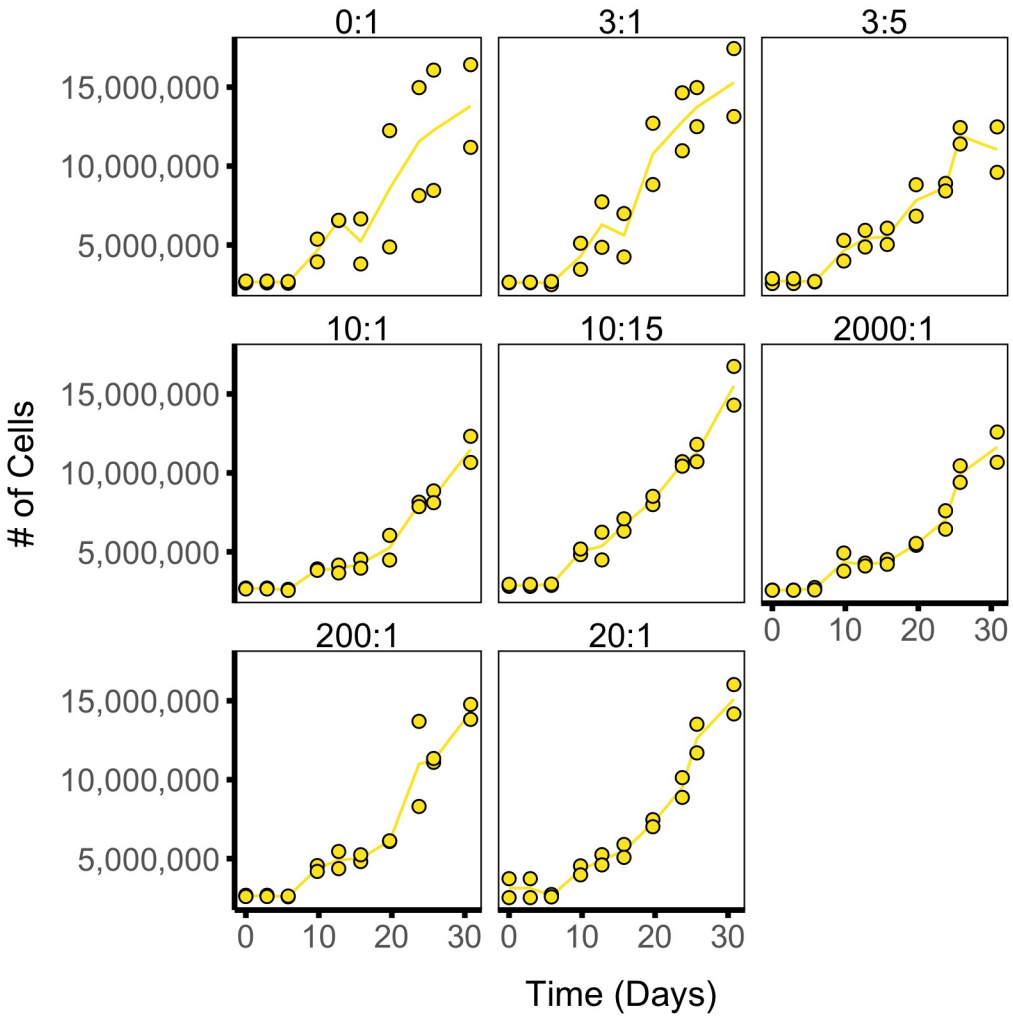

Figure 4.6: Growth of *Microcystis aeruginosa* in different molar ratios of FZ:Fe. Line connects mean cell numbers and points are duplicate measurements of each of two incubations.

addition of FZ at eight different FZ:Fe ratios had no significant difference on the growth of cyanobacterial species. This finding is in contradiction of Kranzler et al. (2011), perhaps because of the different species that were studied or through the photoreduction of Fe(III) to Fe(II).

Further work is required to study the efficacy and the impacts of Fe(II) removing agents on HABs using conditions that are representative of the environment.

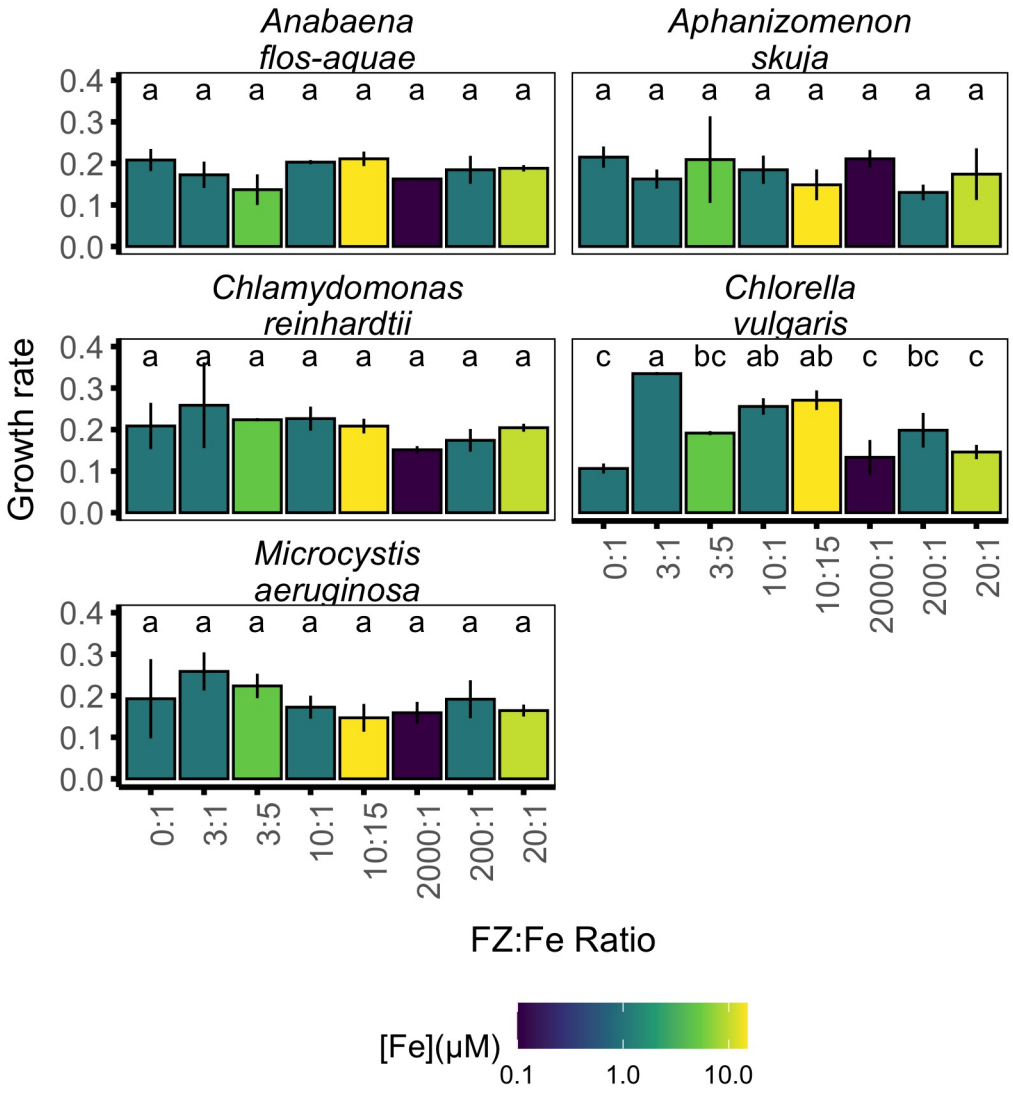

Figure 4.7: Growth rates for each species grown at various FZ:Fe ratios. Colour indicates concentration of Fe, error bars are standard deviation from the mean and lettered groupings indicate statistically different mean growth rates for each species found by an ANOVA.

Chapter 5

Indirect Measurements of Fe-Chelation Strengths of EDTA and Citrate using Ferrozine for use in Cell Culture

Abstract

Iron is an important micronutrient involved in many different biochemical processes. This makes Fe a key ingredient in cell culture to ensure the growth of the organisms being studied. EDTA and citrate have been used in cell culture media as chelators to keep metal ions soluble and bioavailable. However, EDTA has been reported to inhibit growth of some species in cell culture because it is an oxidant. This study evaluated the relative impacts of EDTA and citrate on the formation of the colourimetric iron-binding complex, ferrozine (FZ). We found that citrate had no significant ($p < 0.05$) impact on colour formation of FZ while EDTA did, most likely because it is an oxidizing agent rather than a competitor for Fe(II). Citrate also binds other trace metals, so it may be better suited to culture studies involving Fe(II) than the more widely used EDTA.

5.1 Introduction

Iron is one of the most important elements for the growth of organisms. It has a key role in important cellular functions like cellular respiration, photosynthesis and N-fixation (Shi et al., 2007). Despite being one of the most abundant elements on Earth, iron sometimes limits growth of plants and algae (Kean et al., 2015). This is because in oxygenated environments, Fe exists primarily as Fe(III), which is not very soluble unless bound to an organic chelator, thus rendering it unavailable for uptake by many species (Stumm and Morgan, 1995; Miles and Brezonik, 1981).

Ethylenediaminetetraacetic acid (EDTA) is a molecule which is synthetic, organic and polyprotic with the ability to form strong bonds with metal cations in solution, making the cations soluble (Willet and Rittmann, 2003). It is known that EDTA increases solubility of trace metals and is essential in cell culture for good growth of cells (Waris, 1953; Krauss, 1955; Satpati et al., 2016). While EDTA is non-toxic to humans, it has been found to inhibit growth of cells in certain situations (Willet and Rittmann, 2003; Andersen, 2005). EDTA can bind to Zn so effectively that Zn can be unavailable for cellular uptake and use in DNA synthesis (Saryan and Petering, 1980). In another study, it was noted that EDTA's non-specific metal-binding might stop the growth of biofilms (Chudzik et al., 2007). It is possible that in certain instances, EDTA might be too strong of a chelator for a species to gain access to EDTA-bound trace metals, such as Fe, especially if the EDTA/Fe ratio is high. EDTA has different affinities for forming the metal-EDTA complexes and these are known.

Table 5.1: Formation constants (K_f) for metal-EDTA complexes. This constant is the equilibrium constant for the reaction $M^n + Y^{4-} \rightleftharpoons MY^{n-4}$. All values apply at 25°C and ionic strength of 0.1M unless indicated otherwise. *a*. 20°C, ionic strength = 0.1M, *b*. 20°C, ionic strength = 1M. Table from Harris (2010).

K_f for Metal-EDTA complexes							
Ion	**log K_f**	**Ion**	**log K_f**	**Ion**	**log K_f**	**Ion**	**log K_f**
Li^+	2.95	Fe^{2+}	14.3	Tl^+	6.41	Pm^{3+}	16.9
Na^+	1.86	Co^{2+}	16.45	Pd^{2+}	25.6[a]	Sm^{3+}	17.06

Continuation of Table 5.1							
Ion	**log K_f**	**Ion**	**log K_f**	**Ion**	**log K_f**	**Ion**	**log K_f**
K^+	0.8	Ni^{2+}	18.4	Zn^{2+}	16.5	Eu^{3+}	17.25
Be^{2+}	9.7	Cu^{2+}	18.78	Cd^{2+}	16.5	Gd^{3+}	17.35
Mg^{2+}	8.79	Ti^{3+}	21.3	Hg^{2+}	21.5	Tb^{3+}	17.87
Ca^{2+}	10.65	V^{3+}	25.9[a]	Sn^{2+}	18.3[b]	Dy^{3+}	18.3
Sr^{2+}	8.72	Cr^{3+}	23.4[a]	Pb^{2+}	18	Ho^{3+}	18.56
Ba^{2+}	7.88	Mn^{3+}	25.2	Al^{3+}	16.4	Er^{3+}	18.89
Ra^{2+}	7.4	Fe^{3+}	25.1	Ga^{3+}	21.7	Tm^{3+}	19.32
Sc^{3+}	23.1[a]	Co^{3+}	41.4	In^{3+}	24.9	Yb^{3+}	19.49
Y^{3+}	18.08	Zr^{4+}	29.3	Tl^{3+}	35.3	Lu^{3+}	19.74
La^{3+}	15.36	Hf^{4+}	29.5	Bi^{3+}	27.8[a]	Th^{4+}	23.2
V^{2+}	12.7[a]	VO^{2+}	18.7	Ce^{3+}	15.93	U^{4+}	25.7
Cr^{2+}	13.6[a]	VO_2^+	15.5	Pr^{3+}	16.3		
Mn^{2+}	13.89	Ag^+	7.2	Nd^{3+}	16.51		
End of Table							

Citrate, first isolated in 1874, is a common molecule that has biological relevance. It is found ubiquitously from lemons to human teeth in large proportions (Glusker, 1980). Citric acid is a weak chelating agent of various trace metals, including Fe (Patterson, 1987). In bacteria, citric acid can function as an iron-scavenging siderophore. Siderophores like rhizoferrin and staphyloferrin A have a citric acid molecular backbone in the chelation site of the siderophores (Silva et al., 2009). Both citrate and EDTA are used in cell culture media because they can bind metal ions and keep them soluble and bioavailable (Klein and Manos, 1960; Gour et al., 2018; Andersen, 2005).

Ferrozine (FZ) is an iron-binding complex, specifically binding to Fe(II) (Stookey, 1970). FZ has been used in colourimetric assays to quantify Fe(II) and total Fe (Verschoor and Molot, 2013; Jones and Lee, 2020). FZ has an absorption maximum at 562nm (ε = $2.79\times10^4 mol^{-1}\cdot L\cdot cm^{-1}$) (Stookey, 1970). This colourimetric property of FZ can be used

to estimate relative strengths of other Fe chelators compared to FZ.

The objective of this study was to evaluate the relative impacts of EDTA and citrate on the formation of the FZ-Fe complex. The goals are to understand how EDTA and citrate impact the oxidation of Fe in solution.

5.2 Materials and Methods

A solution of 10 mg/L of Fe (as $FeCl_3$•6 H_2O, Sigma-Aldrich 236489) with 100 mg/L of FZ (Sigma-Aldrich 160601) had either EDTA (Sigma-Aldrich 324503) or citrate (Sigma- Aldrich 71498) added to it in final concentrations of either 10mg/L, 100mg/L or 1000mg/L. One set of solutions had L-ascorbic acid (Sigma-Aldrich 255564) added it to a final concentration of 10% w/v to reduce the Fe(III) to Fe(II) at pH 3. For controls, FZ, Fe with L-ascorbic acid, and FZ with Fe were made and absorbance measurements were blanked with either Fe only, or Fe and L-ascorbic acid only blanks. All solutions were left at room temperature overnight and made in triplicate. After incubation, absorbance at 562nm and pH was recorded. The pH was maintained close to 3 in Fe(II) solutions and between 4 and 5.9 in Fe(III) solutions.

After analysis, a pair-wise two-way ANOVA was conducted grouped by the redox state of Fe, chelator used and concentration of chelator followed by a post-hoc Tukey's HSD.

5.3 Results

Table 5.2 and Fig. 5.1 show the average pH and the average absorbance at 562nm of the various samples. Absorbance at 562nm was higher in the presence of L-ascorbic acid, indicating reduction of Fe(III) by the reagent. Some Fe(II) was produced without ascorbic acid, perhaps from photoreduction generated from overhead lights. In all samples, citrate did not have a significant affect on the absorbance while EDTA lowered the absorbance.

Table 5.3 shows the summary of the pair-wise two-way ANOVA by redox state (containing L-ascorbic acid or not), competitor used (EDTA or citrate) and concentration

Table 5.2: Average absorbance at 562nm corresponding to relative amounts of Fe bound to FZ of samples containing EDTA or citrate at various concentrations. Standard deviation indicated by ± of n = 3. Fe(II) redox state was obtained by adding L-ascorbic acid, ± indicates standard deviation. ANOVA groupings indicate statistically different mean absorbance for each treatment found by a two-way ANOVA followed by a Tukey's HSD.

Fe Redox State	Competing Chelator	Conc. Chelator (mg/L)	pH	Avg. Abs @ 562nm	ANOVA grouping
Fe(II)	FZ-Fe Control	0	3.04 ± 0.05	1.5961 ± 0.0238	A
Fe(II)	Citrate	10	2.99 ± 0.01	1.5400 ± 0.0545	A
Fe(II)	Citrate	100	3.06 ± 0.06	1.6048 ± 0.0309	A
Fe(II)	Citrate	1000	3.15 ± 0.08	1.5932 ± 0.0800	A
Fe(II)	EDTA	10	3.01 ± 0.01	1.0699 ± 0.0806	B
Fe(II)	EDTA	100	3.02 ± 0.02	0.2724 ± 0.0934	C
Fe(II)	EDTA	1000	3.07 ± 0.06	0.0955 ± 0.0081	D
Fe(III)	FZ-Fe Control	0	5.94 ± 0.12	0.7033 ± 0.0624	E
Fe(III)	Citrate	10	5.11 ± 0.13	0.7025 ± 0.0282	E
Fe(III)	Citrate	100	4.48 ± 0.04	0.6673 ± 0.0150	E
Fe(III)	Citrate	1000	4.26 ± 0.02	0.6806 ± 0.0185	E
Fe(III)	EDTA	10	5.94 ± 0.03	0.0263 ± 0.0113	F
Fe(III)	EDTA	100	5.74 ± 0.06	0.0376 ± 0.0088	F
Fe(III)	EDTA	1000	5.42 ± 0.01	0.0189 ± 0.0050	F

of competitor (10, 100, or 1000mg/L). The results indicate that all three of these categorizations were significantly different from one another.

Table 5.3: Output of ANOVA comparing absorbance at 562 of FZ to different competitors, at different concentrations and of different Fe redox state

term	df	sumsq	meansq	statistic	p.value
IronRedox	1	5.22	5.22	2309	1.89×10^{-28}
Competitor	2	8.01	4.01	1772	3.30×10^{-30}
Conc.Comp	2	0.378	0.189	83.68	1.54×10^{-12}
IronRedox:Competitor	2	0.506	0.253	111.8	4.45×10^{-14}
IronRedox:Conc.Comp	2	0.333	0.166	73.63	7.06×10^{-12}
Competitor:Conc.Comp	2	0.433	0.216	95.70	3.04×10^{-13}
IronRedox:Competitor:Conc.Comp	2	0.482	0.241	106.7	7.98×10^{-14}
Residuals	28	0.0633	0.00226		

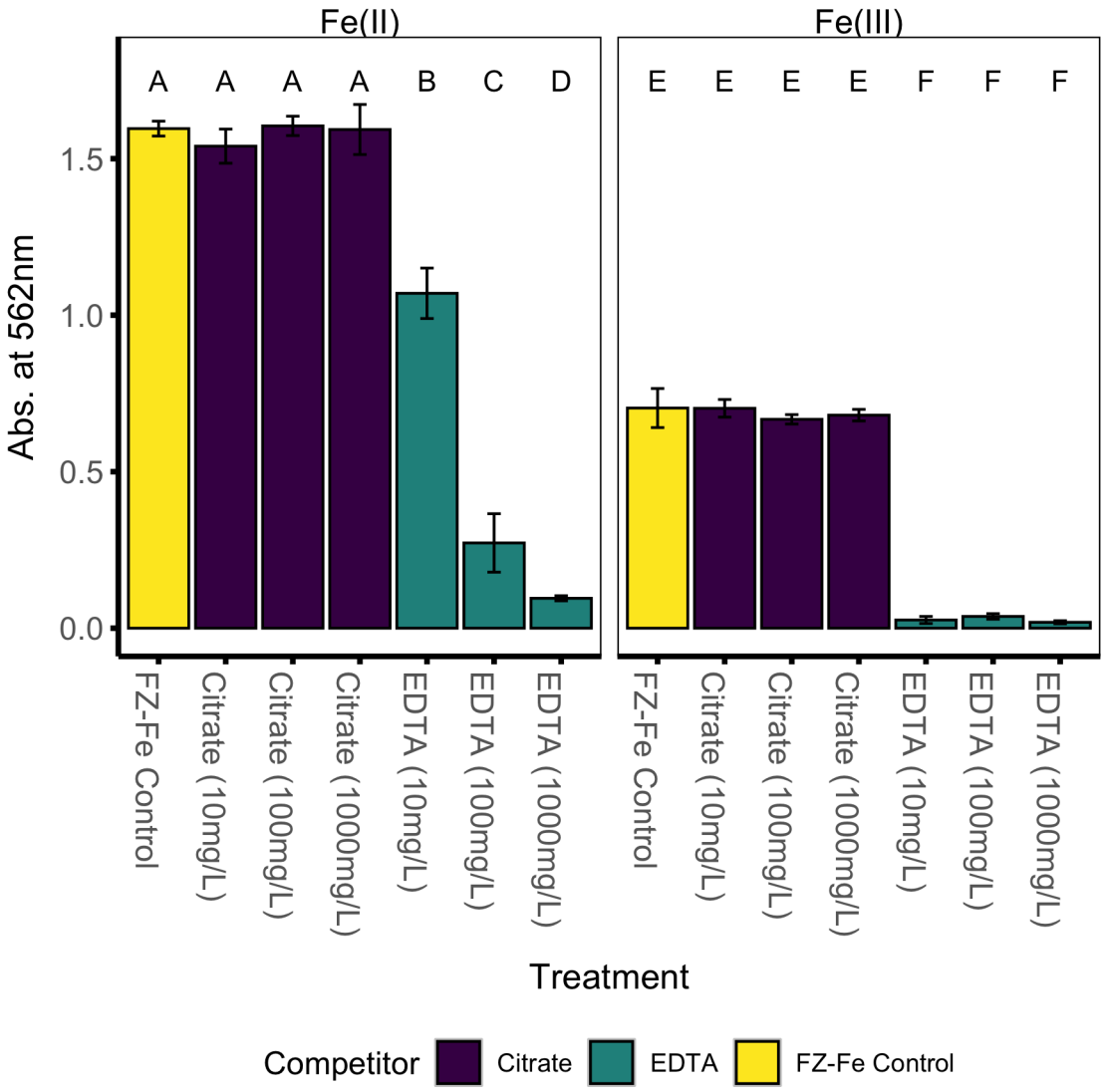

Figure 5.1: Average absorbance at 562nm of FZ with different competitors added at varying concentrations. Lettered groupings indicate statistically different ($p < 0.05$) means as shown by the pair-wise two-way ANOVA followed by a Tukey's HSD (results in Table 5.2). Error bars indicate standard deviation in replicate absorbance measurements

5.4 Discussion

L-ascorbic acid is a strong reducer of Fe resulting in increased absorbance at 562nm (Panel 1, Fig. 5.1) indicating the increased concentration of Fe(II) (Stookey, 1970). This increase in absorbance is also shown in the FZ-Fe control where L-ascorbic acid was added. There also is some reduction of Fe even without L-Ascorbic acid, possibly due to photo-reduction of Fe(III) to Fe(II) (Miles and Brezonik, 1981). FZ is a reagent which binds preferentially to Fe(II), which is the reason why the absorbance at 562nm is higher

in Fe-reduced conditions (where L-ascorbic acid was included) than in the samples where Fe was predominantly Fe(III) (Stookey, 1970).

These results show that citrate is a weaker binder of Fe(II) than FZ, in both Fe treatments because it did not interfere with colour formation by complexed FZ.

In contrast, EDTA strongly interfered with the formation of the coloured FZ-Fe complex which is consistent with its behaviour as an oxidant and Fe(III) chelator (Seibig and van Eldik, 1997; Santana-Casiano et al., 2000; Jones et al., 2015). This has important implications for studies of Fe(II) dynamics in cultures grown with EDTA because EDTA may interfere with Fe(II) acquisition by oxidizing it to Fe(III) (Wubs and Beenackers, 1993; Jones et al., 2015).

This study is consistent with the findings of Fujii et al. (2015), who found that high Ca and Mg concentrations led to greater Fe(II) formation through promotion of photo-reductive dissociation of Fe(III) from EDTA. Then, the Ca and Mg likely bind to the EDTA preventing it from oxidizing Fe(II). Both of these studies show that EDTA has the ability to oxidize Fe(II).

5.5 Conclusion

The aim of this study was to examine the oxidative effects of EDTA and citrate on Fe for use in cell culture media when studying Fe(II). We show that L-ascorbic acid is an effective reducing agent of Fe, but also some reduction of Fe occurs without the presence of acid as seen by the presence of the FZ-Fe complex without the addition of a reductant. Citrate does not appear to oxidize or reduce Fe, while EDTA is capable of oxidizing Fe at a rate that is a function of the concentration of EDTA. We also found that FZ is a stronger Fe(II) chelating agent than citrate.

The findings of this work indicate that when conducting experiments involving Fe(II), citrate may be better suited as a metal chelator than the more widely used EDTA.

Chapter 6

Heterocyst Abundance is Dependent on Cobalt Concentration in Temperate Freshwater Cyanobacteria

Abstract

Harmful algal blooms (HABs) are on the rise in inland waters all over the world. These HABs and specifically cyanobacterial harmful algal blooms (cHABs) cause widespread harm and damage. Understanding the role of nutrients, specifically micronutrients such as Co is key in understanding how these blooms occur, dominate and can be mitigated. The growth and nitrogen fixation rates of N-fixing cyanobacteria are known to increase with increases in Co concentrations by a varying rate based on the measured value. The impact of varying Co concentrations on the growth and heterocyst formation of diazotrophic phytoplankton taxa was investigated, and examined along with previously published data and field data from IISD-ELA. Our results indicate that increases in the Co concentration from 0.17 to 170 nM has a major impact on the frequency of heterocysts produced by four temperate freshwater N-fixing, filamentous cyanobacteria. This study finds that Co availability may increase N-fixation rates by increasing number of heterocysts within a cell population.

6.1 Introduction

External loading of macronutrients such as phosphorus result in increases in biomass and productivity of phytoplankton (Downing et al., 2001; Huisman et al., 2018; Schindler, 2012). However, the impacts of micronutrient on phytoplankton biomass and species dynamics are largely overlooked in freshwater systems due to a large focus on factors such as phosphorus and nitrogen as factors that control harmful algal blooms (Molot et al., 2014). Harmful algal blooms (HABs) and specifically cyanobacterial harmful algal blooms (cHABs) can cause ecological and economic damage through toxin production, creation of foul taste and odour compounds and through harm of wildlife, livestock and humans (Downing et al., 2001; Wolk, 1996). There are many indications that phytoplankton, especially harmful cyanobacteria, are sometimes limited by low levels of micronutrients such as Fe, Mo, Mn, B, Co, or Zn (Goldman, 1966; Baptista and Vasconcelos, 2006; Hawco and Saito, 2018; Fu et al., 2008; Downs et al., 2008). These micronutrients are important cofactors in enzymes which are needed for many metabolic processes (Graham et al., 2016; Andreini et al., 2008). Micronutrient requirements differ amongst phytoplankton species, for example, N-fixing cyanobacteria have a higher requirement for Mo and Fe because these metals are cofactors for their N-fixing nitrogenase enzyme, that catalyzes the conversion of N_2 to NH_3 (Schindelin et al., 1997).

Heterocysts are specialized cells that house the nitrogen fixation machinery in filamentous cyanobacteria, designed with thick walls and high respiration rates to prevent O_2 from deactiviting nitrogenase (Kangatharalingam et al., 1992). During growth, the heterocyst differentiation process is a complex series of cellular events following four stages: induction, patterning, commitment and morphogenesis (Videau et al., 2016). Induction of heterocyst differentiation is caused by N-limited conditions, which results in the production of NtcA, a global nitrogen regulator (Harish and Seth, 2020). NtcA then upregulates the production of HetR. Patterning is determined via HetR-dependent upregulation of PatS which travels laterally to other vegetative cells and inhibits HetR production in those cells, effectively stopping the differentiation process there (Xu et al.,

2020). HetR also causes the synthesis of HetP which is thought to be the point at which the process of heterocyst differentiation is irreversible (Harish and Seth, 2020). HetP activates a series of proteins and transcription factors which change the morphology and physiology of the cell to make the heterocyst microoxic and ideal for nitrogenase activity (Kumar et al., 2010). Nitrogenase is then synthesized and can begin to fix nitrogen (Zhao and Wolk, 2008).

Atomic or ionic Co is a cofactor of key enzymes such as methylmalonyl-CoA mutase, methionine synthase and type II ribonucleotide reductase. Co is also needed to form plant nodules in legumes (Ullrich, 1983). Cobalt is primarily found as a component of vitamin B_{12}, a cofactor in many metabolic pathways (Croft et al., 2006). Vitamin B_{12} is only synthesized by some prokaryotes and species incapable of synthesizing it acquire it from exogenous sources (Rodriguez and Ho, 2015). Some cyanobacteria can manufacture a variant, pseudocobalamin (Helliwell et al., 2016). Thus, the dependency of most species on external vitamin B_{12} can shape the phytoplankton community composition (Rodriguez and Ho, 2015).

Increasing Co concentration has previously been shown to increase rates of photosynthesis and N-fixation in bloom forming alga in Swedish estuaries, *Azotobacter*, *Rhizobium* and in the phytoplankton *Nostoc* and *Calothrix*; where cells grown in 170nM resulted in higher N content in cells than cells grown without Co (Goldman, 1966; Granéli and Haraldsson, 1993; Holm-Hansen et al., 1954; Iswaran and Rao, 1964; Hallsworth et al., 1960; Downs et al., 2008). However, how Co leads to increased rates of N-fixation is unknown. Rodriguez and Ho (2015) characterised the influences of Co and vitamin B_{12} on the marine diazotroph, *Trichodesmium erythraeum* and found that *Trichodesmium* has an absolute requirement for Co. Hawco et al. (2020) quantified the minimal Co usage in *Prochlorococcus*, a marine cyanobacterium and found that *Prochlorococcus* can sustain growth with less than 50 Co atoms per cell. Kelly et al. (2021) studied the growth rates and heterocyst frequencies of two *Dolichospermum* species from Lake Taupō in New Zealand. They found that increasing trace metal (Co, Mo, and Fe) concentrations increased heterocyst frequency.

The objective of this chapter is to assess whether heterocyst formation is dependent on the availability of Co. This was done by growing laboratory cultures of several species of freshwater cyanobacteria at varying concentrations of Co and comparing these results to Co concentrations and corresponding heterocyst frequencies in Lake 227 and with other literature values.

6.2 Materials and Methods

6.2.1 Natural Cobalt Concentrations

Total epilimnetic cobalt concentration from lake water were obtained for the year of 2017 from about 35 Canadian lakes from Saskatchewan, Manitoba, Ontario, Quebec and New Brunswick. Samples were contributed by Helen Baulch (University of Saskatchewan), Jennifer Korosi (York University), Scott Higgins (IISD-ELA), Karen Kidd (McMaster University), Lewis Molot (York University), Sherry Schiff (University of Waterloo), Jason Venkiteswaran (Wilfrid Laurier University), Dan Walters (Nipissing University) and Arthur Zastepa (ECCC).

Unfiltered samples were collected into acid-washed tubes. Samples were acidified with 0.3mL/15mL of concentrated HNO_3 and analyzed with ICP-MS at Trent Water Quality Centre. All acids used were trace metal grade.

6.2.2 Culture and Growth Conditions

Cultures of *Anabaena flos-aqaue* (CPCC 67), *Aphanizomenon flos-aqaue* (NIES 81), *Aphanizomenon skujae* (isolate from Lake 227) and *Dolichospermum lemmermanii* (isolate from Lake Erie) were grown in BG-11_0 (BG-11 without inorganic N). A culture of *Microcystis aeruginosa* (PCC 7005) was grown in BG-11. Phytoplankton were grown at 20°C on a 12:12h light/dark cycle at 100 μmol/m^2/s in BG11 media containing equivalent amount of $FeCl_3$ instead of ferric ammonium citrate (Rippka et al., 1979). *Microcystis aeruginosa* was used in this study as a non N-fixing control species. A 12:12h light cycle was selected to mimic the circadian cycle of cyanobacteria and to ensure that

N-fixation rates remained constant throughout the experiment (Chen et al., 1998).

All species were grown in BG-11_0 before inoculation. 1mL of exponentially growing cells from the starter culture was used to inoculate duplicate metal-free plastic tubes of $BG11_0$ or BG11 containing either 0.17, 17 or 170nM of $CoSO_4$ as the final concentration. To ensure that there was no trace metal contamination, all reagents used were trace metal grade, all flasks and bottles were soaked in 10% HCl over 48 hours and then in Milli-Q water for another 24 hours. Only acid-washed clear pipette tips were used throughout this experiment. All media, glassware and supplies such as pipette tips were UV sterilized under a Laminar flow hood for 15 minutes as autoclave steam can introduce trace metal contamination (Keller et al., 1988).

Growth was assayed by taking absorbance readings at 750nm (A_{750}) using a Cary 100 spectrophotometer. At 750nm, interference from photosynthetic pigments is minimal and can be used as a consistent proxy for cellular growth (Chioccioli et al., 2014).

6.2.3 Heterocyst and Vegetative Cell Counts

Cell and heterocyst counts were done using a hemocytometer under the microscope at 40X magnification. Heterocysts were stained with alcian blue, 0.015% (w/v) for 10 mins (Maldener et al., 2003). A minimum of five squares of the hemocytometer field were counted for each replicate to obtain heterocyst and vegetative cell abundance. Heterocyst frequency was calculated by dividing the number of heterocysts observed by the total number of cells counted.

6.2.4 Calculations and Statistics

The A_{750} was plotted against time and the R package *growthcurver*(version 0.3.0) was used to find the growth rate of each sample (Sprouffske and Wagner, 2016).The package *growthcurver* finds the growth rate by finding the best fit of a given dataset to the logistic growth equation (Eq 6.1).

$$N_t = \frac{K}{1 + (\frac{K - N_0}{N_0})e^{-rt}} \tag{6.1}$$

where N_t is the A_{750} at a given time, K is the carrying capacity (maximum cell biomass), N_0 is the starting A_{750}, r is the growth rate (μ) and t is time. Eq. 6.1 is the solution to Eq 1.9.

Heterocyst counts were calculated as percentage of total cell number and averaged for each species at each concentration of Co. Statistical differences in these mean heterocyst frequencies were found by using two-way ANOVA followed by Tukey's HSD.

6.2.5 Field and Literature Review

To fully understand if Co could play a role in heterocyst differentiation, a literature and field study review was also done. Biological data from IISD-ELA and metal concentration from the same date were compared along with an extensive literature review of culture studies where heterocyst frequency was quantified using defined media where Co concentrations are specified.

Heterocyst frequencies and dissolved Co concentrations from Lake 227 were obtained for the year of 2017. Lake 227 is a small (5ha, mean depth 4.4m, maximum depth 10m), headwater lake that is artificially fertilized by P inputs, located at the IISD-ELA in northwestern Ontario. The lake is dimictic, with thermal stratification defined in the summer occurring at 1-3m. Lake 227 was fertilized with N and P (27:1 molar N:P) from 1969 to 1974, with reduced N loading from 1975 to 1989 (9:1 molar N:P) and with only P from 1990 to present (Findlay et al., 1994; Higgins et al., 2017; Molot et al., 2010). A bloom of the N-fixing cyanobacteria, of the genus *Aphanizomenon*, typically occurs in early summer of each year since 1990 (Schindler et al., 2008).

Dissolved Co concentration from lake samples was collected using 0.45μm Sartorious syringe filters and measured at the Trent Water Quality Centre using ICP-MS.

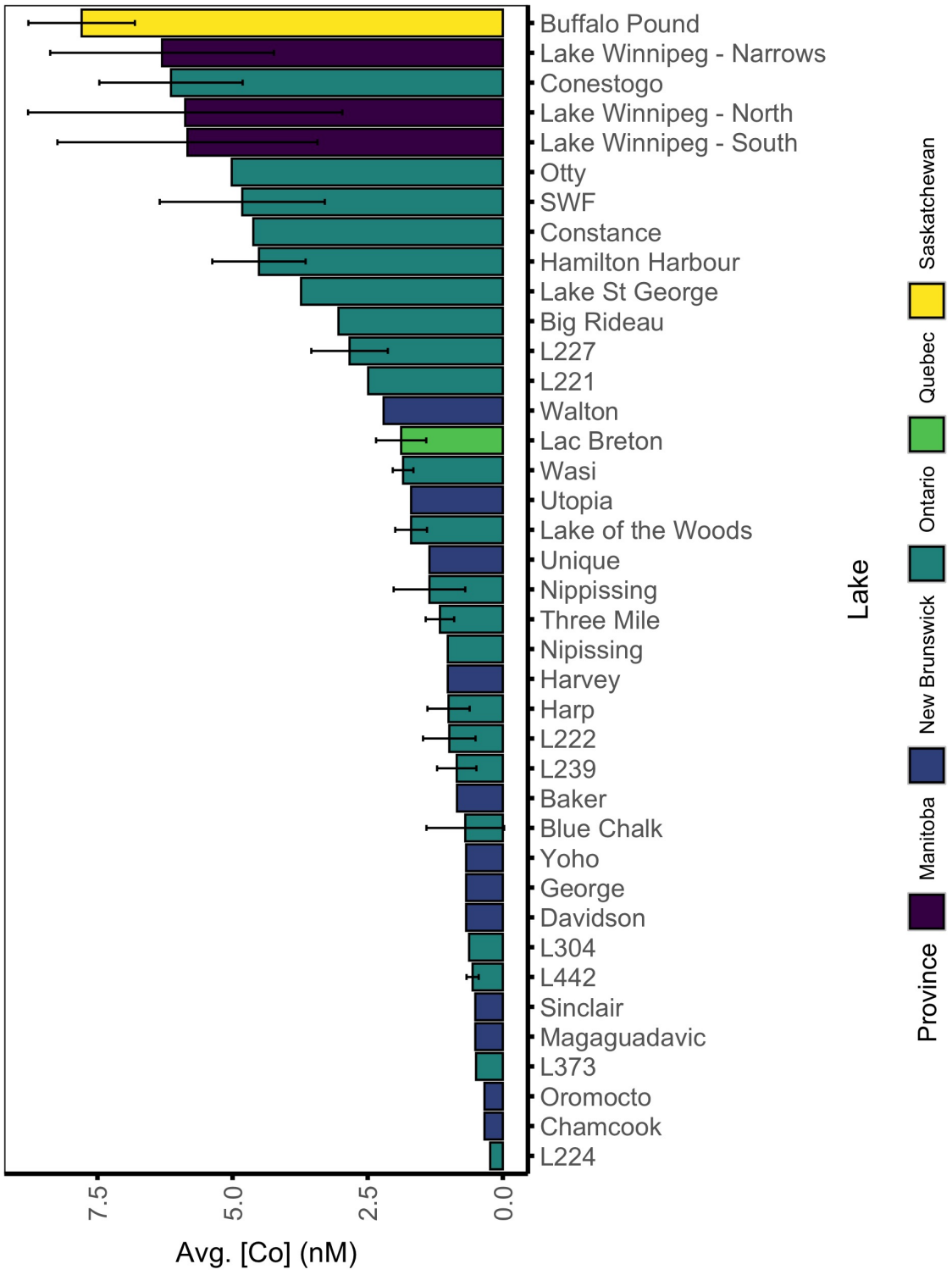

Figure 6.1: Mean epilimnetic dissolved Co concentrations in Canadian Lakes during the field season of 2017. Error bars indicate standard deviation when multiple samples were analyzed for a particular location during the year. Colours indicate the province of the lake. Lake Winnipeg has been categorized in three geographic locations; North Basin, South Basin and Narrows.

6.3 Results

Fig. 6.1 shows the average dissolved cobalt concentration in 39 lakes across Canada in the epilimnion. In all lakes, the mean total Co concentration is below 10nM.

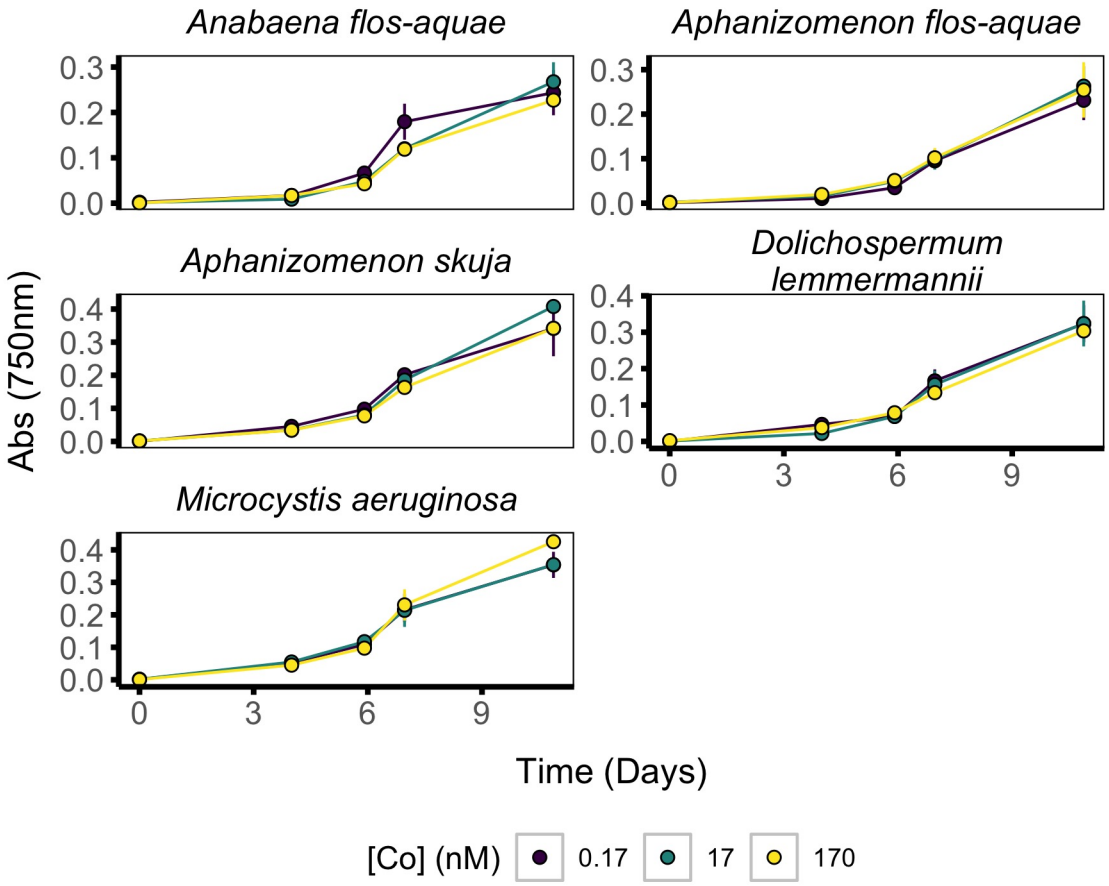

Figure 6.2: Growth curves of phytoplankton species at varying concentrations of Co. Line and points are the mean cell number and bars indicate deviation from the duplicates.

Fig. 6.2 does not indicate a large difference in the growth curves of the various species with relation to concentration of Co. Table 6.1 lists the average growth rates for each species at three different concentrations of Co. The growth rates are variable and do not indicate any pattern in differences with relation to Co concentration. Growth rates also exhibit a small range within each species: *Anabaena flos-aqaue* has the highest range in average growth rates of 0.567 day^{-1}, *Aphanizomenon flos-aqaue* with 0.437 day^{-1}, *Aphanizomenon skuja* with a range of 0.033 day^{-1}, *Dolichospermum lemmermannii* has a range of 0.438, and *Microcystis aeruginosa* has a range of 0.368 day^{-1}.

Table 6.1: Average growth rates of the various phytoplankton species grown at varying concentration of Co, ± indicate standard deviation from the mean of the duplicates.

Species	**[Co] (nM)**	**Mean Growth Rate (day^{-1})**
Anabaena flos-aquae	0.17	1.842 ± 0.18
Anabaena flos-aquae	17	1.275 ± 0.17
Anabaena flos-aquae	170	1.383 ± 0.09
Aphanizomenon flos-aquae	0.17	1.244 ± 0.15
Aphanizomenon flos-aquae	17	0.831 ± 0.27
Aphanizomenon flos-aquae	170	0.807 ± 0.13
Aphanizomenon skuja	0.17	0.908 ± 0.12
Aphanizomenon skuja	17	0.980 ± 0.22
Aphanizomenon skuja	170	0.875 ± 0.06
Dolichospermum lemmermannii	0.17	0.790 ± 0.16
Dolichospermum lemmermannii	17	1.028 ± 0.31
Dolichospermum lemmermannii	170	0.590 ± 0.09
Microcystis aeruginosa	0.17	0.853 ± 0.15
Microcystis aeruginosa	17	0.755 ± 0.19
Microcystis aeruginosa	170	1.123 ± 0.51

Fig. 6.3 shows the mean heterocyst frequency at varying concentration of Co. *Microcystis aeruginosa*, a non-N-fixing cyanobacteria does not produce heterocysts and is shown for comparison. The diazotrophic species have varying results in heterocyst frequency, ranging from 4 to 9%. Lettered groupings as a result of a post-hoc test indicate that the heterocystous frequencies at 0.17nM Co were significantly different from 17nM in all four heterocystous species. The frequencies at 17 and 170nM were also significantly different in *Anabaena flos-aquae*.

Table 6.2: Output of ANOVA of heterocyst frequencies compared to concentration of Co

term	**df**	**sumsq**	**meansq**	**statistic**	**p.value**
[Co] (nM)	2	82.72	41.36	35.85	8.29×10^{-11}
Residuals	57	65.75	1.15		

Fig. 6.4 show the mean heterocyst frequencies of all the N-fixing species (no *Microcystis aeruginosa*) pooled together at the different concentrations of Co. Table 6.2 shows the results of an ANOVA on the heterocyst frequencies observed at different concentrations. There is a significant impact to heterocyst frequencies with rising Co concentrations.

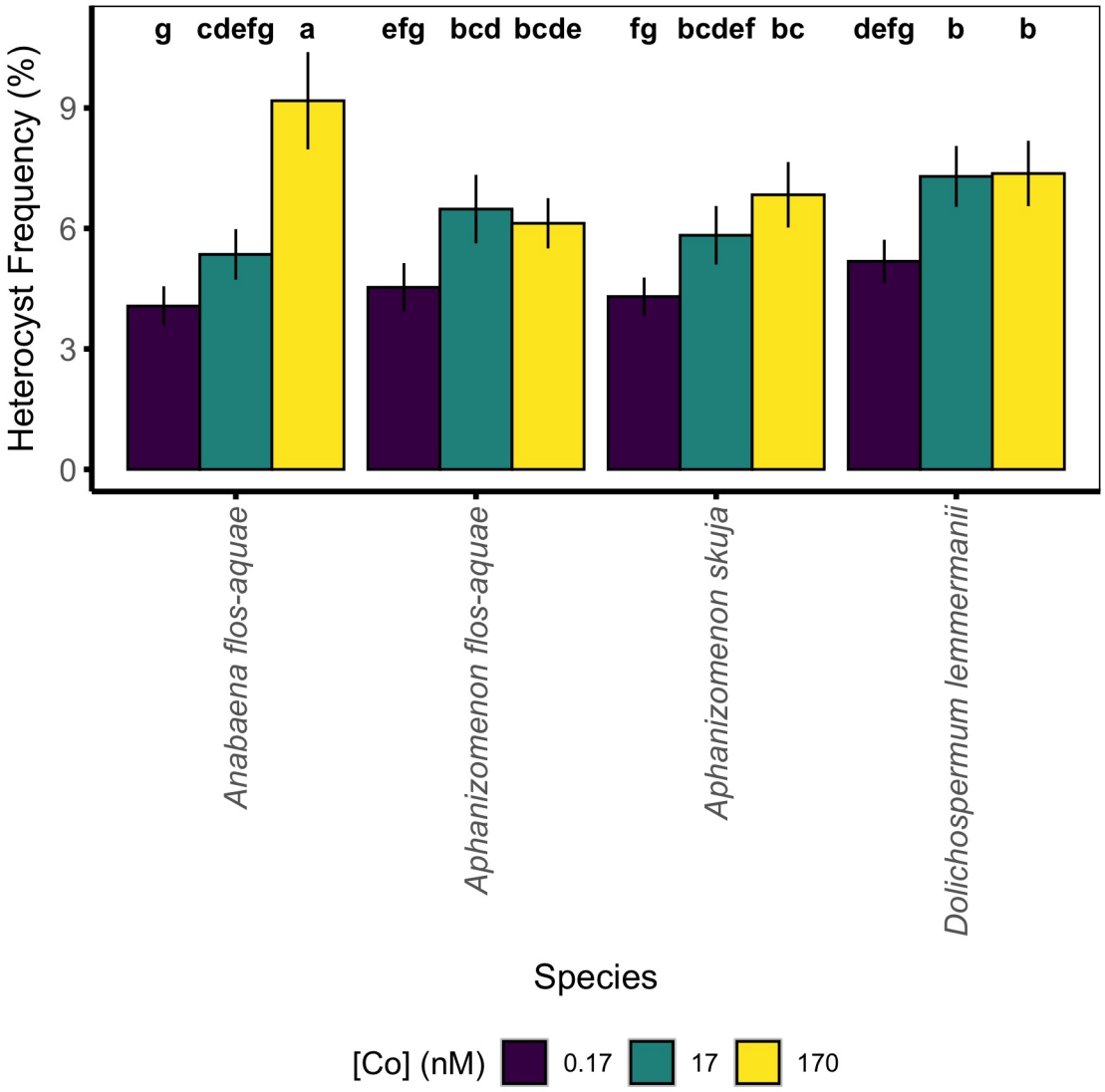

Figure 6.3: Heterocyst frequencies as a percentage of total cell number of the species studied. Each bar represents the mean heterocyst percentage of five counts, bars indicate standard deviation and letters above indicate statistically different means as found by a two-way ANOVA followed by a Tukey's HSD.

6.4 Discussion

Our results indicate that Co can affect the frequency of heterocysts in N-fixing populations. Previous studies have shown that cobalt influences the rates of nitrogen fixation (Granéli and Haraldsson, 1993; Holm-Hansen et al., 1954; Iswaran and Rao, 1964; Hallsworth et al., 1960). However, these studies looked at parameters of nitrogen fixation, using rates of nitrogenase activity or amount of N accumulated in biomass. Here, we show that heterocyst frequency can be used as a response variable when assessing the

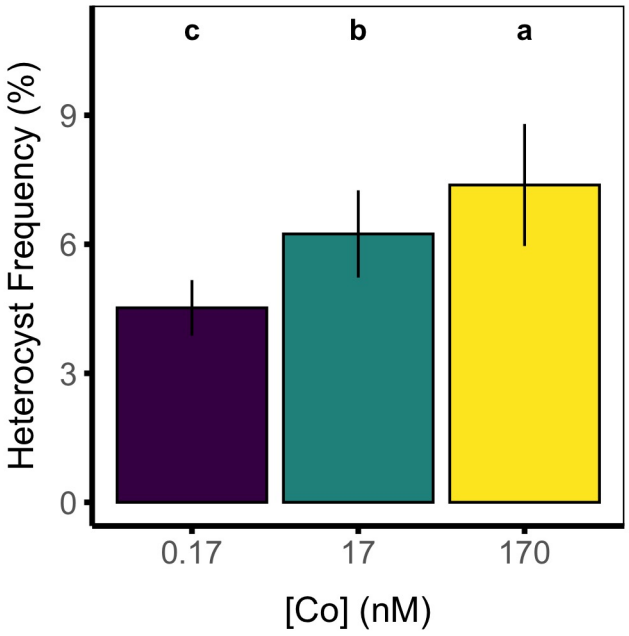

Figure 6.4: Heterocyst frequencies as a percentage of total cell number pooled for all diazotrophic species at the concentrations of Co studied. Each bar represents the mean heterocyst percentage of five counts per species, bars indicate standard deviation and letters above indicate statistically different means as found by an ANOVA followed by a Tukey's HSD.

role of Co in cyanobacterial growth and nitrogen fixation, to our knowledge only (Kelly et al., 2021) have used this variable to study impacts of micronutrients on N-fixation.

Co is an important cofactor in a number of enzymes, however what role they play in heterocyst function is difficult to tease apart. A systematic review by Pernil and Schleiff (2019) of metalloproteins involved in heterocyst metabolism does not reveal a clear requirement for cobalt within the system. The only potential role of cobalt that was hypothesized was that Co^{2+} can replace Zn^{2+} in class II fructose-bisphosphate aldolase (FbaA).

Cobalt and vitamin B_{12} can be a part of other key enzymes such as methionine synthase, ribonucleotide reductase, methylmalonyl-CoA mutase and nitrile hydratase (Ullrich, 1983). While synthesis of methionine and the subunits of DNA through ribonucleotide reductase are important, there is no evidence that either of those are upregulated in heterocysts (Qiu, 2018). Some species of cyanobacteria do not have genes for methylmalonyl-CoA mutase or nitrile hydratase (Hawco et al., 2020).

Vitamin B_{12}-based riboswitches also have been found to regulate proteins associated with heterocysts (Singh et al., 2018). Riboswitches are a regulatory part of an mRNA molecule to which another molecule can bind, causing a change in production of the protein that the mRNA coded for (Tucker and Breaker, 2005). Cobalamin-based riboswitches have been found for a few genes annotated as "metal binding proteins" and the hydrogenase/urease accessory protein encoding genes (*hupE*) (Singh et al., 2018). *HupE* is a transmembrane accessory protein thought to be a Ni/Co transporter to facilitate the Ni-dependent hydrogenase activity (Pernil and Schleiff, 2019; Hoffmann et al., 2006). Mutants of *HupE* were unable to grow at all in medium containing a metal chelator, and growth was only resumed when cobalt or methionine were added pointing to the overall importance of methionine and its synthesis, not to the need for Co specifically in that study (Hoffmann et al., 2006).

This study spans the range of cobalt concentrations found in counts of heterocyst frequency of lake water cyanobacteria and laboratory culture studies (Tables 6.3, 6.4 and Figs. 6.1, 6.2). Examinations of other studies where Co concentration was known and

Table 6.3: Heterocyst frequencies of cyanobacteria and dissolved Co concentrations from Lake 227 at IISD-ELA during the summer of 2017. Heterocyst frequencies were calculated from biomass data provided by IISD-ELA and unpublished Co concentrations were provided by Dr. Lewis Molot.

Organism And Location	**Date**	**Sampling Depth Range (m)**	**[Co] (nM)**	**Het. %**
Aphanizomenon skuja	2017-May-23	0-2	1.26	4.38
Lake 227	2017-May-23	2-4	1.05	2.94
IISD-ELA	2017-June-05	0-1	0.70	3.77
	2017-June-05	0-1	0.76	4.19
	2017-June-19	0-2.3	1.04	3.50
	2017-June-19	2.3-4	1.07	3.81
	2017-July-04	0-1	1.99	5.21
	2017-July-04	1-3	2.07	6.92
	2017-July-17	0-1.3	4.00	4.12
	2017-July-17	1.3-3	0.90	4.08
	2017-Aug-08	0-1.5	1.88	3.53
	2017-Aug-08	1.5-4	2.26	4.02
	2017-Aug-21	0-2	2.56	3.38
	2017-Aug-21	2-3	1.56	3.26
	2017-Sep-05	0-2.5	2.05	3.30

Table 6.4: Mean reported heterocyst frequencies of cyanobacteria from the literature. Literature heterocyst frequencies are reported for only wild-type species.

Organism	[Co] (nM)	Het. %	Ref
Anabaena cylindrica	170	4.10	Jewell and Kulasooriya (1970)
	170	4.70	Kulasooriya et al. (1972)
	170	5.20	Ogawa and Carr (1969)
	170	5.80	Nayak et al. (2007)
Anabaena fertilissima	170	7.40	Nayak et al. (2007)
Anabaena flos-aquae	170	3.20	Ogawa and Carr (1969)
	170	9.20	Kangatharalingam et al. (1992)
Anabaena inequalis	170	5.36	Ogawa and Carr (1969)
Anabaena iyengarii	170	7.61	Nayak et al. (2007)
Anabaena laxa	170	5.10	Nayak et al. (2007)
Anabaena oryzae	170	8.45	Nayak et al. (2007)
Anabaena oscillarioides	170	4.28	Nayak et al. (2007)
Anabaena PCC7108	170	7.80	Nayak et al. (2007)
Anabaena PCC7120	170	6.50	Nürnberg et al. (2015)
	170	7.22	Chaurasia and Apte (2011)
	170	7.50	Berendt et al. (2012)
	170	8.00	Videau et al. (2016)
	170	8.67	Borthakur et al. (2005)
	170	8.90	Rivers et al. (2018)
Anabaena PCC7122	170	8.03	Nayak et al. (2007)
Anabaena sp.	170	6.33	Ahad et al. (2015)
Anabaena sphaerica	170	5.49	Nayak et al. (2007)
Anabaena spiroides	170	4.33	Nayak et al. (2007)
Anabaena vaginicola	170	6.34	Nayak et al. (2007)
Anabaena variabilis	170	4.33	Ogawa and Carr (1969)
	170	5.90	Nayak et al. (2007)
Aphanizomenon aphanizomenoides	42.03	3.17	de Figueiredo et al. (2011)
Aphanizomenon flos-aqaue	16	4.37	Rother and Fay (1979)
Aphanizomenon ovalisporum	170	8.43	Vasas et al. (2013)
Aphanizomenon sp.	42.03	3.72	Mohlin et al. (2012)

heterocyst frequency was measured for *Anabaena* and *Aphanizomenon* species shows a minor increasing trend with a weak positive correlation (R^2 = 0.36). The concentrations of Co from Lake 227 spans the lower part of the range used in the experiments here (0.17 to 17nM) (see Fig. 6.2) and there is a large rise in heterocyst frequency between those concentrations in all heterocystous species studied. Therefore, it can be concluded that heterocyst frequency and consequently the N-fixation rates in lakes is probably affected where low Co concentrations occur.

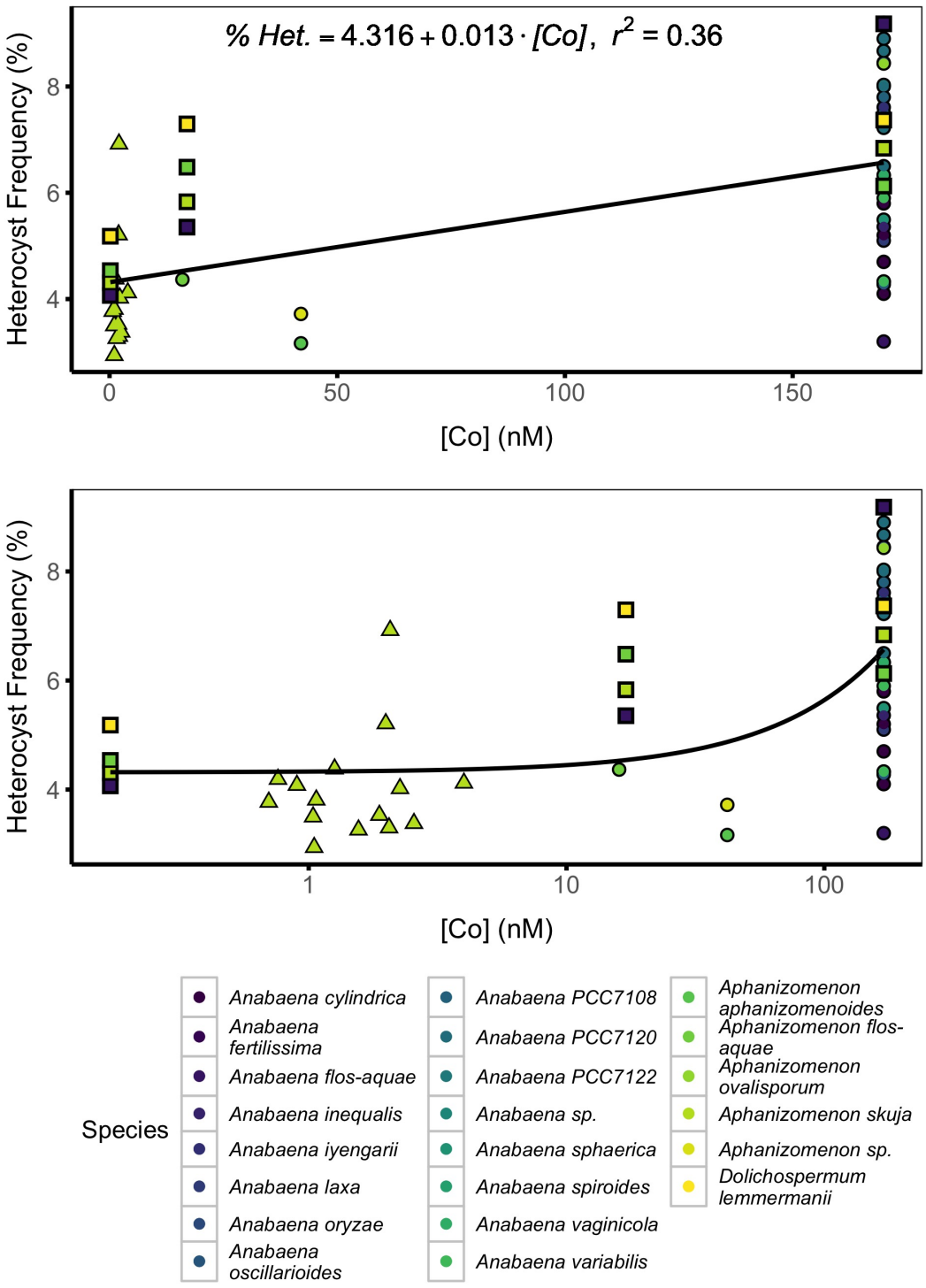

Figure 6.5: Heterocyst frequency (% of all cells) of various freshwater *Aphanizomenon* and *Anabaena* species from this study (□), field (△) and culture studies (○) where Co concentrations could be determined. The equation of the linear relationship is $\%Het. = (4.3 \pm 0.3) + (0.013 \pm 0.002) \times Co.\ Conc.$, $R^2 = 0.36$ and $p < 0.05$. Second panel is same data with log x-axis to better display the spread of the data. Tables 6.3 and 6.4 shows the references where these values were obtained.

There is a wide variability of heterocyst abundance observed at varying Co concentrations in the field data as well culture data at the same concentrations (170nM). The variability in data from Lake 227 might be explained by external factors such as wind, temperature and lake mixing, all of which can influence algal bloom growth in lakes (Wei et al., 2001). Perhaps the variability when many species are compared at the same concentration of cobalt in culture maybe due to species-species variability but also due to the morphological changes that occur in culture especially in heterocyst formation (de Figueiredo et al., 2011). Some diazotrophic species that once formed blooms in N-depleted waters have lost the ability to form heterocysts in culture, hence the variability in heterocyst frequencies observed could be an artefact of that phenomenon (de Figueiredo et al., 2011).

A similar study of impacts of low iron concentration on heterocyst formation by Aly and Andrews (2016) found that iron deficiency led to a delay in heterocyst formation and that only a prolonged iron starvation of about 11-14 days in culture led to a decrease in heterocyst frequency. Fe is an important cofactor of many more processes in heterocysts than cobalt (Pernil and Schleiff, 2019), so achieving cobalt starvation without shut down of cellular growth due to inadequate methionine or dNTP synthesis could be difficult. Hawco et al. (2020) have shown that the cellular demand for cobalt is very low at less than 50 atoms per cell.

Kelly et al. (2021) studied two species of *Dolichospermum*, *Dolichospermum planctonicum* and *Dolichospermum lemmermannii*, the latter also being studied in this work. They did not find a direct increase in heterocyst frequency with the addition of Co in *Dolichospermum lemmermanii*, it was only when both Co and Fe were added that heterocyst frequency increased. Although increasing Co did result in increased heterocyst frequencies for *Dolichospermum planctonicum*. Kelly et al. (2021) suggested that differences in species physiology may be attributable to the variations. In this work, we found that increasing Co 100-fold from 0.17nM to 17nM increased heterocyst frequencies significantly but not when the Co concentration increased to 170nM for *Dolichospermum lemmermannii*. One of the possible reasons why the same species

behaved differently could be due to how they were grown. Kelly et al. (2021) used recently isolated phytoplankton from Lake Taupō, while we used species which had been isolated from Lake Erie but have gone through many generations of being grown in lab culture conditions.

6.5 Conclusion

We used field, literature and experimental data to examine whether heterocyst formation is dependent on the availability of Co. We did this at 0.17, 17 and 170nM of Co. 0.17 to 17nM appears to be the range of Co found in many Canadian lakes. We found that increasing Co significantly increases the frequency of heterocysts found in cell cultures of four diazotrophic cyanobacteria. When compared with literature and field data, the relationship is confirmed although the correlation is weak.

These results suggest that in general Co plays a role in nitrogen fixation and the possible mode of action is by the increased percentage of heterocysts. A major limitation to fully understanding how Co impacts nitrogen fixation is the lack of knowledge about Co and Co-dependent enzymes in the nitrogen fixation and heterocyst differentiation process. Further work in understanding the biochemistry of Co in cyanobacteria is required.

Understanding how Co can play a role in the synthesis of heterocysts and growth of heterocystous cyanobacteria may lead to better understanding of bloom dynamics which may help inform better management decisions in N-limited systems.

Chapter 7

Smartphone App-based Measurements of Temperate Freshwater Phytoplankton Growth

Abstract

Harmful algal blooms (HABs) are increasingly reported and prove a challenge to monitor. News reports, citizen reporting and ecosystem modelling have made predicting and reporting the occurrence of HABs easier, but quantifying biomass quickly, inexpensively and simply is still a challenge. Here, we have devised a unique and simple strategy for sensitive and colourimetric estimation of algal biomass concentration. A colourimetric smartphone app was used to record red, green, blue colour model (RGB) values of algal cell culture of various species for estimation of algal biomass levels. A good linear relationship (R^2 = 0.90) between algal absorbance at 750nm and $(R+G+B)/G$ was obtained. Our results add to the increased number of substances quantified using this method. This new method offers a promising and portable detection method for phytoplankton with simple operation, fast response and very low cost.

7.1 Introduction

Algal blooms are an ever increasing challenge to monitor and to solve (Pick, 2016). Increased occurrences of harmful algal blooms (HABs) and specifically cyanobacterial harmful algal blooms (cHABs) are now being reported in nutrient poor systems adding to the challenge (Verschoor et al., 2017). News reports, citizen reporting and ecosystem modelling have made predicting and reporting HABs easier, however the ability to quantify phytoplankton biomass in the field is still lacking (Pick, 2016). HABs are a nuisance and can negatively impact the tourism and fishing industries (Hudnell, 2010). These blooms can produce foul smells and also produce toxins which can harm life around the impacted area (Downing et al., 2001). Algal blooms have been observed worldwide and are an increasing problem (Song et al., 2013; Pick, 2016).

To better monitor and understand the impacts of HABs and cHABs, a variety of *in situ* field sampling and laboratory techniques have been used. Direct cell counts by microscopy have been used extensively to quantify and identify phytoplankton. It is, however, time consuming and is very dependent on the identification skill of the observer (Butterwick et al., 1982). Indirect measurements of algal biomass are commonly used such as turbidity measurements, chlorophyll *a* (ChlA) quantification (via spectrophotometry, fluorometry or HPLC) and genetic quantification through qPCR (Graham et al., 2016; Hu, 2014; Li et al., 2009; Almomani and Örmeci, 2016; Liu et al., 2020). These techniques require expensive equipment (Butterwick et al., 1982; Hu, 2014). ChlA extractions require time, chemicals such as methanol, ethanol or acetone and transport to the lab from the field site (Gregor and Maršálek, 2004). While spectrophotometric measurements of cell cultures have proved to be an effective proxy for cell number for a variety of phytoplankton species, it also requires expensive equipment (see Appendix A) (Erratt, 2017).

In vivo fluorometry (IVF) uses sondes and probes to measure the fluorometric signal ChlA and phycobilisomes (PBS) within the water column. These probes are able to generate and collect large amount of instantaneous data without the need to do further laboratory analysis. However, the equipment is expensive and costs approximately

$2000 for the most minimal model. The equipment is also temperamental and requires meticulous calibration and handling (Pires, 2010). Moreover, several models are ineffective at detecting cyanobacterial ChlA (L. Molot, personal communication).

While, there are numerous methods for quantifying phytoplankton biomass in use, there are no effective yet simple and inexpensive ways of estimating phytoplankton biomass that can be done with very little training available.

Smartphones are emerging as a powerful analytical tool for colourimetric, fluorometric, chemiluminescence and bioluminescence (Peng et al., 2020). In this study, we assess if an inexpensive smartphone app can be related to algal spectrophotometric results. This method is portable and user-friendly.

7.2 Materials and Methods

7.2.1 Experimental Organisms and Growth Conditions

Algal cultures of *Anabaena flos-aqaue* (CPCC 67), *Aphanizomenon flos-aqaue* (NIES 81), *Aphanizomenon skuja* (isolate from Lake 227), *Dolichospermum lemmermannii* (isolate from Lake Erie), *Microcystis aeruginosa* (PCC 7005), *Chlamydomonas reinhardtii* (CPCC 243), *Chlorella vulgaris* (CPCC 90) and *Coelastrum proboscideum* (SAG 217-2) were obtained from various sources as listed in Table 1.3. These phytoplankton species were selected to represent the various phytoplankton found in freshwater systems. These phytoplankton were grown in batch culture in 250mL Ehrlenmeyer flasks at 20°C on a 12:12h light/dark cycle at 100 $\mu mol/m^2$/s in BG-11 or BBM medium containing equivalent amount of $FeCl_3$ instead of ferric ammonium citrate and equivalent amount of $CoSO_4$ instead of $Co(NO_3)_2$ (Rippka et al., 1979). The N_2-fixing species: *Anabaena flos-aqaue*, *Aphanizomenon flos-aqaue*, *Aphanizomenon skuja* and *Dolichospermum lemmermannii* were also grown in BG-11_0 (BG-11 without inorganic N). A 12:12h light cycle was selected to mimic the circadian cycle of cyanobacteria and to ensure that N-fixation rates remained constant throughout the experiment (Chen et al., 1998). Blanks of BG-11 and BG-11_0 were also made.

7.2.2 Spectrophotometer Measurements

While phytoplankton cultures were growing, samples were withdrawn every 3 or 4 days for absorbance scans from 200nm to 800nm using a Cary 100 (Agilent) and corrected with media blanks. Additionally, a series of dilutions of cell cultures were analyzed by the spectrophotometer. A_{750} was selected for focus as 750nm is used as a proxy for cell growth and is not subject to interference from photosynthetic pigments (Chioccioli et al., 2014).

7.2.3 Smartphone Measurements

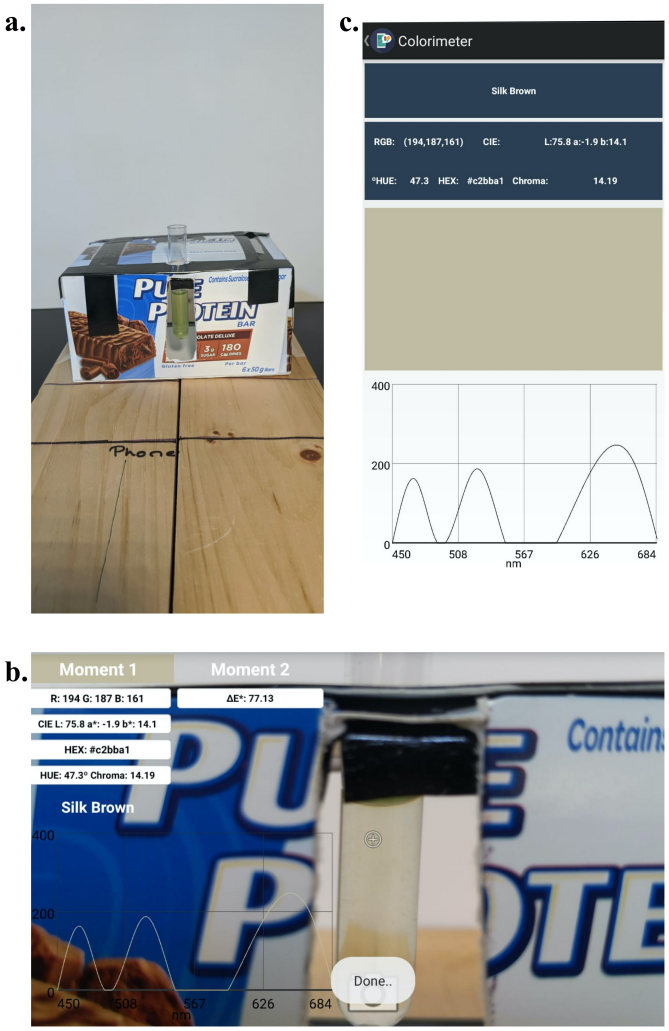

Figure 7.1: *Colorimeter* apparatus for measuring algal samples. **a** Photograph of the apparatus created to hold and measure algal samples using a box. **b** Smartphone app user screen for recording RGB values. **c** Results screen to indicate measured RGB values.

A smartphone app called *Colorimeter* (Version 5.5.1; Lab Tools, São Carlos, São Paulo, Brazil) was purchased on an Android smartphone (equipped with 12.2 megapixel camera) (Ravindranath et al., 2018; Yuan et al., 2019). The app is user-friendly and does not require a wi-fi or network connection.

At the same time that samples were analyzed by the spectrophotometer, samples were analyzed for RGB using the *Colorimeter* app. Phytoplankton and media blank samples were subsampled and placed in 5mL (12mm x 75mm) clear, polystyrene tubes. A cardboard box with a white background was constructed with an opening on the top to hold a sample tube inserted into the box and a section of the front of the box cut out to allow for light to enter (Fig. 7.1a). A cool-white fluorescent lamp to provide a light source was placed in front of the box. The smartphone was consistently placed 10 cm away from the sample tube. RGB values were recorded for each sample.

7.2.4 Data Processing and Statistics

After the absorbance spectra and RGB values for the algal samples were obtained, data was analyzed using R. The *Colorimeter* app reports different parameters in colour space such as RGB, CIE, colour names and chroma (Lab Tools, 2018).

In order to determine the best relationship for the quantification of algal cells, different relationships were analyzed including R, G, B, $(R + G + B)$, $(R + G + B)/R$, $(R + G + B)/G$ and $(R + G + B)/B$ (Peng et al., 2020; Ravindranath et al., 2018; Yuan et al., 2019). Furthermore, we compared relationships of A_{750} with raw RGB values, their sums and the three ratios, and the blank-subtracted (zeroed) RGB values, their sums and their ratios and the absorbance calculated from the RGB values and their ratios using the equation 7.1, where I_0 is the intensity of light measured through a blank solution and I is the intensity of light measured through a sample solution (Peng et al., 2020; Doak et al., 2010).

$$A = -log_{10}\frac{I}{I_0} \tag{7.1}$$

Once a regression model between A_{750} and RGB value-based measurement was found, the model was compared to cell numbers estimated by counting cells and generating standard curves for each organism to correlate cell number to A_{750} (see Appendix A). This conversion was done by substituting A_{750} in the linear regression equation obtained by the RGB value with the modified factor of *Cell Number / (slope of A_{750} to Cell Number ± error)*. This modification was necessary as the linear regression to convert to cell numbers has different slopes for all the species.

7.3 Results

Table 7.1 shows the statistical parameters associated with the different models of correlating A_{750} to RGB parameters. The correlation coefficient, p-value and the AIC are shown. AIC values are used to compare models among each other. The closer the AIC value to 0, the better the fit is considered. Only two models have correlation coefficients of more than 0.75, both being calculated by (R + G + B)/G. The blank-subtracted model has an AIC value closer to 0 than the calculated abs model.

Fig. 7.2 shows the linear correlations between the A_{750} and (R + G + B)/G. Tables 7.2 and 7.3 show the linear models using only the zeroed values. The linear fit through the origin has a better R^2 and lower AIC. Fig. 7.3 shows the data just for zeroed A_{750} and (R + G + B)/G for all the species.

The best equation was:

$$\frac{R+G+B}{G} = (-0.38915 \pm 0.01159) \times A_{750} \tag{7.2}$$

Fig. 7.4 shows the linear relationship for each species and compares the closeness of fit using RMSE. RMSE are also shown as a percentage of the range of the data for each species. The RMSEs reported here span from 7.3 to 54.9% of the ranges of the data presented for each species. The diazotrophic strains of *Anabaena flos-aquae* (54.9%) and *Aphanizomenon flos-aquae* (26.2%) have the highest RMSE as a percentage of the range in data, while the N-replete *Aphanizomenon flos-aquae*, *Microcystis aeruginosa* and

Calculation Method	RGB Parameter	R^2	p-value	AIC
RGB	R	0.1937	8.25×10^{-8}	1142
Zeroed		0.2443	9.67×10^{-10}	1048
Calculated abs		0.2533	4.23×10^{-10}	-587
RGB	G	0.1051	1.00×10^{-4}	1100
Zeroed		0.2114	1.79×10^{-8}	1010
Calculated abs		0.2108	1.90×10^{-8}	-612
RGB	B	0.4154	2.53×10^{-17}	1144
Zeroed		0.6825	3.44×10^{-35}	1058
Calculated abs		0.6554	8.41×10^{-33}	-491
RGB	(R + G + B)	0.2687	1.02×10^{-10}	1412
Zeroed		0.4536	2.63×10^{-19}	1327
Calculated abs		0.4488	4.71×10^{-19}	-578
RGB	(R + G + B) / R	0.1074	9.83×10^{-5}	-291
Zeroed		0.6356	3.64×10^{-31}	-443
Calculated abs		0.6193	6.84×10^{-30}	-937
RGB	(R + G + B) / G	0.7221	4.40×10^{-39}	-442
Zeroed		0.8098	3.95×10^{-50}	-483
Calculated abs		0.8057	1.65×10^{-49}	-990
RGB	(R + G + B) / B	0.4175	1.99×10^{-17}	-33
Zeroed		0.7035	3.42×10^{-37}	-125
Calculated abs		0.7379	8.80×10^{-41}	-720

Table 7.1: Correlation coefficients (R^2), p-values and AIC values of various linear models of A_{750} and various RGB parameters. Zeroed values were found by subtracting blank values from the samples and calculated abs values were determined by using Eq. 7.1. Models with $R^2 > 0.75$ are highlighted.

Table 7.2: Linear relationship of blank corrected A_{750} to blank corrected $(R + G + B)/G$

term	estimate	stnd. error	statistic	p.value
y-intercept	0.015439	0.005489	2.812	0.00566
slope	-0.428322	0.017935	-23.882	$< 2 \times 10^{-16}$
Residual Stnd Error	0.04034		Degrees of Freedom	134
R^2	0.8098		Adjusted R^2	0.8083
F-statistic	570.3		p-value	$< 2.2 \times 10^{-16}$
AIC	-483.3188			

Chlamydomonas reinhardtii have RMSE as percentage of range lower than 10%.

The slope of the regression was found by substituting *Cell Number / (slope of* A_{750} *to Cell Number ± error)* for A_{750} in Eq. 7.2 resulting in:

$$\frac{R+G+B}{G} = \frac{-0.38915 \pm 0.01159}{Slope\ of\ A_{750}\ to\ Cell\ Number \pm error} \times CellNumber \tag{7.3}$$

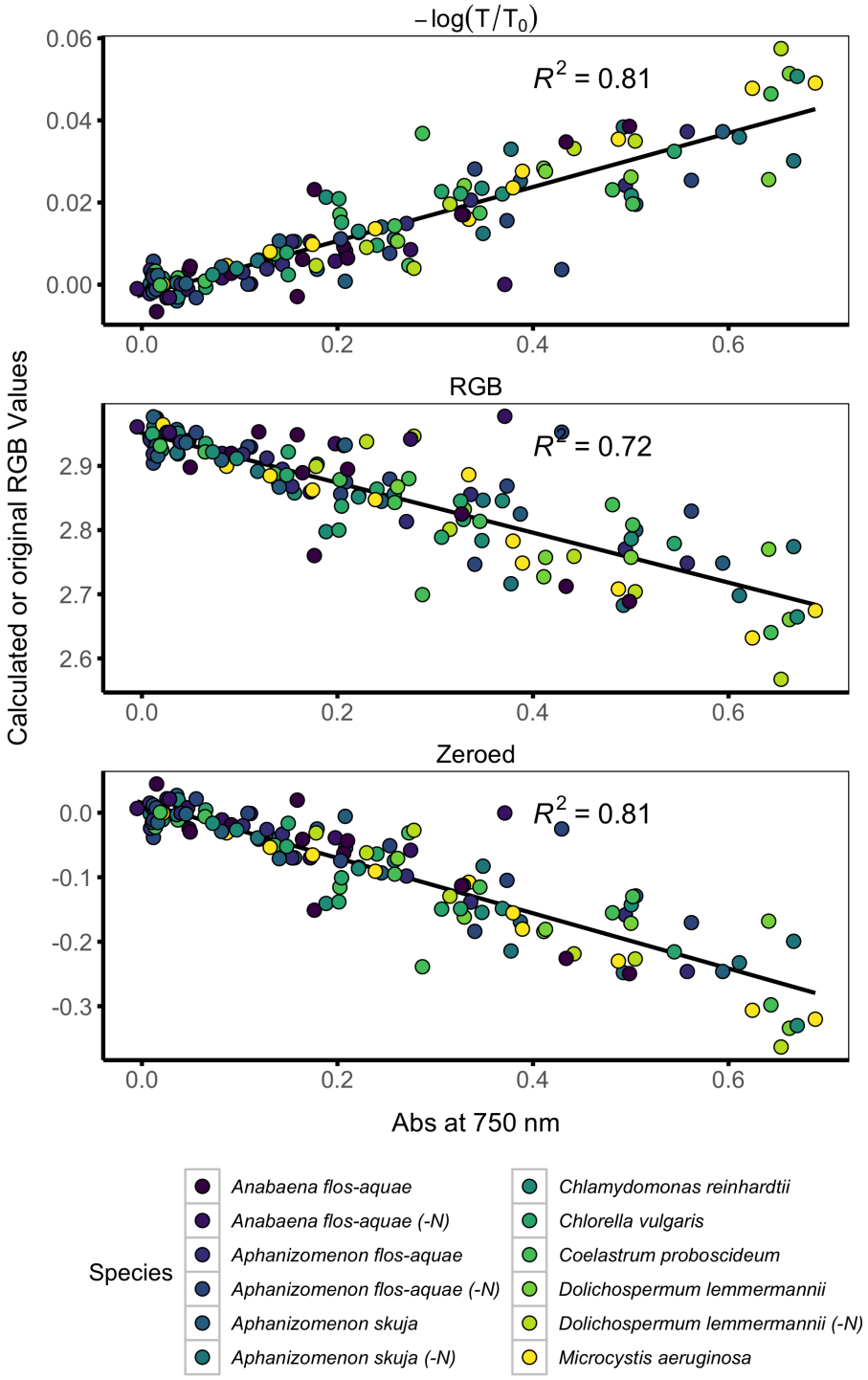

Figure 7.2: Comparison of A_{750} to three different ways of calculating $(R + B + G)/G$. Linear correlation coefficients of relationships are shown and all relationships have $p < 2.2{\times}10^{-16}$. Colours indicate species.

Table 7.3: Linear relationship of blank corrected A_{750} to blank corrected $(R+G+B)/G$, the linear regression is through the origin

term	estimate	stnd. error	statistic	p.value
slope	-0.38915	0.01159	-33.59	$< 2 \times 10^{-16}$
Residual Stnd Error	0.04136		Degrees of Freedom	135
R^2	0.8931		Adjusted R^2	0.8923
F-statistic	1128		p-value	$< 2 \times 10^{-16}$
AIC	-477.5187			

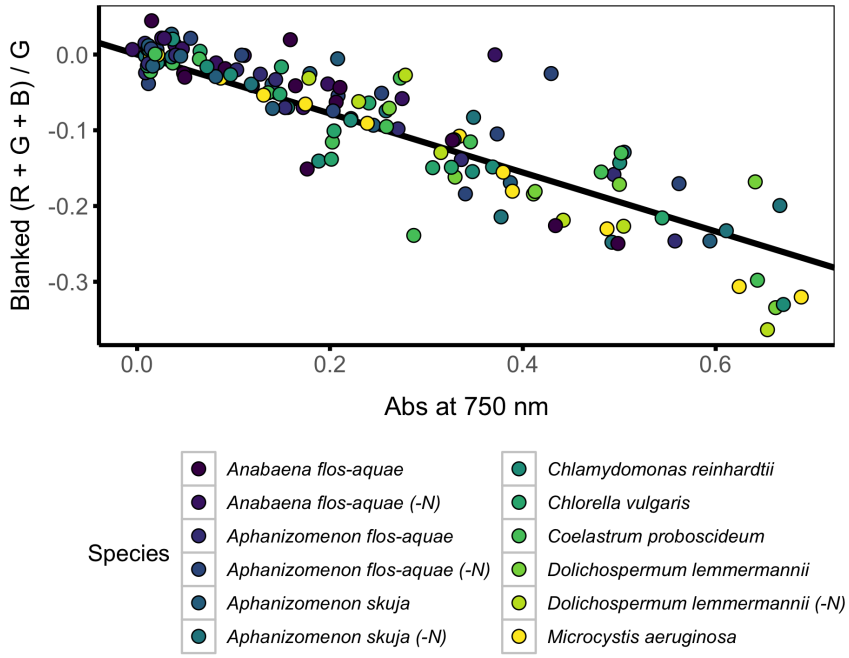

Figure 7.3: Relationship of A_{750} to $(R+G+B)/G$. Equation of the line is $(R+G+B)/G$ = -0.38915 × A_{750}. R^2 is 0.893. Colours indicate species.

7.4 Discussion

The goal of this experiment was to propose a new, inexpensive, portable and user-friendly way to quantify algal biomass *in vivo*. We have demonstrated that this can be done by using a cardboard box with a white background and two openings, an inexpensive light source and the cheap smartphone app, *Colorimeter*.

It should be noted that linear regression forced through the origin yielded a better R^2 and a lower AIC than a linear regression with an intercept. Due to this better R^2 the linear relationship through the origin was selected as the optimal model. Fig. 7.4 shows how a modified model (Eq. 7.3) can be used to relate cell number to the *(R + G + B)/G*,

the RMSE shows the average deviation on the y-axis of each observation from the linear regression as a percentage of the range of the values observed. Ten of the twelve species studied have RMSEs less than 20% of the range of RGB-derived values observed, while only two go over 25% and only one species with over 50% in RMSE. For the ten species with lower than 20% RMSE of range, this method of quantification can be deemed good. More validation and further study may be required into the two species with high deviations.

For many analytical techniques, a R^2 of 0.95 or over is desirable. However, given that this proposed technology uses equipment that are not designed for analytical scientific work, the obtained R^2 of 0.90 is acceptable. This correlation can easily be made stronger with the use of equipment such as a tripod to hold the smartphone at one consistent place and angle during each sampling event.

Further validation of this method with environmental samples and samples containing humic waters is needed.

7.5 Conclusion

The purpose of this study was to assess if a smartphone app can be used to quantify algal biomass, eliminating the need for expensive laboratory equipment or chemicals to extract pigments. This study shows that it is possible to use *Colorimeter* to measure the algal biomass with a high correlation (R^2 = 0.9) using Eq. 7.2. We also found that this correlation to A_{750} can be applied to cell number by using Eq. 7.3.

Our results suggest that using smartphones to measure phytoplankton colorimetrically may be a promising method for rapid quantification of algal biomass in the field, even by citizens. These results also add to the rapidly expanding list of coloured solutions to be quantified using smartphones.

Further work to validate this method is necessary, especially with field samples. This study only used cultures where the only particulate was algal biomass. The next step from this study is to apply this work to environmental samples and use this technique to

quantify algal biomass, or dissolved organic compounds which can give waters a coloured appearance.

Ravindranath et al. (2018) and Peng et al. (2020) used this method to quantify Hg^{2+} and H_2O_2, respectively, in this study we showed this can be applied to algal biomass as well. We believe this technique presents a great opportunity to quantify and characterize a panoply of coloured materials.

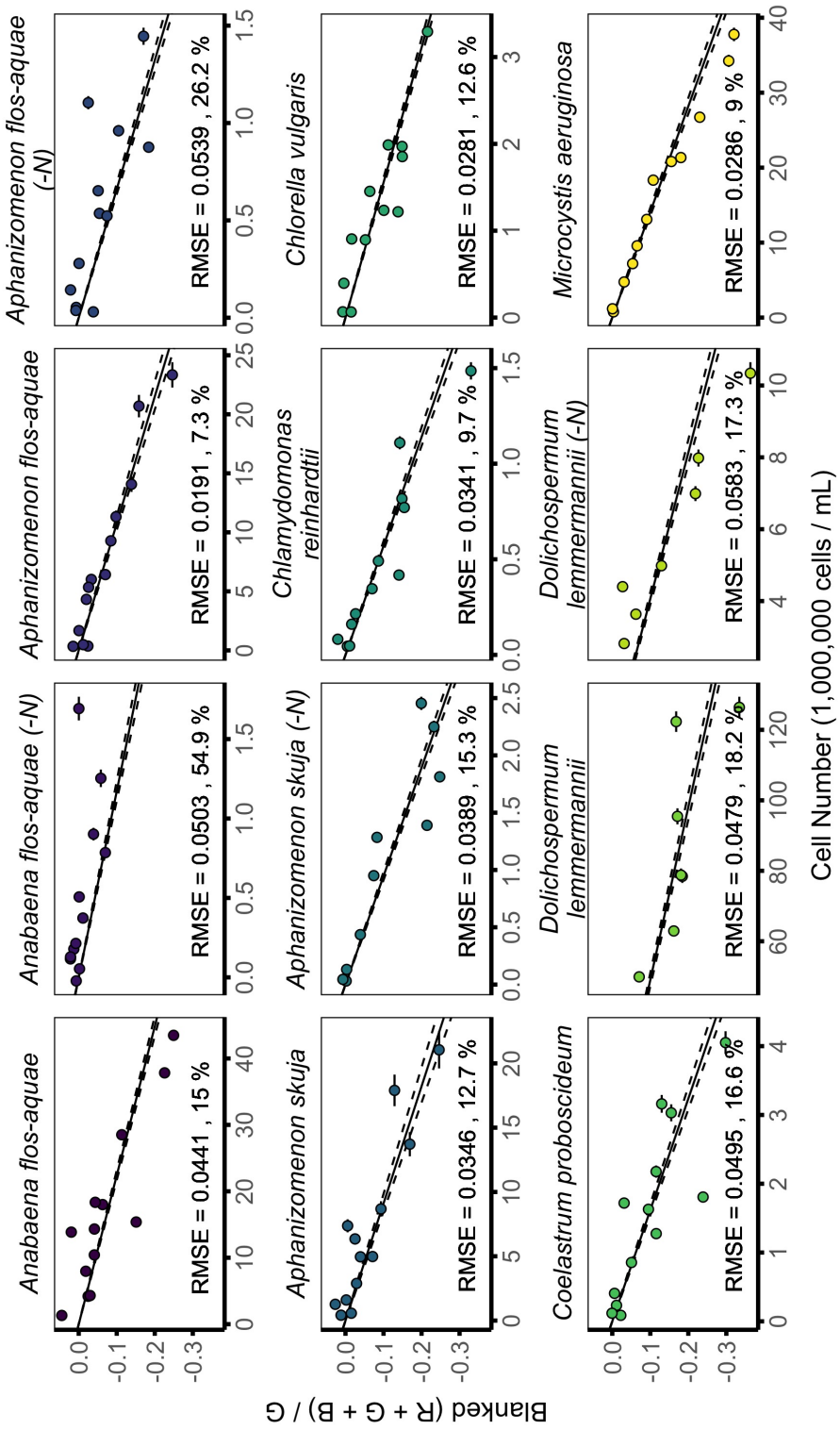

Figure 7.4: Relationship of cell number to $(R + G + B)/G$ linear relationship for each species. Equations of these lines vary as the new conversion is calculated based on the species-specific conversion from A_{750} to cell number. Solid lines are regression lines, dashed lined indicate error on the regression, circles are measured values. RMSE indicate overall average deviation of the observed values from the regression and are presented as a percentage of the range of the data for each species. Horizontal error bars indicate potential error in estimating cell numbers.

Chapter 8

SUMMARY AND FUTURE RESEARCH

Harmful algal blooms are an increasing problem in more and more systems. This project aimed to characterize different aspects of micronutrient dependent growth of phytoplankton to better understand the often-overlooked drivers of algal blooms and taxa within blooms.

We found in chapter 2 the Fe threshold concentrations of various phytoplankton taxa, both eukaryotic and prokaryotic, both N-replete and nitrogen fixing. It was found that N-fixing cyanobacteria in N-replete conditions had the lowest threshold for Fe, followed by eukaryotic algae, followed by cyanobacteria and N-fixing cyanobacteria had the highest threshold for Fe. Affinities for Fe at low Fe concentrations were also estimated and found that cyanobacteria have the highest affinity for low iron concentrations. This understanding of threshold concentrations and affinities allows us to better understand species competition in a given environment. Future research could use this approach to study more organisms or the influence of other nutrients such as Co or Mo.

Stable isotopic fractionation can be used to glean insight into the growth characteristics of phytoplankton cultures (Chapter 3). We developed a model to determine the stable isotopic composition of the newly grown biomass from the bulk sample in culture and used this new isotopic signature to correlate the C and N isotopic fractionation factors to

the growth rate of these cultures. Future research should focus on studying field samples, with a focus on N-fixing species to better understand their growth.

Ferrozine is a chelator which preferentially binds to Fe(II) over Fe(III). In chapter 4, we attempted to see if ferrozine would inhibit cyanobacterial growth in culture as they are dependent solely on Fe(II). It was found that phytoplankton are uninhibited by FZ in their surroundings and will grow in the FZ:Fe ratios studied. In chapter 5, the impacts of EDTA and citrate were explored on the formation of the colourimetric FZ-Fe complex. We found that citrate does not oxidize or reduce Fe in solution while EDTA is capable of oxidizing Fe. Future work involving Fe(II) should use citrate as a chelator than EDTA.

Cobalt is another micronutrient that not much is known about in cyanobacteria. In chapter 6, we aimed to find the role of cobalt in the formation of the specialized nitrogen fixing cells, heterocysts. The heterocyst differentiation process is complex and needs many cofactors and regulatory proteins. Field samples from Lake 227 at IISD-ELA, a literature review for culture studies and the study done here revealed a major role for cobalt in controlling the amount of heterocysts produced. More work needs to be done to understand cobalt biochemistry in cyanobacteria, especially with regards to nitrogen fixation.

Much of this thesis and indeed much of the work with phytoplankton relies on being able to measure biomass quickly and accurately. Chapter 7 introduces a simple, inexpensive and sensitive way of measuring algal cell numbers and biomass with the use of a smartphone app. Further work can be done to validate and develop this method further such as testing it with environmental samples or samples with high background DOM.

The overarching objective of this thesis was to assess the importance of micronutrients such as Fe and Co in the development and growth of algal blooms. New techniques were proposed as a way to elucidate uptake mechanisms, compare chelator strength, and measure phytoplankton biomass accurately with a simple, portable and inexpensive method.

References

Ahad, R., Phukan, T., and Syiem, M. (2015). Random sampling of cyanobacterial diversity from five locations within Eastern Himalayan Biodiversity hot spot. *International Journal of Advanced Research in Biological Sciences*, 2:20–29.

Almomani, F. A. and Örmeci, B. (2016). Estimation of algae concentration in water solutions using spectrophotometry measurements and absorbance first derivative. *Advanced Materials - TechConnect Briefs 2016*, 2:144–147.

Aly, W. S. M. and Andrews, S. C. (2016). Iron Regulation of Growth and Heterocyst Formation in the Nitrogen Fixing Cyanobacterium *Nostoc* sp. PCC 7120. *Journal of Ecology of Health & Environment*, 4(3):103–109.

Andersen, R. A. (2005). *Algal Culture Techniques*. Elsevier Academic Press, Burlington, MA.

Anderson, D. M., Boerlage, S. F. E., and Dixon, M. B. (2017). *Harmful Algal Blooms (HABs) and Desalination: a Guide to Impacts, Monitoring and Management*. United Nations Educational, Scientific, and Cultural Organization, Paris, France.

Anderson, D. M., Glibert, P. M., and Burkholder, J. M. (2002). Harmful algal blooms and eutrophication: Nutrient sources, composition, and consequences. *Estuaries*, 25(4):704–726.

Andreini, C., Bertini, I., Cavallaro, G., Holliday, G. L., and Thornton, J. M. (2008). Metal ions in biological catalysis: from enzyme databases to general principles. *JBIC Journal of Biological Inorganic Chemistry*, 13(8):1205–1218.

Bade, D. L., Pace, M. L., Cole, J. J., and Carpenter, S. R. (2006). Can algal photosynthetic inorganic carbon isotope fractionation be predicted in lakes using existing models? *Aquatic Sciences*, 68(2):142–153.

Baptista, M. S. and Vasconcelos, M. T. (2006). Cyanobacteria Metal Interactions: Requirements, Toxicity, and Ecological Implications. *Critical Reviews in Microbiology*, 32(3):127–137.

Barker, A. V., Pilbeam, D. J., and Pilbeam, D. J. (2015). *Handbook of Plant Nutrition, Second Edition*. CRC Press.

Bauer, C. C., Buikema, W. J., Black, K., and Haselkorn, R. (1995). A short-filament mutant of *Anabaena* sp. strain PCC 7120 that fragments in nitrogen-deficient medium. *Journal of bacteriology*, 177(6):1520–1526.

Bauersachs, T., Schouten, S., Compaoré, J., Wollenzien, U., Stal, L. J., and Sinninghe Damsteé, J. S. (2009). Nitrogen isotopic fractionation associated with growth on dinitrogen gas and nitrate by cyanobacteria. *Limnology and Oceanography*, 54(4):1403–1411.

Berendt, S., Lehner, J., Zhang, Y. V., Rasse, T. M., Forchhammer, K., and Maldener, I. (2012). Cell Wall Amidase AmiC1 Is Required for Cellular Communication and Heterocyst Development in the Cyanobacterium *Anabaena* PCC 7120 but Not for Filament Integrity. *Journal of Bacteriology*, 194(19):5218–5227.

Berg, J. M., Tymoczko, J. L., and Stryer, L. (2002). A Proton Gradient Powers the Synthesis of ATP. In *Biochemistry*, chapter 18.4. W H Freeman, 5th edition.

Bergquist, B. and Boyle, E. (2006). Iron isotopes in the Amazon River system: Weathering and transport signatures. *Earth and Planetary Science Letters*, 248(1-2):54–68.

Borowitzka, M. A. and Moheimani, N. R. (2013). *Algae for Biofuels and Energy*. Springer Netherlands, Dordrecht.

Borthakur, P. B., Orozco, C. C., Young-Robbins, S. S., Haselkorn, R., and Callahan, S. M. (2005). Inactivation of patS and hetN causes lethal levels of heterocyst differentiation in the filamentous cyanobacterium *Anabaena* sp. PCC 7120. *Molecular Microbiology*, 57(1):111–123.

Braddock, J. F., Luong, H. V., and Brown, E. J. (1984). Growth Kinetics of *Thiobacillus ferrooxidans* Isolated from Arsenic Mine Drainage. *Applied and Environmental Microbiology*, 48(1):48–55.

Braun, E. (2007). *Reactive nitrogen in the environment : too much or too little of a good thing*. UNEP DTIE, Sustainable Consumption and Production (SCP) Branch, Paris, Falmouth, MA, USA.

Burkhardt, S., Riebesell, U., and Zondervan, I. (1999). Effects of growth rate, CO_2 concentration, and cell size on the stable carbon isotope fractionation in marine phytoplankton. *Geochimica et Cosmochimica Acta*, 63(22):3729–3741.

Burrows, A., Parsons, A., Pilling, G., and Price, G. (2017). *Chemistry3: introducing inorganic, organic and physical chemistry*. Oxford University Press.

Butterwick, C., Heaney, S., and Talling, J. (1982). A comparison of eight methods for estimating the biomass and growth of planktonic algae. *British Phycological Journal*, 17(1):69–79.

Chaurasia, A. K. and Apte, S. K. (2011). Improved Eco-Friendly Recombinant *Anabaena* sp. Strain PCC7120 with Enhanced Nitrogen Biofertilizer Potential. *Applied and Environmental Microbiology*, 77(2):395–399.

Chen, Y.-B., Dominic, B., Mellon, M. T., and Zehr, J. P. (1998). Circadian Rhythm of Nitrogenase Gene Expression in the Diazotrophic Filamentous Nonheterocystous CyanobacteriumTrichodesmium sp. Strain IMS 101. *Journal of Bacteriology*, 180(14):3598–3605.

Chioccioli, M., Hankamer, B., and Ross, I. L. (2014). Flow cytometry pulse width data enables rapid and sensitive estimation of biomass dry weight in the microalgae *Chlamydomonas reinhardtii* and *Chlorella vulgaris*. *PLoS ONE*, 9(5):1–12.

Chudzik, B., Malm, A., Rajtar, B., and Polz-Dacewicz, M. (2007). In vitro inhibitory activity of EDTA against planktonic and adherent cells of *Candida* sp. *Annals of Microbiology*, 57(1):115–119.

Coplen, T. B. (2011). Guidelines and recommended terms for expression of stable-isotope-ratio and gas-ratio measurement results. *Rapid Communications in Mass Spectrometry*, 25(17):2538–2560.

Creed, I. F., Bergström, A.-K., Trick, C. G., Grimm, N. B., Hessen, D. O., Karlsson, J., Kidd, K. A., Kritzberg, E., McKnight, D. M., Freeman, E. C., Senar, O. E., Andersson, A., Ask, J., Berggren, M., Cherif, M., Giesler, R., Hotchkiss, E. R., Kortelainen, P., Palta, M. M., Vrede, T., and Weyhenmeyer, G. A. (2018). Global change-driven effects on dissolved organic matter composition: Implications for food webs of northern lakes. *Global Change Biology*, 24(8):3692–3714.

Croft, M. T., Warren, M. J., and Smith, A. G. (2006). Algae Need Their Vitamins. *Eukaryotic Cell*, 5(8):1175–1183.

Dauphas, N., John, S. G., and Rouxel, O. (2017). Iron Isotope Systematics. *Reviews in Mineralogy and Geochemistry*, 82(1):415–510.

de Figueiredo, D. R., Goncalves, A. M. M., Castro, B. B., Goncalves, F., Pereira, M. J., and Correia, A. (2011). Differential inter- and intra-specific responses of *Aphanizomenon* strains to nutrient limitation and algal growth inhibition. *Journal of Plankton Research*, 33(10):1606–1616.

Demming, A. (2010). King of the elements? *Nanotechnology*, 21(30):300201.

Dijkstra, P., LaViolette, C. M., Coyle, J. S., Doucett, R. R., Schwartz, E., Hart, S. C., and Hungate, B. A. (2008). ^{15}N enrichment as an integrator of the effects of C and N on microbial metabolism and ecosystem function. *Ecology Letters*, 11(4):389–397.

Doak, J., Gupta, R., Manivannan, K., Ghosh, K., and Kahol, P. (2010). Effect of particle size distributions on absorbance spectra of gold nanoparticles. *Physica E: Low-dimensional Systems and Nanostructures*, 42(5):1605–1609.

Dodds, W. K., Bouska, W. W., Eitzmann, J. L., Pilger, T. J., Pitts, K. L., Riley, A. J., Schloesser, J. T., and Thornbrugh, D. J. (2009). Eutrophication of U.S. Freshwaters: Analysis of Potential Economic Damages. *Environmental Science & Technology*, 43(1):12–19.

Dolan, D. M. and McGunagle, K. P. (2005). Lake Erie Total Phosphorus Loading Analysis and Update: 1996 - 2002. *Journal of Great Lakes Research*, 31:11–22.

Downing, J. A., Watson, S. B., and McCauley, E. (2001). Predicting Cyanobacteria dominance in lakes. *Canadian Journal of Fisheries and Aquatic Sciences*, 58(10):1905–1908.

Downs, T. M., Schallenberg, M., and Burns, C. W. (2008). Responses of lake phytoplankton to micronutrient enrichment: a study in two New Zealand lakes and an analysis of published data. *Aquatic Sciences*, 70(4):347–360.

Einola, E., Rantakari, M., Kankaala, P., Kortelainen, P., Ojala, A., Pajunen, H., Mäkelä, S., and Arvola, L. (2011). Carbon pools and fluxes in a chain of five boreal lakes: A dry and wet year comparison. *Journal of Geophysical Research*, 116(G3):G03009.

Elser, J. J., Marzolf, E. R., and Goldman, C. R. (1990). Phosphorus and Nitrogen Limitation of Phytoplankton Growth in the Freshwaters of North America: A Review and Critique of Experimental Enrichments. *Canadian Journal of Fisheries and Aquatic Sciences*, 47(7):1468–1477.

Environmental Protection Agency (1983). EPA Methods for Chemical Analysis of Water and Wastes. Technical report.

Erratt, K. J. (2017). *Urea as an Effective Nitrogen Source for Cyanobacteria*. PhD thesis, University of Western Ontario.

Falkowski, P. G. and Raven, J. A. (2007). *Aquatic Photosynthesis*. Princeton University Press, Princeton, NJ, 2nd edition.

Farquhar, G. and Richards, R. (1984). Isotopic Composition of Plant Carbon Correlates with Water-use Efficiency of Wheat Genotypes. *Aust. J. Plant Pkysiol*, 11(1):539–52.

Farquhar, G. D., Ehleringer, J. R., and Hubick, K. T. (1989). Carbon Isotope Discrimination and Photosynthesis. *Annual Review of Plant Physiology and Plant Molecular Biology*, 40(1):503–537.

Farrar, K., Bryant, D., and Cope-Selby, N. (2014). Understanding and engineering beneficial plant-microbe interactions: plant growth promotion in energy crops. *Plant Biotechnology Journal*, 12(9):1193–1206.

Fehr, M. A., Andersson, P. S., Hålenius, U., and Mörth, C.-M. (2008). Iron isotope variations in Holocene sediments of the Gotland Deep, Baltic Sea. *Geochimica et Cosmochimica Acta*, 72(3):807–826.

Filstrup, C. T. and Downing, J. A. (2017). Relationship of chlorophyll to phosphorus and nitrogen in nutrient-rich lakes. *Inland Waters*, 2041(November):1–16.

Findlay, D. L., Hecky, R. E., Hendzel, L. L., Stainton, M. P., and Regehr, G. W. (1994). Relationship Between N_2-Fixation and Heterocyst Abundance and its Relevance to the Nitrogen Budget of Lake 227. *Canadian Journal of Fisheries and Aquatic Sciences*, 51(10):2254–2266.

Fogg, G. and Thake, B. (1987). *Algae Cultures and Phytoplankton Ecology*. The University of Winsconsins Press Ltd., London, 3rd edition.

Frey, B. C. and Mutz, A. (2006). The Public Trust in Surface Waterways and Submerged Lands of the Great Lakes States, 40 U. Mich. Technical report.

Fu, F.-X., Mulholland, M. R., Garcia, N. S., Beck, A., Bernhardt, P. W., Warner, M. E., Sañudo-Wilhelmy, S. A., and Hutchins, D. A. (2008). Interactions between changing pCO2, N2 fixation, and Fe limitation in the marine unicellular cyanobacterium *Crocosphaera*. *Limnology and Oceanography*, 53(6):2472–2484.

Fujii, M., Yeung, A. C. Y., and Waite, T. D. (2015). Competitive Effects of Calcium and Magnesium Ions on the Photochemical Transformation and Associated Cellular Uptake of Iron by the Freshwater Cyanobacterial Phytoplankton *Microcystis aeruginosa*. *Environmental Science & Technology*, 49(15):9133–9142.

Galloway, J. N., Dentener, F. J., Capone, D. G., Boyer, E. W., Howarth, R. W., Seitzinger, S. P., Asner, G. P., Cleveland, C. C., Green, P. A., Holland, E. A., Karl, D. M., Michaels, A. F., Porter, J. H., Townsend, A. R., and Vörösmarty, C. J. (2004). Nitrogen Cycles: Past, Present, and Future. *Biogeochemistry*, 70(2):153–226.

Glusker, J. P. (1980). Citrate conformation and chelation: enzymic implications. *Accounts of Chemical Research*, 13(10):345–352.

Goldman, C. R. (1966). Micronutrient limiting factors and their detection in natural phytoplankton populations. *Primary Productivity in Aquatic Environments. Mem. Ist. Ital. Idrobiol*, 18:121–136.

Gour, R. S., Bairagi, M., Garlapati, V. K., and Kant, A. (2018). Enhanced microalgal lipid production with media engineering of potassium nitrate as a nitrogen source. *Bioengineered*, 9(1):98–107.

Graham, L. E., Graham, J. M., Cook, M. E., and Wilcox, L. W. (2016). *Algae*.

Granéli, E. and Haraldsson, C. (1993). Can Increased Leaching of Trace Metals from Acidified Areas Influence Phytoplankton Growth in Coastal Waters? *Ambio*, 22(5):308–311.

Gregor, J. and Maršálek, B. (2004). Freshwater phytoplankton quantification by chlorophyll a: A comparative study of in vitro, in vivo and in situ methods. *Water Research*, 38(3):517–522.

Gu, B., Chapman, A. D., and Schelske, C. L. (2006). Factors controlling seasonal variations in stable isotope composition of particulate organic matter in a softwater eutrophic lake. *Limnology and Oceanography*, 51(6):2837–2848.

Gu, B., Schell, D. M., and Alexander, V. (1994). Stable Carbon and Nitrogen Isotopic Analysis of the Plankton Food Web in a Subarctic Lake. *Canadian Journal of Fisheries and Aquatic Sciences*, 51(6):1338–1344.

Guiry, E. (2019). Complexities of Stable Carbon and Nitrogen Isotope Biogeochemistry in Ancient Freshwater Ecosystems: Implications for the Study of Past Subsistence and Environmental Change. *Frontiers in Ecology and Evolution*, 7(AUG):313.

Hallsworth, E. G., Wilson, S. B., and Greenwood, E. A. N. (1960). Copper and Cobalt in Nitrogen Fixation. *Nature*, 187(4731):79–80.

Hanson, P. C., Hamilton, D. P., Stanley, E. H., Preston, N., Langman, O. C., and Kara, E. L. (2011). Fate of Allochthonous Dissolved Organic Carbon in Lakes: A Quantitative Approach. *PLoS ONE*, 6(7):e21884.

Harish and Seth, K. (2020). Molecular circuit of heterocyst differentiation in cyanobacteria. *Journal of Basic Microbiology*.

Harris, D. C. (2010). *Quantitative Chemical Analysis*. W. H. Freeman, New York, NY, 8th edition.

Hawco, N. J., McIlvin, M. M., Bundy, R. M., Tagliabue, A., Goepfert, T. J., Moran, D. M., Valentin-Alvarado, L., DiTullio, G. R., and Saito, M. A. (2020). Minimal cobalt metabolism in the marine cyanobacterium *Prochlorococcus*. *Proceedings of the National Academy of Sciences*, 12:202001393.

Hawco, N. J. and Saito, M. A. (2018). Competitive inhibition of cobalt uptake by zinc and manganese in a pacific *Prochlorococcus* strain: Insights into metal homeostasis in a streamlined oligotrophic cyanobacterium. *Limnology and Oceanography*, 63(5):2229–2249.

Healey, F. P. (1980). Slope of the Monod equation as an indicator of advantage in nutrient competition. *Microbial Ecology*, 5(4):281–286.

Health Canada (2012). *Guidelines for Canadian Recreational Water Quality*. 3rd edition.

Helliwell, K. E., Lawrence, A. D., Holzer, A., Kudahl, U. J., Sasso, S., Kräutler, B., Scanlan, D. J., Warren, M. J., and Smith, A. G. (2016). Cyanobacteria and Eukaryotic Algae Use Different Chemical Variants of Vitamin B12. *Current biology : CB*, 26(8):999–1008.

Herrero, A., Stavans, J., and Flores, E. (2016). The multicellular nature of filamentous heterocyst-forming cyanobacteria. *FEMS Microbiology Reviews*, 40(6):831–854.

Higgins, S. N., Paterson, M. J., Hecky, R. E., Schindler, D. W., Venkiteswaran, J. J., and Findlay, D. L. (2017). Biological Nitrogen Fixation Prevents the Response of a Eutrophic Lake to Reduced Loading of Nitrogen: Evidence from a 46-Year Whole-Lake Experiment. *Ecosystems*, pages 1–13.

Hill, R. D., Rinker, R. G., and Wilson, H. D. (1980). Atmospheric Nitrogen Fixation by Lightning. *Journal of the Atmospheric Sciences*, 37(1):179–192.

Hill, W. R., Fanta, S. E., and Roberts, B. J. (2009). Quantifying phosphorus and light effects in stream algae. *Limnology and Oceanography*, 54(1):368–380.

Ho, J. C. and Michalak, A. M. (2015). Challenges in tracking harmful algal blooms: A synthesis of evidence from Lake Erie. *Journal of Great Lakes Research*, 41(2):317–325.

Hoffmann, D., Gutekunst, K., Klissenbauer, M., Schulz-Friedrich, R., and Appel, J. (2006). Mutagenesis of hydrogenase accessory genes of *Synechocystis* sp. PCC 6803. *FEBS Journal*, 273(19):4516–4527.

Holben, W. E. and Ostrom, P. H. (2000). Monitoring Bacterial Transport by Stable Isotope Enrichment of Cells. *Applied and Environmental Microbiology*, 66(11):4935–4939.

Holm-Hansen, O., Gerloff, G. C., and Skoog, F. (1954). Cobalt as an Essential Element for Blue-Green Algae. *Physiologia Plantarum*, 7(4):665–675.

Hood, R. R., Laws, E. A., Armstrong, R. A., Bates, N. R., Brown, C. W., Carlson, C. A., Chai, F., Doney, S. C., Falkowski, P. G., Feely, R. A., Friedrichs, M. A., Landry, M. R., Keith Moore, J., Nelson, D. M., Richardson, T. L., Salihoglu, B., Schartau, M., Toole, D. A., and Wiggert, J. D. (2006). Pelagic functional group modeling: Progress, challenges and prospects. *Deep Sea Research Part II: Topical Studies in Oceanography*, 53(5-7):459–512.

Hu, W. (2014). *Dry weight and cell density of individual algal and cyanobacterial cells for algae research and development*. PhD thesis, University of Missouri–Columbia.

Hudnell, H. K. (2010). The state of U.S. freshwater harmful algal blooms assessments, policy and legislation. *Toxicon*, 55(5):1024–1034.

Huisman, J., Codd, G. A., Paerl, H. W., Ibelings, B. W., Verspagen, J. M. H., and Visser, P. M. (2018). Cyanobacterial blooms. *Nature Reviews Microbiology*, 16(8):471–483.

IAEA (2009). *Manual for the Use of Stable Isotopes in Entomology*. Non-serial Publications. International Atomic Energy Agency, Vienna.

Irwin, A. J., Nelles, A. M., and Finkel, Z. V. (2012). Phytoplankton niches estimated from field data. *Limnology and Oceanography*, 57(3):787–797.

Iswaran, V. and Rao, W. V. B. S. (1964). Role of Cobalt in Nitrogen Fixation by *Azotobacter chroococcum*. *Nature*, 203(4944):549.

Jewell, W. J. and Kulasooriya, S. A. (1970). The Relation of Acetylene Reduction to Heterocyst Frequency in Blue-Green Algae. *Journal of Experimental Botany*, 21(4):874–880.

Jiang, M., Zhou, Y., Cao, X., Ji, X., Zhang, W., Huang, W., Zhang, J., and Zheng, Z. (2019). The concentration thresholds establishment of nitrogen and phosphorus considering the effects of extracellular substrate-to-biomass ratio on cyanobacterial growth kinetics. *Science of The Total Environment*, 662:307–312.

Johnson, C. M. and Beard, B. L. (2006). Fe isotopes: An emerging technique for understanding modern and ancient biogeochemical cycles. *GSA Today*, 16(11):4.

Johnson, C. M., Beard, B. L., and Roden, E. E. (2008). The Iron Isotope Fingerprints of Redox and Biogeochemical Cycling in Modern and Ancient Earth. *Annual Review of Earth and Planetary Sciences*, 36(1):457–493.

Jones, A. M., Griffin, P. J., and Waite, T. D. (2015). Ferrous iron oxidation by molecular oxygen under acidic conditions: The effect of citrate, EDTA and fulvic acid. *Geochimica et Cosmochimica Acta*, 160:117–131.

Jones, M. R. and Lee, K. (2020). Sequential injection analysis Ferrozine spectrophotometry versus Luminol chemiluminescence for continuous online monitoring of the concentration and speciation of iron. *Microchemical Journal*, 157(December 2019):104881.

Kane, D. D., Conroy, J. D., Peter Richards, R., Baker, D. B., and Culver, D. A. (2014). Re-eutrophication of Lake Erie: Correlations between tributary nutrient loads and phytoplankton biomass. *Journal of Great Lakes Research*, 40(3):496–501.

Kangatharalingam, N., Priscu, J. C., and Paerl, H. W. (1992). Heterocyst envelope thickness, heterocyst frequency and nitrogenase activity in *Anabaena flos-aquae*: influence of exogenous oxygen tension. *Journal of General Microbiology*, 138(12):2673–2678.

Karsh, K., Trull, T., Sigman, D., Thompson, P., and Granger, J. (2014). The contributions of nitrate uptake and efflux to isotope fractionation during algal nitrate assimilation. *Geochimica et Cosmochimica Acta*, 132:391–412.

Kean, M. A., Brons Delgado, E., Mensink, B. P., and Bugter, J. (2015). Iron chelating agents and their effects on the growth of *Pseudokirchneriella subcapitata*, *Chlorella vulgaris*, *Phaeodactylum tricornutum* and *Spirulina platensis* in comparison to Fe-EDTA. *J. Algal Biomass Utln.*, 6(1):56–73.

Keller, M. D., Bellows, W. K., and Guillard, R. R. (1988). Microwave treatment for sterilization of phytoplankton culture media. *Journal of Experimental Marine Biology and Ecology*, 117(3):279–283.

Kelly, L. T., Champeaud, M., Beuzenberg, V., Goodwin, E., Verburg, P., and Wood, S. A. (2021). Trace metal and nitrogen concentrations differentially affect bloom forming cyanobacteria of the genus Dolichospermum. *Aquatic Sciences*, 83(2):34.

Kendall, B., Anbar, A. D., Kappler, A., and Konhauser, K. O. (2012). The Global Iron Cycle. In Knoll, A. H., Canfield, D. E., and Konhauser, K. O., editors, *Fundamentals of Geobiology*, chapter 6, pages 65–92. Blackwell Publishing Ltd, 1st edition.

Khan, F. A. and Ansari, A. (2005). Eutrophication: An Ecological Vision. *The Botanical Review*, 71(4):449–482.

Kilham, S. S. (1975). Kinetics of Silicon-Limited Growth in the Freshwater Diatom *Asterionella formosa*. *Journal of Phycology*, 11(4):396–399.

Klein, R. M. and Manos, G. E. (1960). Use of Metal Chelates for Plant Tissue Cultures. *Annals of the New York Academy of Sciences*, 88(2):416–425.

Knowles, J. R. (1980). Enzyme-Catalyzed Phosphoryl Transfer Reactions. *Annual Review of Biochemistry*, 49(1):877–919.

Kranzler, C., Lis, H., Finkel, O. M., Schmetterer, G., Shaked, Y., and Keren, N. (2014). Coordinated transporter activity shapes high-affinity iron acquisition in cyanobacteria. *The ISME Journal*, 8(2):409–417.

Kranzler, C., Lis, H., Shaked, Y., and Keren, N. (2011). The role of reduction in iron uptake processes in a unicellular, planktonic cyanobacterium. *Environmental Microbiology*, 13(11):2990–2999.

Krauss, R. W. (1955). Nutrient Supply for Large-Scale Algal Cultures. *The Scientific Monthly*, 80(1):21–28.

Kukert, H. and Riebesell, U. (1998). Phytoplankton carbon isotope fractionation during a diatom spring bloom in a Norwegian fjord. Technical report.

Kulasooriya, S. A., Lang, N. J., and Fay, P. (1972). The heterocysts of blue-green algae. III. Differentiation and nitrogenase activity. *Proceedings of the Royal Society of London. Series B. Biological Sciences*, 181(1063):199–209.

Kumar, K., Mella-Herrera, R. A., and Golden, J. W. (2010). Cyanobacterial Heterocysts. *Cold Spring Harbor Perspectives in Biology*, 2(4):a000315–a000315.

Kurihara, H., Ikeda, N., and Umezawa, Y. (2018). Diurnal and seasonal variation of particle and dissolved organic matter release by the coral *Acropora tenuis*. *PeerJ*, 6(11):e5728.

Lab Tools (2018). Colorimeter (5.5.1) [Mobile Application Software]. Retrieved from https://play.google.com.

Laws, E. A., Bidigare, R. R., and Popp, B. N. (1997). Effect of growth rate and CO 2 concentration on carbon isotopic fractionation by the marine diatom *Phaeodactylum tricornutum*. *Limnology and Oceanography*, 42(7):1552–1560.

Leenheer, J. and Croué, J.-P. (2003). Characterizing aquatic dissolved organic matter. *Environmental Science & Technology*, 37:19A–26A.

Lehmann, M. F., Bernasconi, S. M., McKenzie, J. A., Barbieri, A., Simona, M., and Veronesi, M. (2004). Seasonal variation of the δC and δN of particulate and dissolved carbon and nitrogen in Lake Lugano: Constraints on biogeochemical cycling in a eutrophic lake. *Limnology and Oceanography*, 49(2):415–429.

Li, Y., Veilleux, D. J., and Wikfors, G. H. (2009). Particle removal by Northern bay scallops *Argopecten irradians irradians* in a semi-natural setting: Application of a flow-cytometric technique. *Aquaculture*, 296(3-4):237–245.

Lis, H., Kranzler, C., Keren, N., and Shaked, Y. (2015). A Comparative Study of Iron Uptake Rates and Mechanisms amongst Marine and Fresh Water Cyanobacteria: Prevalence of Reductive Iron Uptake. *Life*, 5(1):841–860.

Liu, J. Y., Zeng, L. H., Ren, Z. H., Du, T. M., and Liu, X. (2020). Rapid in situ measurements of algal cell concentrations using an artificial neural network and single-excitation fluorescence spectrometry. *Algal Research*, 45(November 2019):101739.

Loftus, S. E. and Johnson, Z. I. (2019). Reused Cultivation Water Accumulates Dissolved Organic Carbon and Uniquely Influences Different Marine Microalgae. *Frontiers in Bioengineering and Biotechnology*, 7.

Mackensen, A. and Schmiedl, G. (2019). Stable carbon isotopes in paleoceanography: atmosphere, oceans, and sediments. *Earth-Science Reviews*, 197:102893.

Maldener, I., Hannus, S., and Kammerer, M. (2003). Description of five mutants of the cyanobacterium *Anabaena* sp. strain PCC 7120 affected in heterocyst differentiation and identification of the transposon-tagged genes. *FEMS Microbiology Letters*, 224(2):205–213.

McClanahan, T. and Humphries, A. (2012). Differential and slow life-history responses of fishes to coral reef closures. *Marine Ecology Progress Series*, 469:121–131.

Michalak, A. M., Anderson, E. J., Beletsky, D., Boland, S., Bosch, N. S., Bridgeman, T. B., Chaffin, J. D., Cho, K., Confesor, R., Daloglu, I., DePinto, J. V., Evans, M. A., Fahnenstiel, G. L., He, L., Ho, J. C., Jenkins, L., Johengen, T. H., Kuo, K. C., LaPorte, E., Liu, X., McWilliams, M. R., Moore, M. R., Posselt, D. J., Richards, R. P., Scavia, D., Steiner, A. L., Verhamme, E., Wright, D. M., and Zagorski, M. A. (2013). Record-setting algal bloom in Lake Erie caused by agricultural and meteorological trends consistent with expected future conditions. *Proceedings of the National Academy of Sciences*, 110(16):6448–6452.

Miles, C. J. and Brezonik, P. L. (1981). Oxygen consumption in humic-colored waters by a photochemical ferrous-ferric catalytic cycle. *Environmental Science & Technology*, 15(9):1089–1095.

Mohlin, M., Roleda, M. Y., Pattanaik, B., Tenne, S.-J., and Wulff, A. (2012). Interspecific Resource Competition-Combined Effects of Radiation and Nutrient Limitation on Two Diazotrophic Filamentous Cyanobacteria. *Microbial Ecology*, 63(4):736–750.

Moisander, P. H., Hench, J. L., Kononen, K., and Paerl, H. W. (2002). Small-scale shear effects on heterocystous cyanobacteria. *Limnology and Oceanography*, 47(1):108–119.

Molot, L. A. and Brown, E. J. (1986). Method for determining the temporal response of microbial phosphate transport affinity. *Applied and Environmental Microbiology*, 51(3):524–531.

Molot, L. A., Li, G., Findlay, D. L., and Watson, S. B. (2010). Iron-mediated suppression of bloom-forming cyanobacteria by oxine in a eutrophic lake. *Freshwater Biology*, 55(5):1102–1117.

Molot, L. A., Schiff, S. L., Venkiteswaran, J. J., Baulch, H. M., Higgins, S. N., Zastepa, A., Verschoor, M. J., and Walters, D. (2021). Low sediment redox promotes cyanobacteria blooms across a trophic range: implications for management. *Lake and Reservoir Management*, pages 1–33.

Molot, L. A., Watson, S. B., Creed, I. F., Trick, C. G., McCabe, S. K., Verschoor, M. J., Sorichetti, R. J., Powe, C., Venkiteswaran, J. J., and Schiff, S. L. (2014). A novel model for cyanobacteria bloom formation: the critical role of anoxia and ferrous iron. *Freshwater Biology*, 59(6):1323–1340.

Monod, J. (1950). The technique of continuous culture. *Ann. Inst. Pasteur*, 79:390–410.

Muchowska, K. B., Varma, S. J., and Moran, J. (2019). Synthesis and breakdown of universal metabolic precursors promoted by iron. *Nature*, 569(7754):104–107.

Mutshinda, C. M., Finkel, Z. V., Widdicombe, C. E., and Irwin, A. J. (2016). Ecological equivalence of species within phytoplankton functional groups. *Functional Ecology*, 30(10):1714–1722.

Nayak, S., Prasanna, R., Prasanna, B. M., and Sahoo, D. B. (2007). Analysing diversity among Indian isolates of *Anabaena* (Nostocales, Cyanophyta) using morphological, physiological and biochemical characters. *World Journal of Microbiology and Biotechnology*, 23(11):1575–1584.

Nürnberg, D. J., Mariscal, V., Bornikoel, J., Nieves-Morión, M., Krauß, N., Herrero, A., Maldener, I., Flores, E., and Mullineaux, C. W. (2015). Intercellular Diffusion of a Fluorescent Sucrose Analog via the Septal Junctions in a Filamentous Cyanobacterium. *mBio*, 6(2):1–12.

Ogawa, R. E. and Carr, J. F. (1969). The Influence of Nitrogen on Heterocyst Production in Blue-Green Algae. *Limnology and Oceanography*, 14(3):342–351.

Orihel, D. M., Baulch, H. M., Casson, N. J., North, R. L., Parsons, C. T., Seckar, D. C., and Venkiteswaran, J. J. (2017). Internal phosphorus loading in Canadian fresh waters: a critical review and data analysis. *Canadian Journal of Fisheries and Aquatic Sciences*, 74(12):2005–2029.

Ota, S. and Kawano, S. (2017). Extraction and Molybdenum Blue-based Quantification of Total Phosphate and Polyphosphate in *Parachlorella*. *BIO-PROTOCOL*, 7(17).

Owens, J. and Legan, J. (1987). Determination of the Monod substrate saturation constant for microbial growth. *FEMS Microbiology Letters*, 46(4):419–432.

Padisák, J., Vasas, G., and Borics, G. (2016). Phycogeography of freshwater phytoplankton: traditional knowledge and new molecular tools. *Hydrobiologia*, 764(1):3–27.

Paerl, H. W., Hall, N. S., and Calandrino, E. S. (2011). Controlling harmful cyanobacterial blooms in a world experiencing anthropogenic and climatic-induced change. *Science of the Total Environment*, 409(10):1739–1745.

Park, R. and Epstein, S. (1961). Metabolic fractionation of C^{13} & C^{12} in plants. *Plant Physiology*, 36(2):133–138.

Patterson, J. W. (1987). *Metals speciation separation and recovery*, volume 1. CRC Press.

Peng, B., Xu, J., Fan, M., Guo, Y., Ma, Y., Zhou, M., and Fang, Y. (2020). Smartphone colorimetric determination of hydrogen peroxide in real samples based on B, N, and S co-doped carbon dots probe. *Analytical and Bioanalytical Chemistry*, 412(4):861–870.

Pernil, R. and Schleiff, E. (2019). Metalloproteins in the Biology of Heterocysts. *Life*, 9(2):32.

Peterson, B. J., Wollheim, W. M., Mulholland, P. J., Webster, J. R., Meyer, J. L., Tank, J. L., Marti, E., Bowden, W. B., Valett, H. M., Hershey, A. E., McDowell, W. H., Dodds, W. K., Hamilton, S. K., Gregory, S., and Morrall, D. D. (2001). Control of Nitrogen Export from Watersheds by Headwater Streams. *Science*, 292(5514):86–90.

Pick, F. R. (2016). Blooming algae: a Canadian perspective on the rise of toxic cyanobacteria. *Canadian Journal of Fisheries and Aquatic Sciences*, 73(7):1149–1158.

Pires, M. D. (2010). Evaluation of fluorometers for the in situ monitoring of chlorophyll and/or cyanobacteria. Technical report.

Popp, B. N., Laws, E. A., Bidigare, R. R., Dore, J. E., Hanson, K. L., and Wakeham, S. G. (1998). Effect of Phytoplankton Cell Geometry on Carbon Isotopic Fractionation. *Geochimica et Cosmochimica Acta*, 62(1):69–77.

Qiu, Y. (2018). *Proteogenomic Study of Nitrogen-Fixing Cyanobacterium Anabaena Cylindrica*. PhD thesis, South Dakota State University.

Ravindranath, R., Periasamy, A. P., Roy, P., Chen, Y. W., and Chang, H. T. (2018). Smart app-based on-field colorimetric quantification of mercury via analyte-induced enhancement of the photocatalytic activity of TiO_2-Au nanospheres. *Analytical and Bioanalytical Chemistry*, 410(18):4555–4564.

Rippka, R., Deruelles, J., Waterbury, J. B., Herdman, M., and Stanier, R. Y. (1979). Generic Assignments, Strain Histories and Properties of Pure Cultures of Cyanobacteria. *Microbiology*, 111(1):1–61.

Rivers, O. S., Beurmann, S., Dow, A., Cozy, L. M., and Videau, P. (2018). Phenotypic Assessment Suggests Multiple Start Codons for HetN, an Inhibitor of Heterocyst Differentiation, in *Anabaena* sp. Strain PCC 7120. *Journal of Bacteriology*, 200(16).

Rodriguez, I. B. and Ho, T.-Y. (2015). Influence of Co and B12 on the growth and nitrogen fixation of *Trichodesmium*. *Frontiers in Microbiology*, 6(JUN):1–9.

Rother, J. and Fay, P. (1979). Blue-green algal growth and sporulation in response to simulated surface bloom conditions. *British Phycological Journal*, 14(1):59–68.

Saito, M. A., Moffett, J. W., and DiTullio, G. R. (2004). Cobalt and nickel in the Peru upwelling region: A major flux of labile cobalt utilized as a micronutrient. *Global Biogeochemical Cycles*, 18(4):n/a–n/a.

Santana-Casiano, J., González-Dávila, M., Rodríguez, M., and Millero, F. J. (2000). The effect of organic compounds in the oxidation kinetics of Fe(II). *Marine Chemistry*, 70(1-3):211–222.

Saryan, L. A. and Petering, D. H. (1980). Effects of Ethylenediaminetetraacetic Acid and 1,10-Phenanthroline on Cell Proliferation and DNA Synthesis of Ehrlich Ascites Cells. *Cancer Research*, 40(11):4092–4099.

Satpati, G. G., Gorain, P. C., and Pal, R. (2016). Efficacy of EDTA and Phosphorous on Biomass Yield and Total Lipid Accumulation in Two Green Microalgae with Special Emphasis on Neutral Lipid Detection by Flow Cytometry. *Advances in Biology*, 2016:1–12.

Schiff, S. L., Tsuji, J. M., Wu, L., Venkiteswaran, J. J., Molot, L. A., Elgood, R. J., Paterson, M. J., and Neufeld, J. D. (2017). Millions of Boreal Shield Lakes can be used to Probe Archaean Ocean Biogeochemistry. *Scientific Reports*, 7:46708.

Schindelin, H., Kisker, C., Schlessman, J. L., Howard, J. B., and Rees, D. C. (1997). Structure of ADP·AlF_4^--stabilized nitrogenase complex and its implications for signal transduction. *Nature*, 387(6631):370–376.

Schindler, D. W. (1974). Eutrophication and Recovery in Experimental Lakes: Implications for Lake Management. *Science*, 184(4139):897–899.

Schindler, D. W. (1975). Whole-lake eutrophication experiments with phosphorus, nitrogen and carbon. *SIL Proceedings, 1922-2010*, 19(4):3221–3231.

Schindler, D. W. (2006). Recent advances in the understanding and management of eutrophication. *Limnology and Oceanography*, 51(1part2):356–363.

Schindler, D. W. (2012). The dilemma of controlling cultural eutrophication of lakes. *Proceedings of the Royal Society B: Biological Sciences*, 279(1746):4322–4333.

Schindler, D. W., Hecky, R. E., Findlay, D. L., Stainton, M. P., Parker, B. R., Paterson, M. J., Beaty, K. G., Lyng, M., and Kasian, S. E. M. (2008). Eutrophication of lakes cannot be controlled by reducing nitrogen input: Results of a 37-year whole-ecosystem experiment. *Proceedings of the National Academy of Sciences*, 105(32):11254–11258.

Seibig, S. and van Eldik, R. (1997). Kinetics of [Fe^{II}(edta)] Oxidation by Molecular Oxygen Revisited. New Evidence for a Multistep Mechanism. *Inorganic Chemistry*, 36(18):4115–4120.

Shaked, Y., Kustka, A. B., Morel, F. M., and Erel, Y. (2004). Simultaneous determination of iron reduction and uptake by phytoplankton. *Limnology and Oceanography: Methods*, 2(5):137–145.

Sharp, Z. (2017). *Principles of Stable Isotope Geochemistry*.

Sheftel, J., Loechl, C., Mokhtar, N., and Tanumihardjo, S. A. (2018). Use of Stable Isotopes to Evaluate Bioefficacy of Provitamin A Carotenoids, Vitamin A Status, and Bioavailability of Iron and Zinc. *Advances in Nutrition*, 9(5):625–636.

Shi, T., Sun, Y., and Falkowski, P. G. (2007). Effects of iron limitation on the expression of metabolic genes in the marine cyanobacterium *Trichodesmium erythraeum* IMS101. *Environmental Microbiology*, 9(12):2945–2956.

Silva, A. M. N., Kong, X., Parkin, M. C., Cammack, R., and Hider, R. C. (2009). Iron(III) citrate speciation in aqueous solution. *Dalton Transactions*, (40):8616.

Simon, N., Cras, A.-L., Foulon, E., and Lemée, R. (2009). Diversity and evolution of marine phytoplankton. *Comptes Rendus Biologies*, 332(2-3):159–170.

Singh, P., Kumar, N., Jethva, M., Yadav, S., Kumari, P., Thakur, A., and Kushwaha, H. R. (2018). Riboswitch regulation in cyanobacteria is independent of their habitat adaptations. *Physiology and Molecular Biology of Plants*, 24(2):315–324.

Smayda, T. J. (1997). What is a bloom? A commentary. *Limnology and Oceanography*, 42(5part2):1132–1136.

Smil, V. (2000). Phosphorus in the Environment : Natural Flows and Human Interferences. *Annual Review of Energy and the Environment*, 25(1):53–88.

Smith, V. H. and Schindler, D. W. (2009). Eutrophication science: where do we go from here? *Trends in Ecology & Evolution*, 24(4):201–207.

Song, K., Li, L., Tedesco, L., Clercin, N., Hall, B., Li, S., Shi, K., Liu, D., and Sun, Y. (2013). Remote estimation of phycocyanin (PC) for inland waters coupled with YSI PC fluorescence probe. *Environmental Science and Pollution Research*, 20(8):5330–5340.

Sprouffske, K. and Wagner, A. (2016). *Growthcurver*: an R package for obtaining interpretable metrics from microbial growth curves. *BMC Bioinformatics*, 17(1):172.

Steel, J. A. (1971). *Microbial Aspects of Pollution.* Academic Press, New York, New York, us edition edition.

Stein, J. R., Hellebust, J. A., and Craigie, J. S. (1973). *Handbook of phycological methods: culture methods and growth measurements*. Cambridge University Press.

Stookey, L. L. (1970). Ferrozine—a new spectrophotometric reagent for iron. *Analytical Chemistry*, 42(7):779–781.

Stumm, W. and Morgan, J. J. (1995). *Aquatic Chemistry: Chemical Equilibria and Rates in Natural Waters*. John Wiley & Sons, New York, NY, 3rd edition.

Sunda, W. G. and Huntsman, S. A. (2015). High iron requirement for growth, photosynthesis, and low-light acclimation in the coastal cyanobacterium *Synechococcus bacillaris*. *Frontiers in Microbiology*, 6:1–13.

Sutton, M. A. and Bleeker, A. (2013). The shape of nitrogen to come. *Nature*, 494(7438):435–437.

Suzuki, K., Yang, S.-Y., Shimizu, S., Morishita, E. C., Jiang, J., Zhang, F., Hoque, M. M., Sato, Y., Tsunoda, M., Sekiguchi, T., and Takénaka, A. (2011). The unique structure of carbonic anhydrase αCA1 from Chlamydomonas reinhardtii. *Acta Crystallographica Section D Biological Crystallography*, 67(10):894–901.

Tanaka, Y., Miyajima, T., Yamada, K., Hori, M., Hasegawa, N., Umezawa, Y., and Koike, I. (2008). Specific growth rate as a determinant of the carbon isotope composition of the temperate seagrass Zostera marina. *Aquatic Botany*, 89(3):331–336.

Taylor, T. C., Backlund, A., Bjorhall, K., Spreitzer, R. J., and Andersson, I. (2001). First Crystal Structure of Rubisco from a Green Alga, *Chlamydomonas reinhardtii*. *Journal of Biological Chemistry*, 276(51):48159–48164.

Teutsch, N., von Gunten, U., Porcelli, D., Cirpka, O. A., and Halliday, A. N. (2005). Adsorption as a cause for iron isotope fractionation in reduced groundwater. *Geochimica et Cosmochimica Acta*, 69(17):4175–4185.

Thiel, T. (2005). Nitrogen Fixation in Heterocyst-Forming Cyanobacteria. In Klipp, W., Masepohl, B., Gallon, J. R., and Newton, W. E., editors, *Genetics and Regulation of Nitrogen Fixation in Free-Living Bacteria*, volume 2 of *Nitrogen Fixation: Origins, Applications, and Research Progress*, pages 73–110. Kluwer Academic Publishers, Dordrecht.

Tuck, A. F. (1976). Production of nitrogen oxides by lightning discharges. *Quarterly Journal of the Royal Meteorological Society*, 102(434):749–755.

Tucker, B. J. and Breaker, R. R. (2005). Riboswitches as versatile gene control elements. *Current Opinion in Structural Biology*, 15(3):342–348.

Ullrich, W. R. (1983). *Uptake and Reduction of Nitrate: Algae and Fungi*, pages 376–397. Springer Berlin Heidelberg, Berlin, Heidelberg.

Van Mooy, B. A. S., Fredricks, H. F., Pedler, B. E., Dyhrman, S. T., Karl, D. M., Koblížek, M., Lomas, M. W., Mincer, T. J., Moore, L. R., Moutin, T., Rappé, M. S., and Webb, E. A. (2009). Phytoplankton in the ocean use non-phosphorus lipids in response to phosphorus scarcity. *Nature*, 458(7234):69–72.

Vasas, G., Surányi, G., Bácsi, I., M-Hamvas, M., Máthé, C., Gonda, S., and Borbely, G. (2013). Alteration of Cylindrospermopsin Content of *Aphanizomenon ovalisporum* (Cyanobacteria, Nostocales) due to Step-Down from Combined Nitrogen to Dinitrogen. *Advances in Microbiology*, 03(08):557–564.

Verschoor, M. J. and Molot, L. A. (2013). A comparison of three colorimetric methods of ferrous and total reactive iron measurement in freshwaters. *Limnology and Oceanography: Methods*, 11(3):113–125.

Verschoor, M. J., Powe, C. R., McQuay, E., Schiff, S. L., Venkiteswaran, J. J., Li, J., and Molot, L. A. (2017). Internal iron loading and warm temperatures are preconditions for cyanobacterial dominance in embayments along Georgian Bay, Great Lakes. *Canadian Journal of Fisheries and Aquatic Sciences*, 74(9):1439–1453.

Videau, P., Rivers, O. S., Hurd, K., Ushijima, B., Oshiro, R. T., Ende, R. J., O'Hanlon, S. M., and Cozy, L. M. (2016). The heterocyst regulatory protein HetP and its homologs modulate heterocyst commitment in Anabaena sp. strain PCC 7120. *Proceedings of the National Academy of Sciences*, 113(45):E6984–E6992.

Walker, G. M. (1998). *Yeast physiology and biotechnology*. John Wiley & Sons.

Wallace, J. M. and Hobbs, P. V. (2006). *Atmospheric Science: An Introductory Survey*. Elsevier Academic Press, 2nd edition.

Waris, H. (1953). The Significance for Algae of Chelating Substances in the Nutrient Solutions. *Physiologia Plantarum*, 6(3):538–543.

Waser, N. A. D., Harrison, P. J., Nielsen, B., Calvert, S. E., and Turpin, D. H. (1998). Nitrogen isotope fractionation during the uptake and assimilation of nitrate, nitrite, ammonium, and urea by a marine diatom. *Limnology and Oceanography*, 43(2):215–224.

Watson, S. B., Ridal, J., and Boyer, G. L. (2008). Taste and odour and cyanobacterial toxins: impairment, prediction, and management in the Great Lakes. *Canadian Journal of Fisheries and Aquatic Sciences*, 65(8):1779–1796.

Wei, B., Sugiura, N., and Maekawa, T. (2001). Use of artificial neural network in the prediction of algal blooms. *Water Research*, 35(8):2022–2028.

Wilhelm, S. (1995). Ecology of iron-limited cyanobacteria: a review of physiological responses and implications for aquatic systems. *Aquatic Microbial Ecology*, 9(3):295–303.

Willet, A. I. and Rittmann, B. E. (2003). Slow complexation kinetics for ferric iron and EDTA complexes make EDTA non-biodegradable. *Biodegradation*, 14(2):105–121.

Williams, J. J., Beutel, M., Nurse, A., Moore, B., Hampton, S. E., and Saros, J. E. (2016). Phytoplankton responses to nitrogen enrichment in Pacific Northwest, USA Mountain Lakes. *Hydrobiologia*, 776(1):261–276.

Williamson, C. E., Morris, D. P., Pace, M. L., and Olson, O. G. (1999). Dissolved organic carbon and nutrients as regulators of lake ecosystems: Resurrection of a more integrated paradigm. *Limnology and Oceanography*, 44(3part2):795–803.

Winter, J. G., DeSellas, A. M., Fletcher, R., Heintsch, L., Morley, A., Nakamoto, L., and Utsumi, K. (2011). Algal blooms in Ontario, Canada: Increases in reports since 1994. *Lake and Reservoir Management*, 27(2):107–114.

Wolf, D., Georgic, W., and Klaiber, H. A. (2017). Reeling in the damages: Harmful algal blooms' impact on Lake Erie's recreational fishing industry. *Journal of Environmental Management*, 199:148–157.

Wolk, P. C. (1996). Heterocyst Formation. *Annual Review of Genetics*, 30(1):59–78.

Wu, L., Beard, B. L., Roden, E. E., and Johnson, C. M. (2011). Stable Iron Isotope Fractionation Between Aqueous Fe(II) and Hydrous Ferric Oxide. *Environmental Science & Technology*, 45(5):1847–1852.

Wubs, H. J. and Beenackers, A. A. C. M. (1993). Kinetics of the oxidation of ferrous chelates of EDTA and HEDTA in aqueous solution. *Industrial & Engineering Chemistry Research*, 32(11):2580–2594.

Xu, H., Paerl, H. W., Qin, B., Zhu, G., Hall, N. S., and Wu, Y. (2015). Determining Critical Nutrient Thresholds Needed to Control Harmful Cyanobacterial Blooms in Eutrophic Lake Taihu, China. *Environmental Science & Technology*, 49(2):1051–1059.

Xu, X., Risoul, V., Byrne, D., Champ, S., Douzi, B., and Latifi, A. (2020). HetL, HetR and PatS form a reaction-diffusion system to control pattern formation in the cyanobacterium Nostoc PCC 7120. *eLife*, 9.

Yin, C., Lan, Z., Zhao, M., and Bernhardt, H. (1992). Determination of phosphorus concentration threshold for algal growth in eutrophic Chaohu Lake, china. *Journal of Environmental Science and Health . Part A: Environmental Science and Engineering and Toxicology*, 27(2):433–443.

Yuan, J., Christensen, P. R., and Wolf, M. O. (2019). Dynamic anti-counterfeiting security features using multicolor dianthryl sulfoxides. *Chemical Science*, 10(43):10113–10121.

Yuan, T., Li, J. C., and Zhou, J. F. (2007). Effects of Temperature on the Threshold of Phosphorus for Algal Blooms. In *New Trends in Fluid Mechanics Research*, pages 646–646. Springer Berlin Heidelberg, Berlin, Heidelberg.

Zhao, J. and Wolk, C. P. (2008). Developmental Biology of Heterocysts, 2006. In Whitworth, D. E., editor, *Myxobacteria: Multicellularity and Differentiation*, chapter Developmen, pages 397–418. American Society of Microbiology, Washington, D.C.

Zhen, S. and Zhu, W. (2018). Determination of the in situ growth rate of Microcystis based on carbon and nitrogen stable isotope fractionation. *Water Supply*, 18(3):984–993.

APPENDICES

Appendix A

Conversion of Abs to Cell Number

A.1 Purpose

To convert absorbance units to cell numbers via linear models. These models were used when cell numbers were presented.

A.2 Methods

Cultures of *Anabaena flos-aqaue* (CPCC 67), *Aphanizomenon flos-aqaue* (NIES 81), *Aphanizomenon skujae* (isolate from Lake 227) and *Dolichospermum lemmermanii* (isolate from Lake Erie) were grown in both BG-11 and BG-11_0. Culture of *Microcystis aeruginosa* (PCC 7005) was grown in BG-11 and cultures of *Coelastrum proboscideum* (SAG 217-2), *Chlorella vulgaris* (CPCC 90) and *Chlamydomonas reinhardtii* (CPCC 243) were grown in BBM. All species were grown at 20°C on a 12:12h light/dark cycle at 100 μmol/m^2/s in media containing equivalent amount of $FeCl_3$ instead of ferric ammonium citrate and equivalent amount of $CoSO_4$ instead of $Co(NO_3)_2$ with (BG11) or without (BG11_0) nitrate (Rippka et al., 1979; Stein et al., 1973). A 12:12h light cycle was selected to mimic the circadian cycle of cyanobacteria and to ensure that N-fixation rates remained constant throughout the experiment (Chen et al., 1998).

Absorbance scans were taken for a dilution series of each species from 200 nm to 800 nm using a Cary 100 (Agilent) spectrophotometer. A_{750} was selected as a proxy for

cell concentration because at 750 nm, the interference from photosynthetic pigments is minimal (Chioccioli et al., 2014; Borowitzka and Moheimani, 2013).

Cell counts were done on the same samples using a hemocytometer under the microscope at 40X magnification. A minimum of five squares were counted for each of the replicate and a calibration curve was constructed for each species. The linear models were forced through the origin with the general equation:

$$NumberofCells = \mathrm{A}_{750} \times slope \tag{A.1}$$

A.3 Results

Table A.1: The conversions for each species from A_{750} to cell number. R^2 are indicated

Species	Species Type	Slope of Line	% Error	R^2	p-value
Anabaena flos-aquae	Cyanobacteria	87199488 ± 1233644	1.4%	0.996	$< 2 \times 10^{-16}$
Anabaena flos-aquae (N-Fixing)	Cyanobacteria	4558954 ± 200900	4.4%	0.992	2.234×10^{-05}
Aphanizomenon flos-aquae	Cyanobacteria	41843061 ± 1922319	4.6%	0.956	2.556×10^{-16}
Aphanizomenon flos-aquae (N-Fixing)	Cyanobacteria	2572011 ± 78403	3.0%	0.996	5.149×10^{-06}
Aphanizomenon skuja	Cyanobacteria	35436153 ± 2433351	6.9%	0.955	4.654×10^{-08}
Aphanizomenon skuja (N-Fixing)	Cyanobacteria	3681562 ± 86554	2.4%	0.998	1.826×10^{-06}
Chlamydomonas reinhardtii	Chlorophyte	2216571 ± 67617	3.1%	0.996	5.164×10^{-06}
Chlorella vulgaris	Chlorophyte	6046780 ± 83884	1.4%	0.997	$< 2 \times 10^{-16}$
Coelastrum proboscideum	Chlorophyte	6297438 ± 256948	4.1%	0.965	$< 2 \times 10^{-16}$
Dolichospermum lemmermannii	Cyanobacteria	190841800 ± 4557838	2.4%	0.994	1.448×10^{-12}
Dolichospermum lemmermannii (N-Fixing)	Cyanobacteria	15818843 ± 470152	3.0%	0.996	4.654×10^{-06}
Microcystis aeruginosa	Cyanobacteria	54845244 ± 1303300	2.4%	0.990	$< 2 \times 10^{-16}$

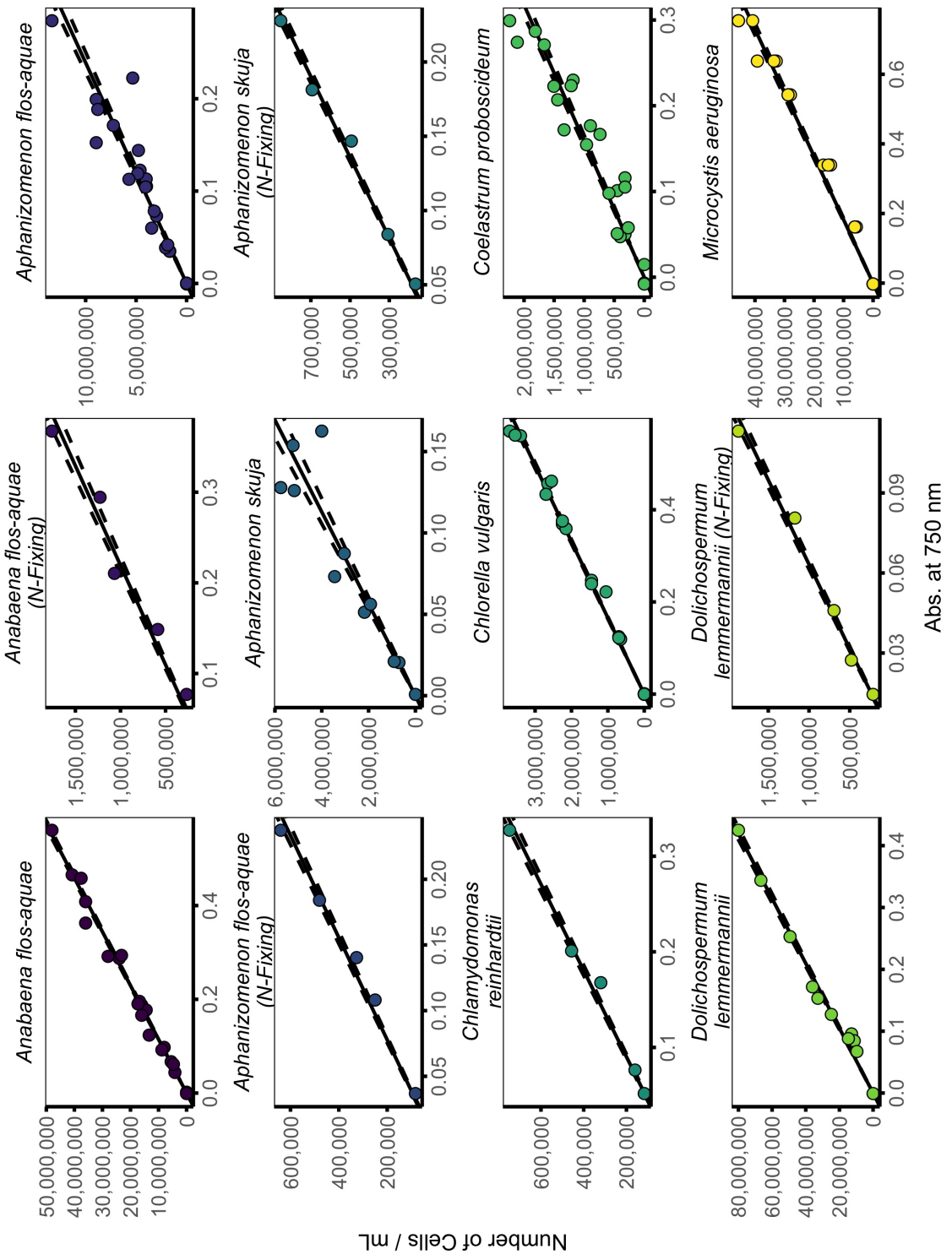

Figure A.1: Linear relationships of cell number to A_{750}. Dashed lines indicate error in slope estimates.

Appendix B

Supplemental Data for Chapter 3

B.1 Results

B.1.1 Growth Rates

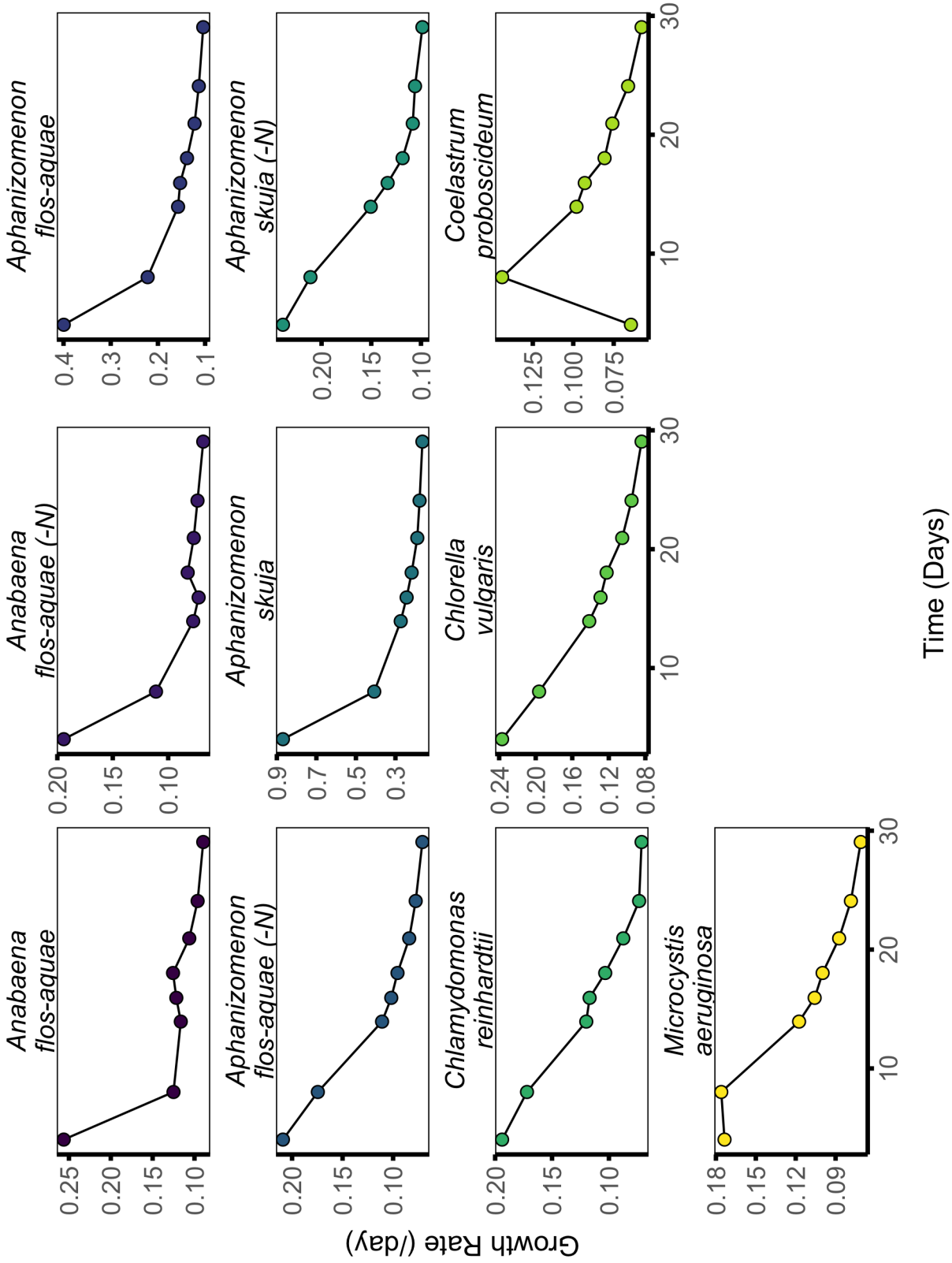

Figure B.1: Growth rates (μ) of each species calculated by using Eq. 3.1.

B.1.2 Dissolved Nutrients

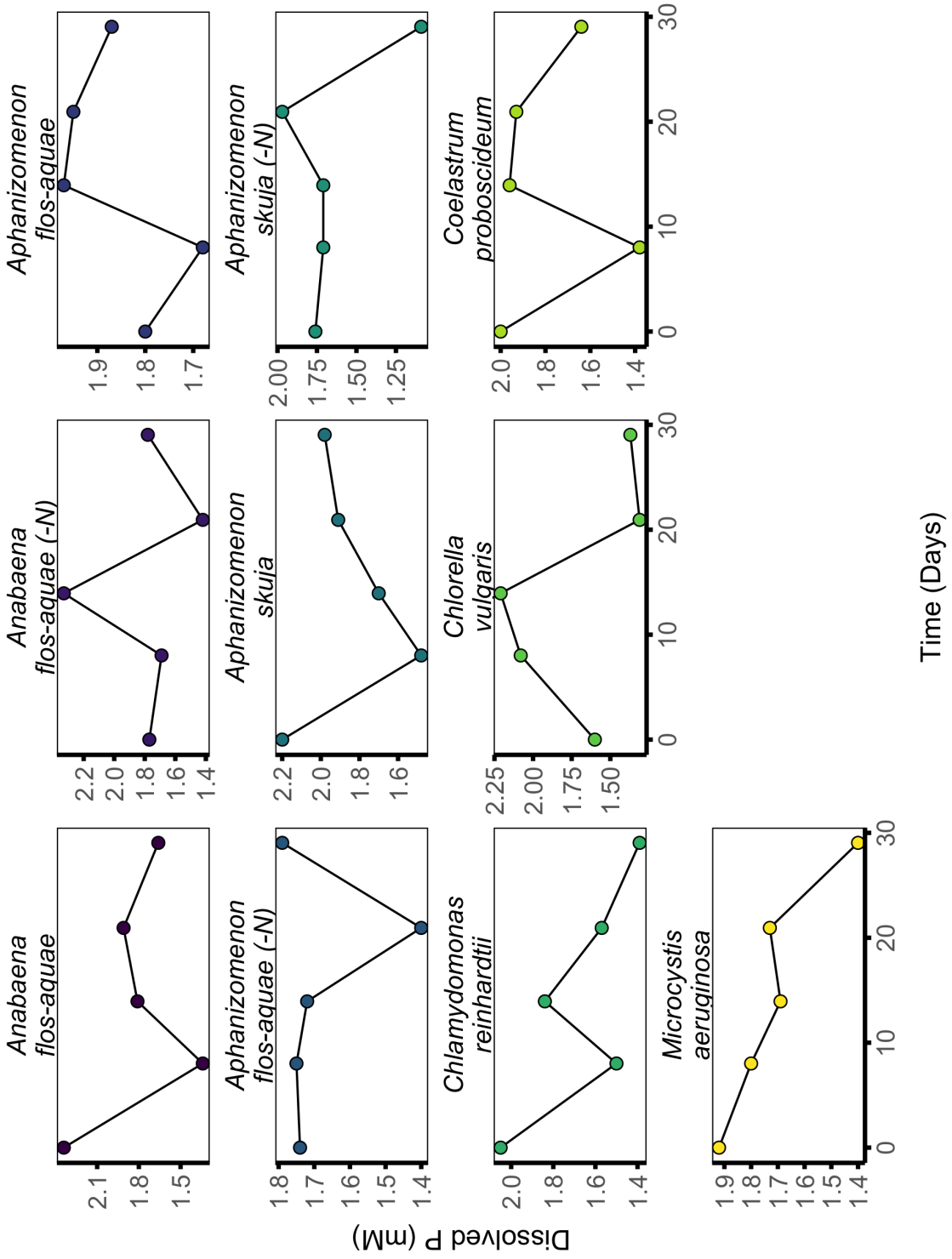

Figure B.2: Dissolved phosphorus concentrations during growth of each species. Dissolved P is reported as mM of P. Species labelled with (-N) are grown without inorganic N in the media and are N-fixing.

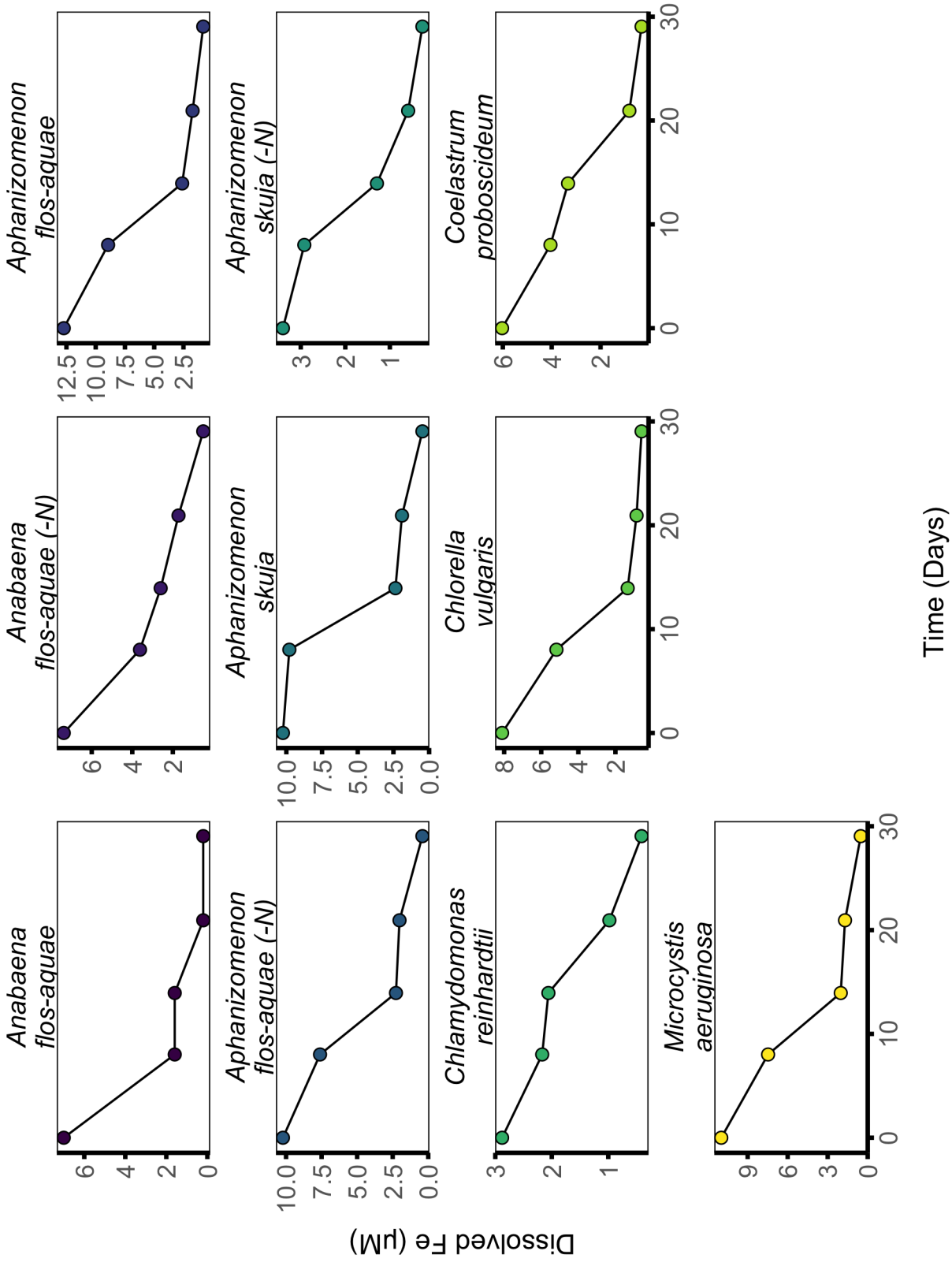

Figure B.3: Dissolved iron concentrations during growth of each species. Dissolved Fe is reported as μM of Fe. Species labelled with (-N) are grown without inorganic N in the media and are N-fixing.

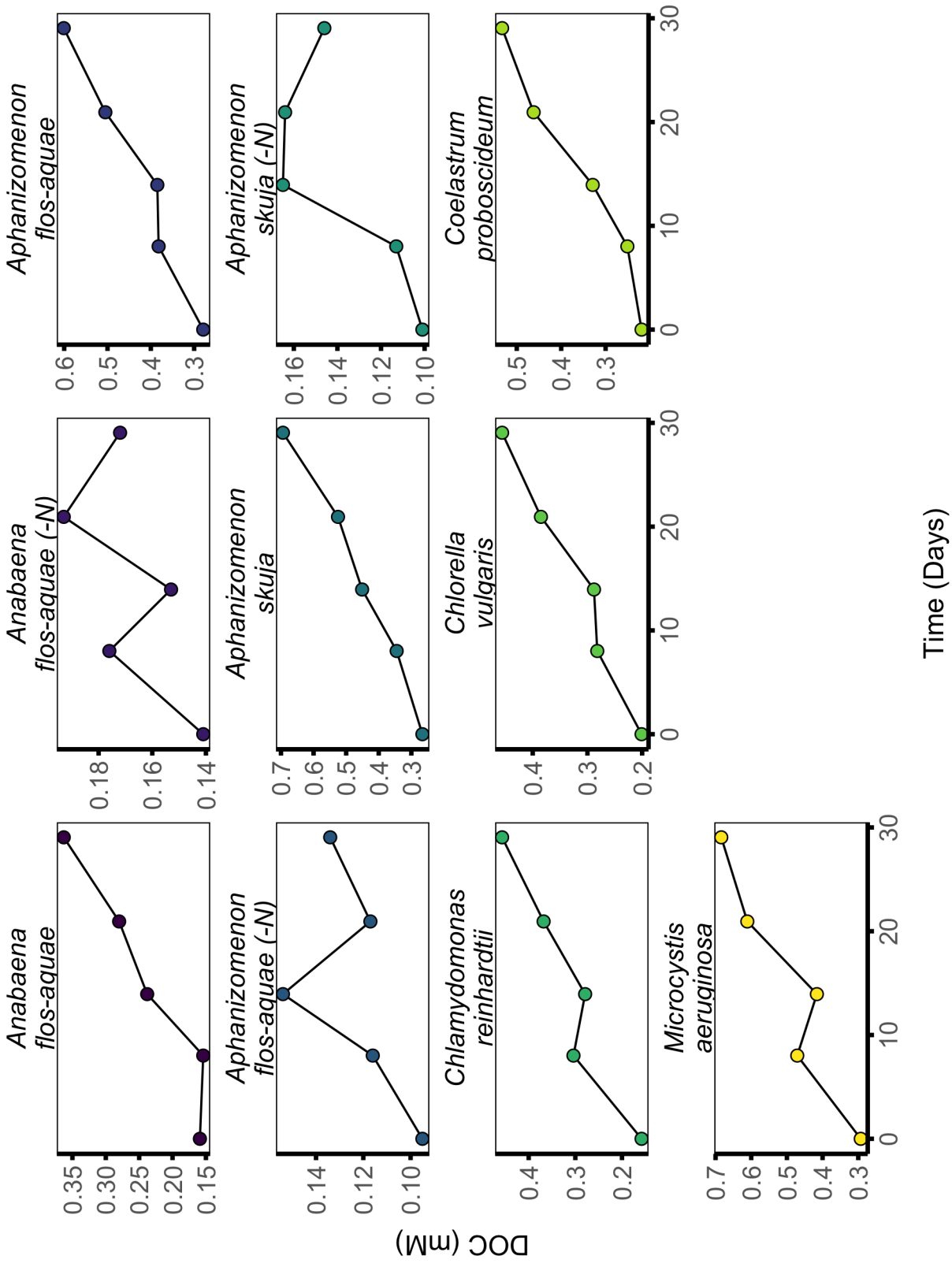

Figure B.4: Dissolved organic carbon (DOC) concentrations during growth of each species. DOC is reported as mM of C. Species labelled with (-N) are grown without inorganic N in the media and are N-fixing. Precision is ±0.25mM C.

B.1.3 C:N Ratios

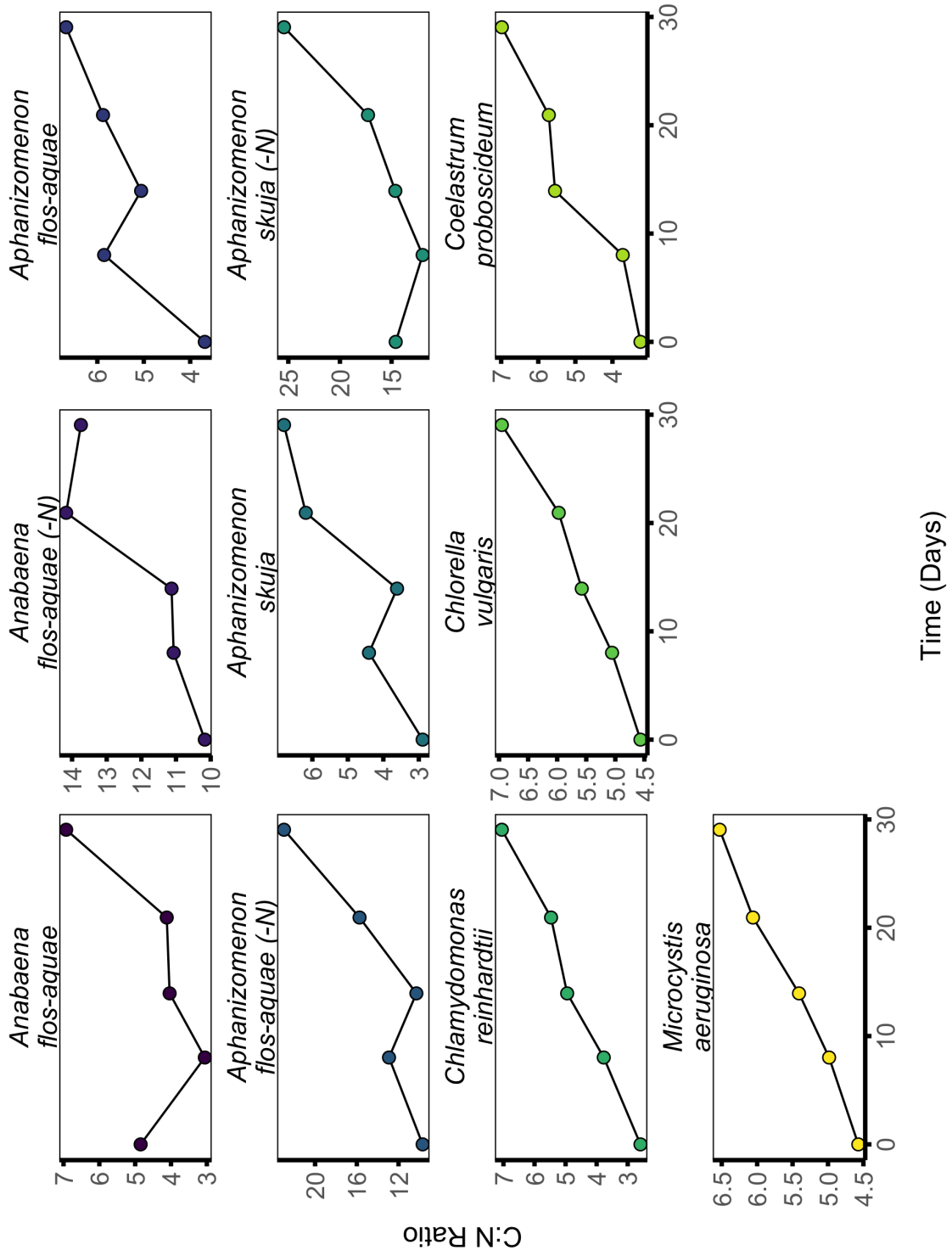

Figure B.5: C:N elemental ratios during growth of each species. Species labelled with (-N) are grown without inorganic N in the media and are N-fixing.

B.1.4 Isotopic Composition

B.1.4.1 δ^{13}C-POC

Table B.1: Time series carbon isotopic composition for each species with δ^{13}C of DIC, bulk POC and calculated new biomass POC (using Eq. 3.2). Stable isotopic fractionation factor calculated between the DIC and the new POC are presented as α and ϵ.

Species	Day	A_{750}	δ^{13}C-DIC	δ^{13}C-POC_{Bulk}	δ^{13}C-POC_{New}	α	ϵ
Anabaena	0.00	0.0182	-4.72	-19.50			
flos-aquae	8.02	0.0496	-4.21	-19.46	-19.43	1.0150	15.0
	13.94	0.0921	0.35	-17.58	-15.38	1.0113	11.3
	20.94	0.1682	2.39	-16.60	-15.41	1.0160	16.0
	29.05	0.2451	1.91	-15.28	-12.40	1.0150	15.0
Anabaena	0.00	0.0039	-7.10	-19.94			
flos-aquae	8.02	0.0096	-11.15	-18.30	-17.15	1.0102	10.2
(N-Fixing)	13.94	0.0116	-11.69	-18.10	-17.13	1.0061	6.1
	20.94	0.0197	-11.53	-18.58	-19.27	1.0077	7.7
	29.05	0.0287	-11.32	-18.89	-19.56	1.0082	8.2
Aphanizomenon	0.00	0.0121	-2.83	-18.71			
flos-aquae	8.02	0.0714	-2.47	-20.13	-20.42	1.0180	18.0
	13.94	0.1082	0.06	-21.03	-22.79	1.0208	20.8
	20.94	0.1568	0.33	-21.01	-20.96	1.0215	21.5
	29.05	0.2477	1.19	-22.35	-24.65	1.0256	25.6
Aphanizomenon	0.00	0.0055	-8.55	-19.31			
flos-aquae	8.02	0.0223	-8.40	-18.44	-18.16	1.0098	9.8
(N-Fixing)	13.94	0.0258	-8.30	-17.79	-13.63	1.0053	5.3
	20.94	0.0320	0.33	-19.81	-28.31	1.0206	20.6
	29.05	0.0432	-8.63	-18.51	-14.82	1.0154	15.4
Aphanizomenon	0.00	0.0029	-1.90	-20.76			
skuja	8.02	0.0756	-1.84	-16.95	-16.80	1.0152	15.2
	13.94	0.1301	1.53	-17.59	-18.47	1.0169	16.9
	20.94	0.1522	0.89	-19.27	-29.20	1.0317	31.7
	29.05	0.3334	1.88	-21.24	-22.90	1.0243	24.3
Aphanizomenon	0.00	0.0032	-9.33	-21.17			
skuja	8.02	0.0174	-8.69	-19.47	-19.09	1.0099	9.9
(N-Fixing)	13.94	0.0261	-8.15	-18.16	-15.53	1.0070	7.0
	20.94	0.0309	-10.94	-17.97	-16.96	1.0090	9.0
	29.05	0.0561	-6.02	-17.65	-17.25	1.0064	6.4
Chlamydomonas	0.00	0.0190	-8.86	-17.59			
reinhardtii	8.02	0.0754	-4.29	-18.46	-18.75	1.0101	10.1
	13.94	0.1011	-0.70	-19.97	-24.42	1.0206	20.6
	20.94	0.1185	-0.09	-21.36	-29.42	1.0296	29.6
	29.05	0.1508	0.87	-22.12	-24.93	1.0255	25.5
Chlorella	0.00	0.0164	-5.94	-18.43			
vulgaris	8.02	0.0793	-5.52	-18.50	-18.52	1.0128	12.8

Continuation of Table B.1

Species	Day	A_{750}	δ^{13}C-DIC	δ^{13}C-POC_{Bulk}	δ^{13}C-POC_{New}	α	ϵ
	13.94	0.1180	-1.57	-18.80	-19.43	1.0142	14.2
	20.94	0.1492	-1.41	-19.55	-22.38	1.0213	21.3
	29.05	0.1892	0.45	-19.79	-20.69	1.0197	19.7
Coelastrum	0.00	0.0268	-10.47	-17.24			
proboscideum	8.02	0.0851	-3.20	-19.75	-20.90	1.0107	10.7
	13.94	0.1052	0.21	-19.19	-16.82	1.0139	13.9
	20.94	0.1313	0.11	-20.67	-26.63	1.0276	27.6
	29.05	0.1437	0.66	-20.99	-24.38	1.0251	25.1
Microcystis	0.00	0.0443	-6.73	-17.20			
aeruginosa	8.02	0.1816	-0.37	-17.59	-17.71	1.0112	11.2
	13.94	0.2278	0.25	-19.40	-26.55	1.0269	26.9
	20.94	0.2759	0.02	-21.56	-31.76	1.0331	33.1
	29.05	0.3491	1.18	-22.82	-27.58	1.0284	28.4

B.1.4.2 δ^{15}N-PON

Table B.2: Time series carbon isotopic composition for each species with δ^{15}N of DIN, bulk PON and calculated new biomass PON (using Eq. 3.2). Stable isotopic fractionation factor calculated between the DIN and the new PON are presented as α and ϵ.

Species	Day	A_{750}	δ^{15}N-DIN	δ^{15}N-PON$_{Bulk}$	δ^{15}N-PON$_{New}$	α	ϵ
Anabaena	0.00	0.0182	-15.1	-15.38			
flos-aquae	8.02	0.0496	-15.1	-15.26	-15.19	1.0001	0.1
	13.94	0.0921	-15.1	-15.68	-16.18	1.0011	1.1
	20.94	0.1682	-15.1	-16.79	-18.13	1.0031	3.1
	29.05	0.2451	-15.1	-19.89	-26.67	1.0119	11.9
Anabaena	0.00	0.0039	0	-11.13			
flos-aquae	8.02	0.0096	0	-12.50	-13.46	1.0136	13.6
(N-Fixing)	13.94	0.0116	0	-15.00	-27.00	1.0277	27.7
	20.94	0.0197	0	-12.17	-8.13	1.0082	8.2
	29.05	0.0287	0	-19.03	-34.08	1.0353	35.3
Aphanizomenon	0.00	0.0121	-15.1	-15.15			
flos-aquae	8.02	0.0714	-15.1	-17.21	-17.63	1.0026	2.6
	13.94	0.1082	-15.1	-16.11	-13.97	0.9989	-1.1
	20.94	0.1568	-15.1	-17.10	-19.32	1.0043	4.3
	29.05	0.2477	-15.1	-18.01	-19.58	1.0046	4.6
Aphanizomenon	0.00	0.0055	0	-12.61			
flos-aquae	8.02	0.0223	0	-9.78	-8.85	1.0089	8.9
(N-Fixing)	13.94	0.0258	0	-11.77	-24.37	1.0250	25.0
	20.94	0.0320	0	-12.44	-15.22	1.0155	15.5
	29.05	0.0432	0	-11.52	-8.93	1.0090	9.0
Aphanizomenon	0.00	0.0029	-15.1	-14.96			
skuja	8.02	0.0756	-15.1	-14.00	-13.96	0.9988	-1.2
	13.94	0.1301	-15.1	-15.79	-18.28	1.0032	3.2
	20.94	0.1522	-15.1	-16.71	-22.10	1.0072	7.2
	29.05	0.3334	-15.1	-16.24	-15.84	1.0008	0.8
Aphanizomenon	0.00	0.0032	0	-10.12			
skuja	8.02	0.0174	0	-9.71	-9.61	1.0097	9.7
(N-Fixing)	13.94	0.0261	0	-11.28	-14.42	1.0146	14.6
	20.94	0.0309	0	-11.34	-11.70	1.0118	11.8
	29.05	0.0561	0	-15.67	-20.98	1.0214	21.4
Chlamydomonas	0.00	0.0190	-15.1	-18.10			
reinhardtii	8.02	0.0754	-15.1	-15.54	-14.67	0.9996	-0.4
	13.94	0.1011	-15.1	-16.79	-20.48	1.0055	5.5
	20.94	0.1185	-15.1	-17.54	-21.90	1.0070	7.0
	29.05	0.1508	-15.1	-18.81	-23.45	1.0085	8.5
Chlorella	0.00	0.0164	-15.1	-15.87			
vulgaris	8.02	0.0793	-15.1	-15.47	-15.37	1.0003	0.3
	13.94	0.1180	-15.1	-16.47	-18.52	1.0035	3.5
	20.94	0.1492	-15.1	-16.07	-14.55	0.9994	-0.6

Continuation of Table B.2

Species	Day	A_{750}	δ^{15}N-DIN	δ^{15}N-PON_{Bulk}	δ^{15}N-PON_{New}	α	ϵ
	29.05	0.1892	-15.1	-16.91	-20.03	1.0050	5.0
Coelastrum	0.00	0.0268	-15.1	-15.53			
proboscideum	8.02	0.0851	-15.1	-16.50	-16.95	1.0019	1.9
	13.94	0.1052	-15.1	-16.29	-15.42	1.0003	0.3
	20.94	0.1313	-15.1	-17.11	-20.41	1.0054	5.4
	29.05	0.1437	-15.1	-17.87	-25.98	1.0112	11.2
Microcystis	0.00	0.0443	-15.1	-16.33			
aeruginosa	8.02	0.1816	-15.1	-16.07	-15.99	1.0009	0.9
	13.94	0.2278	-15.1	-15.83	-14.90	0.9998	-0.2
	20.94	0.2759	-15.1	-16.82	-21.48	1.0065	6.5
	29.05	0.3491	-15.1	-17.60	-20.53	1.0055	5.5